BIOACTIVE TITANIA COLLOIDAL PARTICLES:

PREPARATION, CHARACTERIZATION

AND APPLICATIONS

BIOACTIVE TITANIA COLLOIDAL PARTICLES:

PREPARATION, CHARACTERIZATION

AND APPLICATIONS

By

LU (LUCY) YE, B. Eng., M. Sci.

A Thesis

Submitted to the School of Graduate Studies

In Partial Fulfillment of the Requirements

for the Degree

Doctor of Philosophy

McMaster University

DOCTOR OF PHILOSOPHY

(Chemical Engineering)

McMaster University

Hamilton, Ontario

TITLE: Bioactive Titania Colloidal Particles: Preparation, Characterization, and Applications

AUTHOR: Lu (Lucy) Ye, M. Sci., B. Eng., (Beijing University of Chemical Technology, P. R. China)

SUPERVISORS: Professor Robert H. Pelton & Professor Michael A. Brook

NUMBER OF PAGES: xix, 205

ABSTRACT

Photocatalytic TiO_2, used for oxidizing organic compounds and biological entities, has been extensively studied. However, biomolecules conjugated to photocatalytic TiO_2 colloidal particles and their applications have rarely been reported. In this work, a novel platform for fabricating biomolecules conjugated to TiO_2 using biotin-streptavidin/avidin bioconjugation and biotin coated photocatalytic TiO_2 was developed and the properties and applications of the biomolecules conjugated photocatalytic TiO_2 colloidal particles were studied.

Photocatalytic TiO_2 particles were treated with 3-aminopropyltriethoxysilane (APTS) and then N-hydroxysuccinimidobiotin (NHS-biotin) to give a biotin coating. The resulting aminosilanized and biotinylated TiO_2 particles were characterized by a variety of methods, including nuclear magnetic resonance spectroscopy (NMR), Fourier transform infrared spectroscopy (FT-IR), transmission electron microscopy (TEM), electrophoretic mobility, light diffraction, nitrogen adsorption, polyelectrolyte titration, conductometric titration, biotin assays, X-ray photoelectron spectroscopy (XPS), and confocal laser scanning microscopy (CLSM), giving insight into the strategies necessary to control the density of grafted amino groups, organosilane thickness, and surface charges of the resulting aminosilanized TiO_2. Ultimately, the key parameters for photocatalytic performace relied on the ability to tune the surface modification reaction, and the conditions for conjugating the biotinylated TiO_2 to streptavidin.

The impact of UV irradiation to the aminosilanized cationic TiO_2 colloidal particles was studied. The results show that an oxidization reaction occurs on TiO_2 surfaces, resulting in the removal of the amino groups and the change of surface charge from positive to negative. A new light-triggered flocculation system was developed based on this surface charge conversion.

Biomolecules conjugated to colloidal titania particles exhibit combined properties of the biological functions of bound biomolecules and the photocatalytic properties of titania. Two applications related to biomolecules conjugated photocatalytic TiO_2 were studied in this work. One is the selective binding and killing of bacteria by using antibody coated photocatalytic TiO_2 under UV irradiation. The antibody-TiO_2 was prepared by coupling biotinylated TiO_2 particles to biotinylated *Escherichia coli* (*E. coli*) antibody with streptavidin. In a medium containing antibody-TiO_2 particles, *E. coli*, and *Pseudomonas putida* (*P. putida*), when UV irradiation is applied, the selective binding and killing of *E. coli* was confirmed by electrophoretic mobility measurement, turbidity tests, optical microscopy, scanning electron microscopy (SEM), confocal microscopy, and plate counting. The other application is the immobilization of TiO_2 particles on cellulose fibers with a homogeneous distribution through multi-linker bioconjugation of CBM2a-*Strep*-tag II/streptavidin/biotinylated TiO_2. The immobilized TiO_2 efficiently decolorizes UV sensitive dye within about 10 hours, demonstrating the efficiency of photocatalysis of the resulting TiO_2-containing paper.

ACKNOWLEDGEMENTS

First of all, I would like to express my greatest gratitude to my supervisors, Dr. Robert Pelton and Dr. Michael Brook. I am very lucky to have two supervisors and belong to two research groups. I appreciate very much the freedom Dr. Pelton and Dr. Brook gave me to do research within this thesis, which has given me opportunities to freely gain knowledge in several disciplines. I am very grateful for Dr. Pelton and Dr. Brook's constant encouragement, numerous and priceless guidance, helpful scientific suggestions in all the time of research and writing of this thesis. In addition, I want to express my appreciation to Dr. Brook and Dr. Pelton for giving me a of lot help in many aspects of my life.

I would like to acknowledge the members of my Ph.D. committee, Dr. Carlos Filipe and Dr. John Brennan, for their valuable discussion and advice, good ideas, and consistent encouragement through my whole Ph.D. research work. I am also grateful to Dr. Steve Koprich for his help with scanning electron microscopy, to Dr. Laura Harrington for her help with nuclear magnetic resonance, to Ms. Marcia West and Mr. Marnie Timleck for their help with transmission electron microscopy and confocal laser scanning microscopy, and to Mr. Frank Gibbs for his help with thermogravimetric analysis. Furthermore, Dr. Haifeng Wang and Dr. Luba Brovko in University of Guelph are thanked for their help with *P. putida* and related support in the biological manipulation of the organism; Dr. Michael D. McLean in University of Guelph is thanked

Finally, I am greatly indebted to my family for their love, understanding, encouragement and support throughout my graduate study. They are firm boosters not only in my academic career but also in every decision in my life. Particularly, my son, Jason (Jiasheng) Miao, born on Oct 15 2007, is one of my biggest achievements during my Ph.D. study period.

我首先要感谢我的父母，感谢他们多年来的养育之恩。我在人生道路上所取得的每一点成绩，每一个进步，都是和他们的教育和支持分不开的。在我读博士的最后半年，我的丈夫离开我们去温哥华工作了，我则留在汉密尔顿继续我的博士学业。我的母亲，陈利音女士，只身从中国杭州来到我身边，帮助我照顾我只有 7 个月大的儿子，好让我专心完成学业。我的父亲，叶亦聪先生，因为病重无法和我母亲一同前来，但为了不耽误我的学业，他极少向我提及自己的病情，反而一再嘱咐我全心关注自己的工作。他们是伟大的父亲母亲，深爱我和哥哥，我永远都感谢他们。我也要感谢我的哥哥，叶迅，以及我父亲这边的众多亲属，是他们在我父亲病重期间全力照顾他，使我无后顾之忧。没有他们的帮助，我很难如期完成我的博士学业。在此一并表示深深的感谢。

我其次要感谢的是我的丈夫，苗传威。他一直都是我最坚定的支持者和最重要的人生伴侣。我们在科研上相互鼓励帮助，共同爱护我们的小家。我非常感谢他多

年来的对我们的家庭和我的事业所作出的努力。 我也感谢我的儿子苗嘉盛，他的出生给我的生活带来了无可比拟的幸福感和成就感。

我特别要感谢我的公公婆婆。他们一直对我的事业和家庭都非常的支持。尤其是我的婆婆，许桂荣女士，由于签证原因，在儿子出生一个月时婆婆一人从中国的辽源来到我们汉密尔顿，在生活上对我和孩子给予了很大的帮助，在此表示深深的感谢。

TABLE OF CONTENTS

LIST OF TABLES

LIST OF SCHEMES

Chapter 1   Introduction

"Smart" materials have been attracting much attention because they can perform special tasks. Smart materials are normally those that can be stimulated to perform a certain task. For instance, smart polymers such as poly(N-isopropylacrylamide) (pNIPAM) can respond to various stimuli from the environment; hence smart materials can be used as advanced drug delivery materials, meeting certain special requirements, such as targeted controlled delivery.[1,2] Photocatalytic TiO_2 has been extensively studied and used to oxidize organic pollutants and pathogens. However, "smart" TiO_2 is a new concept. Our group has been interested in the exploiting these photocatalytic properties in a 'smart' way, for example, by selectively killing bacteria.

This thesis describes the preparation of biomolecule-conjugated TiO_2 colloidal particles and their applications, including biotin-TiO_2, streptavidin-TiO_2 and antibody-

TiO$_2$. In each case, the surface biomolecules provided a recognition function causing specific interaction with a target. This work required various research fields, involving chemical surface modification of colloidal TiO$_2$ particles, photocatalytic chemistry with TiO$_2$, microbiology, cellulose fibers and bio-conjugation. For this reason, this section will provide a variety of different introductions to: TiO$_2$ particles (including crystalline structure, colloidal properties and photocatalytic activity); bacteria; the interaction between bacteria and photo-irradiated TiO$_2$ particles; and key biomolecules (including biotin, avidin / streptavidin, and carbohydrate-binding modules) that were involved in this thesis. The methods of surface modification of TiO$_2$ colloidal particles and conventional preparation of biomolecules derivatized TiO$_2$ are reviewed in Chapter 1, and therefore, not included in this introduction.

1. 1   TiO$_2$

TiO$_2$ exists naturally in three crystalline forms: rutile, anatase and brookite. Some physical constants of TiO$_2$ are summarized in Table 1-1 and the three crystalline forms are shown in Figure 1-1.[3] Rutile and anatase, have not only been extensively used to improve opacity and whiteness in papermaking, paints and coatings, cosmetic, plastic and ceramics products because of their high refractive indices,[4] but also played a significant role in photo-assisted degradation of organic compounds, and in killing pathogens in air and water due to their photocatalytic properties.[5] Some studies in comparing the photo-activities of commercial anatase and rutile show that the photooxidation activity of anatase is much higher than that of rutile.[6, 7] The reason probably lies in the difference in

extent and nature of the hydroxyl groups (-OH) on TiO_2 surface of the TiO_2 structure.[8, 9] Brookite, although it also displays photo-activity and a high refractive index, however, has been rarely used in these ways. The reason probably lies in the difficulty of its preparation.[8, 10-12]

Crystal structure		Rutile	Anatase	Brookite
system		Tetragonal	tetragonal	Rhombohedral
Density (kg/m^3)		4240	3830	4170
Refractive index		2.947	2.569	2.809
Band gap (eV)		3.0	3.2	-
Lattice constants (nm)	a	0.458	0.373	0.544
	b	-	-	0.917
	c	0.295	0.937	0.514
The main application		White pigment	photocatalyst	-

Table 1-1 Some physical constants of rutile, anatase and brookite[3]
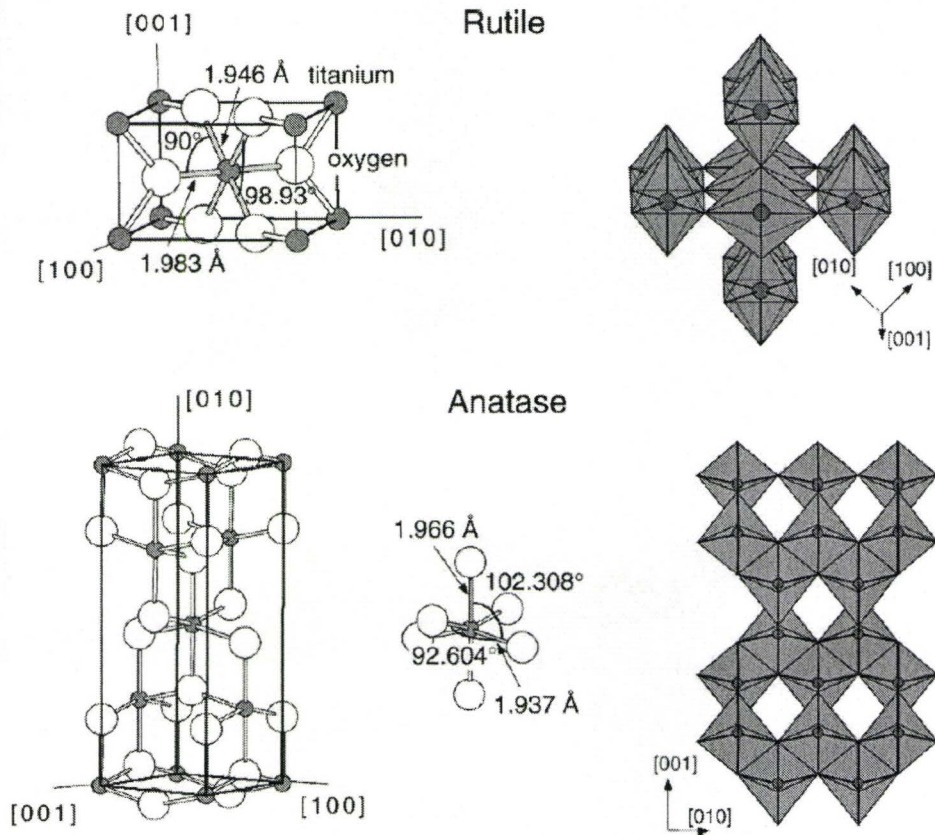
Figure 1-1 Crystalline structure of rutile and anatase – graphic taken from *Surface Science Reports* **2003**, 48, (5-8), 53-229[3]

1.1.1. Colloidal properties of TiO₂ particles

The colloidal properties of TiO_2 particles are affected by a variety of factors, including the surface structure of TiO_2 crystals, surface modification, size and size distribution, the sample preparation and processing, and local environmental conditions such as pH values[13] and ionic strength.[14]

On the TiO_2 surface, amphoteric titanol groups (TiOH) participate in acid-base equilibria, shown in Figure 1-2, to give different surface charges at different pH

values.[15-17]   Many studies have shown that the isoelectric point (point of zero zeta potential) of TiO_2 samples varies in the range 2.3-8.0, strongly depending on the preparation and processing including the annealing history and aging time.[18-22] Table 1-2 shows the isoelectric points of some commercial rutile and anatase samples prepared and pretreated by various methods.[21]

$$TiOH_2^+ \xrightleftharpoons{pK_{a1}} TiOH + H^+ \qquad \text{Eq. (1)}$$

$$TiOH \xrightleftharpoons{pK_{a2}} TiO^- + H^+ \qquad \text{Eq. (2)}$$
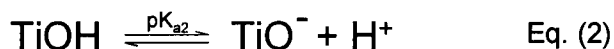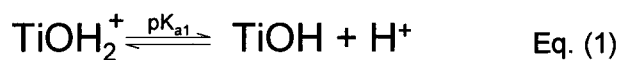
Figure 1-2 Acid-base equilibria of amphoteric titanol groups[15]

The hydroxyl groups (-OH) on TiO_2 surfaces, originating from contact with moisture in air, are the reactive groups in surface reactions. The density of hydroxyl groups on the surface of TiO_2 has been found to be correlated with its photo-activity.[17] In Mueller's report, the densities of hydroxyl groups on TiO_2 particles have been calculated, by thermogravimetric analysis, to be in the range $4.8\sim6.1$ nm^{-2}.[23]

Size and size distribution also influence the colloidal behavior of TiO_2 particles in aqueous solutions, particularly for nano-sized TiO_2 particles.[22] Due to the van der waals force, these nano-sized TiO_2 particles have a tendency to aggregate and even agglomerate spontaneously in water.[22, 24, 25]

	Pretreatment	pH at iep
Rutile A	Sample used shortly after preparation	4.8
	After 12 successive soxhlet wash/ heat in air at 450°C treatments	5.0
	After acid leaching/ soxhlet wash treatment	5.0
	Aged in air 6 months	5.5
	Aged in air for a further 6 months	5.5
	After acid leaching/soxhlet wash treatment	5.5
	Heated in air t 850 °C for 24 hr	4.8
	Aged in air 6 months	4.8
	Dispersion aged for 1 month	3.7
	Dispersion aged for a further 3 months	3.4
Rutile C	Sample used as received from manufacturer	4.2
	After soxhlet washing	4.3
	After acid leaching/ soxhlet wash treatment	4.8
	Aged in air 6 months	4.3
	After acid leaching/soxhlet wash treatment	4.8
	Dispersion aged for 4 months	3.4
Anatase 1 (0.3% rutile)	Sample used shortly after preparation	5.9
	Aged in air 6 months	4.5
	After soxhlet washing	5.0
	After acid leaching/soxhlet washing	6.0

continued

	Pretreatment	pH at iep
Anatase 2 (4.8% rutile)	After heating in air 850 °C for 5 min	5.7
Anatase 3 (5.0% rutile)	After heating in air 850 °C for 10 min	4.5
	Aged in air 6 months	4.0
	Aged in air for a further 4 months	3.4
	After soxhlet washing	4.8
	After acid leaching/ soxhlet washing	5.8
Anatase 4 (7.0% rutile)	After heating in air 850 °C for 15 min	4.6
	Aged in air 6 months	2.7
Anatase 5 (83.2% rutile)	After heating in air 850 °C for 16 hr	4.6
	Aged in air 6 months	3.6
	Aged in air for a further 6 months	3.5
	After acid leaching/ soxhlet washing	4.3

Table 1-2 The isoelectric point values of some commercial rutile and anatase crystalline measured by Furlong[21]

Degussa P25 TiO_2, a commonly studied commercial photocatalytic TiO_2, is produced by the hydrolysis of $TiCl_4$ in a hot flame (Degussa Chemical Company, Germany). In the work reported in this thesis, P25 TiO_2 has also been used. The composition and some important physical parameters of P25 TiO_2 are summarized in Table 1-3.[8, 15, 26]

composition	anatase (80%) + rutile (20%)
Particle size	30nm primary particles
specific surface area	55 ± 15 m^2/g

pKa	pKa$_1$	4.5
	pKa$_2$	8

(point of zero charge) pzc	6.2
theoretical maximum surface density (/nm^2) of hydroxyl groups (-OH) groups, calculated from the crystalline structure[26]	5.5

Table 1-3 Some physical parameters of Degussa P25 TiO$_2$[8, 15]

1.1.2. Photocatalytic properties of TiO$_2$

There is a large body of literature, including numerous reviews,[3, 5, 6, 8, 15, 16, 27-29] describing the photocatalytic chemistry of TiO$_2$. Most of this literature focuses on three aspects: (1) exploring photocatalytic mechanisms; (2) improving the efficiency of the photoactivity of TiO$_2$; and (3) photodegradation of organic compounds and photodisinfection of microorganisms and cells.

1.1.2.1. Photocatalytic mechanism of TiO$_2$

Upon irradiation with the energy of light greater than or equal to its band gap energy (~3.2 eV for anatase, ~3.0 eV for rutile),[30] TiO$_2$ can be electronically excited so as to generate a variety of reactive oxygen species (ROS) such as hydroxyl radicals, superoxide ions and/or hydrogen peroxide.[6, 15, 31] These ROS are extremely aggressive in oxidizing

organic substances (into CO_2 and H_2O ultimately) and in killing biological entities. The reactions on the surfaces of UV-irradiated TiO_2 in water are shown in Table 1-4.[16]

$TiO_2 + h\nu \leftrightarrow h^+ + e^-$	Eq. (3)
$h^+ + H_2O \rightarrow H^+ + \bullet OH$	Eq. (4)
$h^+ + OH^- \rightarrow \bullet OH$	Eq. (5)
$e^- + O_2 \rightarrow O_2^{\bullet-}$	Eq. (6)
$O_2^{\bullet-} + H^+ \rightarrow HO_2$	Eq. (7)
$\bullet OH + \bullet OH \rightarrow H_2O_2$	Eq. (8)
$e^- + H_2O_2 \rightarrow \bullet OH + OH^-$	Eq. (9) photo-Fenton rxn.
$H_2O_2 + Fe^{2+} \rightarrow HO^\bullet + OH^- + Fe^{3+}$	Eq. (10) Fenton rxn.

Table 1-4 Reactions of UV-irradiated TiO_2 in water[16]

Light adsorption is the first step. It is found that light with wavelength above ~380nm leads to a sharp decrease in photocatalytic activity of anatase. Blake et al. have summarized the effects of light sources on TiO_2 catalyzed reactions.[32] TiO_2 without light has no obvious photo-activity. Though light sources with a wavelength of <300nm can kill bacteria directly,[32] the effect of light plus TiO_2 is greater than that of light alone. Typically, UV light sources can be classified according to their wavelength into UVA (380-315nm), UVB (315-280nm) and UVC (<280nm). In the photo-excited TiO_2 experiments, it appears that the light with the wavelength of 365nm has mostly been used

because it matches the band gap of anatase well. In Nosaka's report, the penetration depth of absorbed light into TiO_2 was estimated to be 25 nm.[33]

When light with energy greater than the band gap of TiO_2 reaches TiO_2 surfaces, electro-hole pairs are photogenerated: electrons (e^-) in the conduction band and holes (h^+) in the valence band. The electrons and holes are then separated by traps on the TiO_2. The holes include interior holes that cannot facilitate reactions, and the ones trapped on the surface, which catalyze the following photocatalysis reaction.[34] The separated electrons and holes induce chemical reactions of the substances adsorbed on the surfaces of TiO_2. The recombination of electrons and holes is in direct competition with the process of trapping which favors the photocatalyzed reaction.[8]

The generation of hydroxyl radicals from the reactions of holes with water (Table 1-4, Eq. (4)), and of adsorption of hydroxide anions on the surface of TiO_2 (Table 1-4, Eq. (5)) is the most significant step in the entire photocatalytic process for killing pathogens and oxidizing organic compounds.[6, 16, 35] The efficiency of the production of hydroxyl radicals has been found to be sensitive to the presence of oxygen and H_2O_2, but not sensitive to TiO_2 concentration or light flux.[35-37] The factors affecting the efficiency of photocatalytic activity of TiO_2 have been extensively studied. These factors, including crystalline structure,[7, 38] size and size distribution,[7, 39] surface area,[39] porosity, the density of surface hydroxyl groups, chemisorption on TiO_2 surfaces,[27] and doping TiO_2 with foreign ions,[8] influence the generation process of electron-hole pairs, the recombination of electrons and holes, the chemical reaction, and the adsorption and desorption of target substances. The high efficiency of P25 photocatalytic activity is probably due to the

unique composition of P25 TiO_2, which promotes electron-hole pair separation and inhibits recombination.[38] Although there is abundant literature on the photochemistry of TiO_2, the answers to some of the fundamental problems, such as the length of the lifetimes of ROS, the distance they can travel in different media, and how these ROS exert their actions in the photooxidation process, are still unknown or present data with contradictory evidence. In the entire photocatalytic process, the lifetimes of ROS[15, 27] and their effective diffusion lengths are the key to decomposing organic compounds and microbiological entities. Kawahara and Tatsuma's experimental results suggest that ROS can diffuse as far as 50-70 μm through the vapor phase.[40, 41] However, Kikuchi points out that 50 μm is too far for hydroxyl radicals to travel, and he concluded that for long-range bactericidal effects, the active disinfection agents was H_2O_2, generated by the coupling of hydroxyl radicals.[42] In summary, further evidence of how these ROS exactly contribute to the photocatalytic process is needed.

1.1.2.2.   Decomposing organic compounds

The photocatalytic chemistry of TiO_2 in decomposing organic materials has attracted much interest since the first report of photocatalytic splitting of water on TiO_2 electrodes by Fujishima and Honda in 1972.[31] The ROS excited from photo-irradiated TiO_2 are extremely reactive, being able to convert all organic compounds to CO_2 and H_2O, as long as the target is exposed to photo-irradiated TiO_2 for enough time. Because TiO_2 has this huge potential application for total degradation of organic compounds and displays environmental-friendly characteristics, it has become one of the most active research

areas in heterogeneous photocatalysis. To date, numerous organic compounds have been

reported to be decomposed by photo-irradiated TiO_2. In Hoffmann's review, many

examples of chlorinated aromatics, chlorinated aliphatic and olefinic compounds,

nitrogen compounds, hydrocarbons, carboxylic acids, alcohols, halocarbons, and

heteroatom compounds were reported to be degraded by UV-TiO_2 system.[15] In all these

articles, the adsorption of target to TiO_2 surfaces was reported to be a significant factor in

affecting the efficiency of photodegradation. The apparent adsorption constants K and

the apparent photodegradation rate constants k vary drastically, according to the

experimental conditions.[15] Turchi and Ollis have studied four different reaction schemes,

and suggest that K is independent of reaction schemes whereas k is a function of catalyst

properties.[43]

1.1.2.3. Bactericidal effect

Removing or killing pathogens is important to humans, particularly in special

circumstances such as hospital areas where biological contamination must be prevented.

The most widely used traditional methods of disinfecting pathogens include filter (size

exclusion),[44] Pasteur sterilization, bleaching, chlorination, ozonation, germicidal lamps,

biocides, and washing with disinfectants.[45] Various forms of these traditional disinfection

methods are briefly described in Blake's review.[32] TiO_2, particularly Degussa P25, has

been reported to be an effective photocatalyst in the killing of a variety of

microorganisms including viruses,[46] bacteria,[47, 48] and fungi.[49] UV-irradiated TiO_2 shows

a greater effect on killing pathogens than near ultraviolet light; however, the sensitivity of

different pathogens to UV-irradiated TiO_2 systems varies over a wide range of levels, depending strongly on the nature of pathogens, the type and loading of TiO_2, light resources, buffer properties, the reactor, the temperature, and other experimental conditions.[32]   In Table 1-5, the experimental parameters and results of some photodisinfection experiments on *E. coli* with photo-irradiated TiO_2 are given.

Pfu or cfu/mL / Medium	TiO_2 Type/ Loading	Light Source/ Output	reactor	Kill Fraction	Time (min)	Comment and ref
10^3/phosphate buffer	P25/ 0.4g/L	Xenon 300W, 60mE/sec/m^2	Optical fiber reactor	100	120	[50]
10^6/DI water	P25/ 0.1 g/L	Sunlight	Petri dishes	100	30	100% killing in dark due to temperature rise [51]
10^3/phosphate buffer	P25 (10% Pt) 2.5 g/L	500W white fluorescent 400W metal halide 4.6mE/sec/m2 from top	Slurry	80	60	[52]
10^9/saline	P25/ 0.01-0.5 g/L	500W high-pressure mercury lamp / 0-60W/m^2 externally	Rectangular bubble-column (40×40×250mm) solution height 170 mm	100	4-12	[49]

Table 1-5 Some photodisinfection experiments on *E. coli*[32]

Researchers working on photocatalytic chemistry may not be very familiar with microbiology, and vice versa. Thus, I believe this thesis will be more accessible for various audiences to read if a brief introduction to bacteria is given before the description of the photooxidation of microorganisms by photoactive TiO_2.

1.1.2.3.1. Bacteria

Bacteria are microorganisms that are ubiquitous in nature. They exhibit a wide diversity of sizes (typically 0.5-5 micrometers in length) and morphologies: spherical (cocci), rod-shaped (bacilli or vibrio), and spiral (spirilla or spirochaetes). Unlike cells of animals and other eukaryotes, in which the chromosomes are enveloped by a double membrane, bacterial cells do not contain a nucleus or a nuclear membrane to separate DNA molecules from the cytoplasm (Figure 1-3a). Microorganisms including bacteria, viruses, fungi, protozoa and algae all have evolved a variety of defense and repair mechanisms against various types of environment damages for example, ultraviolet rays from natural sunlight.[53] For instance, a superoxide dismutase, produced in some aerobic life forms, is responsible for converting O_2^- to H_2O_2 and O_2.[54, 55] However, the ability of microorganisms to survive such stresses varies. In the work in this thesis, we only consider *Escherichia coli* (*E. coli*) and *Pseudomonas putida* (*P. putida*). Thus, we have focussed on these two microorganisms in this introduction.

E. coli was discovered by Theodor Escherich, a German paediatrician and bacteriologist in 1885. *E. coli* is a Gram-negative bacterium (see below), with a size of 0.5 μm in diameter and about 2 μm in length.[58] Some *E. coli* strains have flagella, and others do not. *E. coli* can be commonly found in the intestine of warm-blood animals, but are not only confined to the intestine. They also can survive outside the body. Most *E. coli* strains are harmless and even beneficial to humans, because they produce vitamin K_2[59] or/and inhibit the growth of some detrimental bacteria.[60, 61] However, some *E. coli* strains such as serotype O157:H7 are very dangerous to humans.[62] Ingestion by humans

of food contaminated by these strains can cause very serious illness. *E. coli* is one of the best-studied prokaryotic bacteria and has been used as a model organism in biological engineering and industrial microbiology due to the easily-manipulated growth conditions and its relatively simple genetics.[63-65] *P putida* is also a Gram-negative rod-shaped bacterium. Living in soil, it can clean up the pollutants in soil[66, 67] and even protect some plants from certain plants diseases.[68] It can be used in biosafety level 1 laboratories because it is a relative safe bacterium.
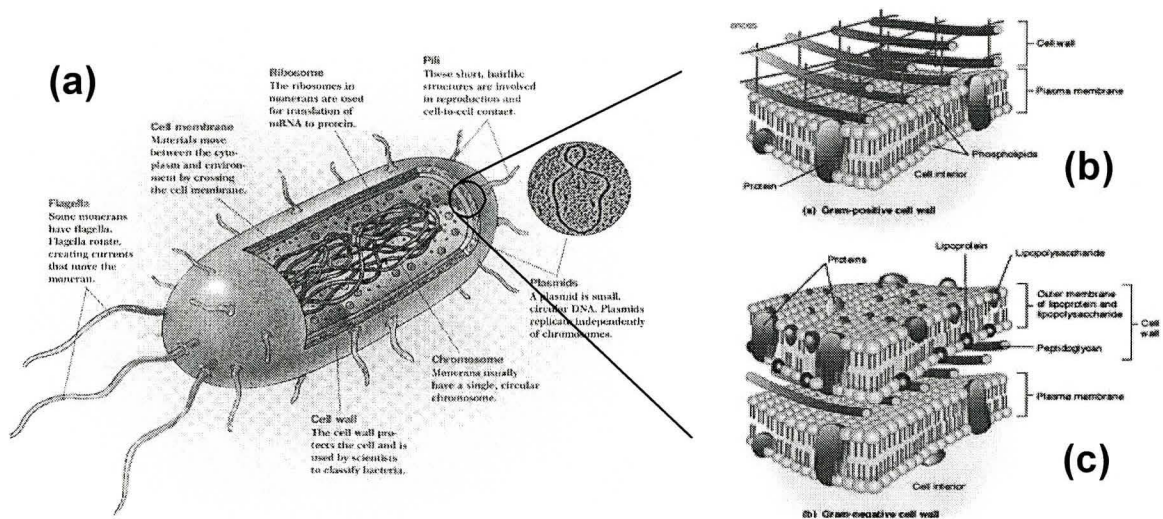
Figure 1-3 (a) Bacterial structure;[56] (b): the cell wall of Gram-positive bacteria;[57] (c) the cell wall of Gram-negative bacteria[57]

The cell walls of bacteria are important in protecting the cells from various environmental damage.[69, 70] According to whether or not their cell walls can be stained by the Gram stain, bacteria are divided into two classes, Gram-positive and Gram-negative. The cell walls of Gram-positive bacteria are 20-80 nm in thickness, composed of a peptidoglycan polymer (80%), teichoic acids (10-20%), and minor amounts of lipids, proteins and lipopolysaccharides (Figure 1-3b).[71, 72] The cell walls of Gram-negative bacteria are composed of a thin peptidoglycan polymer layer (2-6 nm, 10%) and an outer membrane (6-18nm, 90%) containing lipopolysaccharides, phospholipids, and lipoproteins (Figure 1-3c).[73]

Not only cell walls, but also cell membranes, are important in maintaining the viability of cells.[74] The cell membrane is crucial for selective permeability, osmotic equilibrium, electron-transport and oxidative phosphorylation reactions, and serving as the binding site to which certain enzymes and DNA molecules are anchored.[70, 75] Therefore, any disruption of cell membranes can lead to the death of cells.[76]

1.1.2.3.2. Mechanisms of killing bacteria by photocatalytic TiO$_2$

The mechanisms for killing bacteria by photo-irradiated TiO$_2$ have been studied since 1985.[52] However, so far only two mechanisms have been proposed that are supported with direct evidence. In the first, following generation of ROS on the surface of UV-irradiated TiO$_2$, cell membranes are oxidatively destroyed thereby leading to cell death. That is, during the photocatalytic process, the unsaturated phospholipid in the cell membranes is oxidized by ROS, and major rupture of cell membranes was observed by

electron micrographs.[77] Direct evidence of cell membrane damage was provided by the work of Sunada and his colleagues.[78] They detected the presence of endotoxin in the medium, which is evidence for the destruction of cell membranes, since the endotoxin is released only when the outer membrane is damaged. The disruption of cell membranes further leads to the leakage of the cell contents including potassium ions, acidic cellular components, and even large biomolecules such as proteins and RNA. After the cell membranes are broken, TiO_2 particles can enter the cells and mineralize directly on the essential intracellular components including some toxic compounds.[78] Thus, TiO_2 can be used as both a bactericidal and a detoxifying agent.

The other mechanism for killing bacteria by photoirradiation of TiO_2, for which direct evidence exists, is its oxidative effect on DNA and RNA molecules. DNA and RNA are biomolecules that are very important for the viability of cells. They are thus potential targets for photocatalytic reaction with UV-irradiated TiO_2: damage to DNA and RNA can lead to the death of cells. In Dunford's work, the plasmid DNA strand was broken under the attack of the hydroxyl radicals generated from the UV-TiO_2 system and finally converted to a linear form.[79] Hidaka has also given convincing evidence for the breakdown of DNA and RNA backbones, and even demonstrated mineralization reactions in the experiments of UV-irradiated TiO_2 killing bacteria.[80]

1.2 Biotin, streptavidin/avidin

In the work reported in this thesis, the surface of TiO_2 was modified, first with a silane coupling agent, and then with a biotin derivative, to give TiO_2 a biotin coating. Based on

this, other biotinylated biomolecules were attached to TiO$_2$ surfaces through the biological coupling of biotin and streptavidin/avidin to prepare bioactive TiO$_2$. Biotin, streptavidin/avidin and their conjugation have therefore been involved in the entire work described in this thesis. Therefore, it is necessary to give an introduction to these two chemicals.

Biotin, or *cis*-hexahydro-2-oxo-1H-thieno [3, 4] imidazole-4-pentanoic acid (Figure 1-4), is one of the water-soluble B vitamins, which can be found in the liver, kidney and pancreas.[81] Some of its physical and chemical properties are shown in Table 1-6. The absorbance of biotin at 280 nm is minimal, which allows biotinylated proteins to be monitored by UV absorbance without interference.[82]
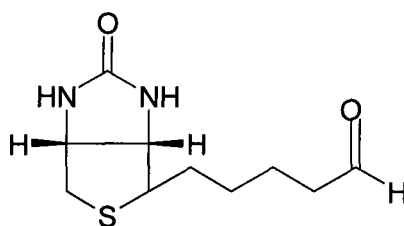
Figure 1-4   the structure of biotin

pH at iep		3.5
Melting point		232-233°C
Solubility at 25°C	In water	~0.22 mg/ mL
	In 95% alcohol	~0.8 mg/ mL
pH value of a 0.01% aqueous solution		4.5

Table 1-6   some properties of biotin [82]

Avidin, existing in chicken egg white and the tissues of birds, is a tetrameric glycoprotein with four identical subunits. Avidin is soluble in water and solutions are stable over wide pH and temperature ranges.[83] The absorbance of avidin at 282 nm is reported to be $\varepsilon^{1\%}_{282}=15.5$.[82] One avidin molecule can bind up to four biotin molecules or fragments with a very high binding constant ($K_a=10^{15}$ M^{-1}).[83] This interaction is very stable, and the products are able to withstand high temperatures (up to 132 °C), extreme changes in pH values (2-13), organic solvents and even some denaturing agents such as 8M guanidine-HCl.[82, 83]

Streptavidin, similar to avidin, is also a biotin-binding protein produced by *Streptomyces avidinii*.[84] Streptavidin also can bind up to four biotins with a similar binding constant.[83, 84] Although streptavidin and avidin share similar affinities with regard to binding to biotin, they are different in many other respects (Table 1-7 and Table 1-8).

	avidin	streptavidin
Protein	glycoprotein	not possess any carbohydrate
Molecular weight	69000 for tetramer[83]	60,000 for tetrameric
Isoelectric point (pI)[82]	~10	5-6
Size of the tetramer	5.5nm×5.5nm×4.1nm [83]	5.5nm × 4.5nm [85, 86]
Solubility in water	Very soluble	Less soluble

Table 1-7 Properties of avidin and streptavidin

Amino acid composite No. of residues/subunit [87, 88]			
avidin		streptavidin	
Ala	5	Ala	25
Arg	8	Arg	4
Asn	10	Asn	10
Asp	5	Asp	8
Cys	2	Cys	0
Gln	3	Gln	6
Glu	7	Glu	5
Gly	11	Gly	18
His	1	His	2
Ile	7.5	Ile	4
Leu	7	Leu	8
Lys	9	Lys	8
Met	2	Met	0
Phe	7	Phe	2
Pro	2	Pro	4
Ser	9	Ser	14
Thr	20.5	Thr	19
Trp	4	Trp	6
Tyr	1	Tyr	6
Val	7	Val	10

Table 1-8 Amino acid composite No. of residues/subunit of avidin and streptavidin

1.3 Carbohydrate-binding module family 2a

An important part of the work described in this thesis concerns the immobilization of TiO$_2$ nanoparticles on fibers through multi-linker bioconjugation, in which CBM2a (CBM = carbohydrate-binding module) was involved. CBM2a is not very well known to many chemists and chemical engineers, who may be among the readers of this thesis. For this reason, a general introduction to CBM2a is now provided. More details information on CBM2a is presented in Chapter 5.

Cellulases, the cellulose degrading enzymes, have three domains: a catalytic domain, a carbohydrate-binding module (CBM), and a highly O-glycosylated linker between the former two domains. CBMs have been found to be responsible for binding the enzyme to cellulose surfaces with a high affinity ($K_a = 10^6$ M^{-1}).[89, 90] CBMs are classified into more than 30 families, the first 14 of which are also known as cellulose binding domains (CBDs),[91] according to their amino acid sequence. CBM2a is the family 2a carbohydrate-binding module. Enzymes in this family have a β-barrel-type backbone that contains aromatic amino acids on a relatively flat surface. CBM2a can bind to crystalline cellulose, including bacterial microcrystalline cellulose (BMCC) and phosphoric acid-swollen cellulose (PASC). The binding is driven by sorbent and protein dehydration and is irreversible. Jervis and coworkers, using fluorescence recovery techniques, showed that CBM2a is mobile on the surface of crystalline cellulose and the interaction between CBM2a and cellulose is dynamic.

The high affinity between CBM and cellulose has been used in many applications. In the textile industry, the affinity of detergents to the textile substrate is greatly improved

by fusing some enzymes to CBMs. Fuglsang and Tsuchiya also found that CBM on its own, or fused with other enzymes, can remove dental plaque or prevent its formation. The use of CBMs, particularly when recombined with other biomolecules, can be used as an affinity tag for expression, recovery, and purification. This use is wide, probably because cellulose is a relatively cheap support matrix, especially for a large-scale protein purification process. Many other interesting applications with CBMs, including bioprocessing, targeting, cell immobilization, protein engineering, diagnostics, fiber modification, and in vivo cell wall modification, are summarized in Levy's review.[91]

1.4 Objectives of the Projects

The key aim of this work is to explore bioactive TiO_2 colloidal particles, including three main parts: their preparation, characterization and applications. The detailed objectives of each part are listed as following:

1.4.1. The preparation of bioactive TiO_2 colloidal particles:

The ultimate goal of this aspect of the research is to develop a platform for preparing photocatalytic TiO_2 colloidal particles conjugated to biomolecules of interest. Since most biomolecules can be biotinylated easily and the bioconjugation of biotin/streptavidin is very stable, biotinylation of TiO_2 is the key to attach various biomolecules to the surfaces of TiO_2 particles. For this reason, covalently attaching biotin to TiO_2 is the main objective.

1.4.2. The characterization of surface modified TiO_2

The objectives of this part of work consist of a series of characterizations of modified TiO_2 including aminosilanized TiO_2, biotinylated TiO_2, streptavidin conjugated TiO_2, and protein conjugated TiO_2, and studying the influences of UV irradiation on modified TiO_2. This work is important as it gives insight into understanding both the correlation between the preparations and the applications of bioactive TiO_2 and the unique, combined properties of TiO_2 colloidal particles with respect to bioactive and photocatalytic aspects.

1.4.3. The applications of bioactive TiO$_2$

There are two main aims associated with this part: to apply *E. col*i antibody coated photoactive TiO$_2$ in a bacteria-containing environment to obtain selective binding and killing of specific bacteria; and to immobilize photocatalytic TiO$_2$ on cellulose fibers via bioconjugation to achieve a uniform distribution of TiO$_2$ particles on paper.

1.5 Thesis outline

This thesis consists of 6 chapters. All of the achievements in this work are reported in this thesis according to the following outline:

Chapter 1 gives a brief introduction to the background required for this thesis, concerning TiO$_2$ and its properties, bacteria (particularly the key bacteria – *E. coli* and *P. putida*), and the main biomolecules involved in this thesis such as biotin, streptavidin and carbohydrate-binding modules. Some related research is reviewed. The objectives and thesis outline are also given.

Chapter 2 describes the details of preparing aminosilanized and biotinylated TiO$_2$ colloidal particles. The characterization is shown and the methods of controlling the density of amino groups are discussed. The conjugation of biotinylated TiO$_2$ colloidal particles with streptavidin is also studied.   In addition, the synthesis of biotinyltriethoxysilane, the compound grafted on TiO$_2$ surfaces for biotinylation, is also

described in detail. This work has led to one publication in *Langmuir*[92] and two U.S. patents application.[93, 94]

Chapter 3 illustrates the effect of UV irradiation on aminosilanized TiO_2 colloidal particles. The charge conversion and the removal of organosilane coating from TiO_2 surfaces are described. The photo-trigged flocculation system is also exploited. This work has led to one publication in *Langmuir*.

Chapter 4 describes the preparation and characterization of *E. coli* antibody conjugated TiO_2. This chapter also demonstrates selective binding (flocculation) and killing of *E. coli* using *E. coli* antibody conjugated TiO_2 colloidal particles in a complex medium containing control bacteria. This work is pending submission to *Biomacromolecules*.

Chapter 5 exploits the application of non-aggregated immobilization of photocatalytic TiO_2 nanoparticles on cellulose fibers via bioconjugation. The photoactivity of the resulting paper is demonstrated. The impact of UV irradiation on bioconjugation is also studied and discussed. This work has led to a publication in the *Journal of Materials Chemistry*. This publication is in press.

Chapter 6 summarizes the main conclusions and contributions that reported in this thesis.

Reference:

1. Moselhy, J.; Wu, X. Y.; Nicholov, R.; Kodaria, K., Interaction of poly(NIPAm/MAA) nanoparticles with human blood cells and proteins. *Proceedings of the International Symposium on Controlled Release of Bioactive Materials* **2000,** 27th, 1110-1111.

2. Moselhy, J.; Wu, X. Y.; Nicholov, R.; Kodaria, K., In vitro studies of the interaction of poly(NIPAm/MAA) nanoparticles with proteins and cells. *Journal of biomaterials science. Polymer edition* **2000,** 11, (2), 123-47.

3. Diebold, U., The surface science of titanium dioxide. *Surface Science Reports* **2003,** 48, (5-8), 53-229.

4. Braun, J. H., Titanium dioxide-a review. *Journal of Coatings Technology* **1997,** 69, (868), 59-72.

5. Fox, M. A.; Dulay, M. T., Heterogeneous photocatalysis. *Chemical Reviews (Washington, DC, United States)* **1993,** 93, (1), 341-57.

6. Hashimoto, K.; Irie, H.; Fujishima, A., TiO$_2$ photocatalysis: A historical overview and future prospects. *Japanese Journal of Applied Physics, Part 1: Regular Papers, Brief Communications & Review Papers* **2005,** 44, (12), 8269-8285.

7. Gao, L.; Zhang, Q., Effects of amorphous contents and particle size on the photocatalytic properties of TiO$_2$ nanoparticles. *Scripta Materialia* **2001,** 44, (8/9), 1195-1198.

8. Wold, A., Photocatalytic properties of titanium dioxide (TiO$_2$). *Chemistry of Materials* **1993,** 5, (3), 280-3.

9. Maruska, H. P.; Ghosh, A. K., Photocatalytic decomposition of water at semiconductor electrodes. *Solar Energy* **1978,** 20, (6), 443-58.

10. Di Paola, A.; Addamo, M.; Bellardita, M.; Cazzanelli, E.; Palmisano, L., Preparation of photocatalytic brookite thin films. *Thin Solid Films* **2007,** 515, (7-8), 3527-3529.

11. Isley, S. L.; Penn, R. L., Relative Brookite and Anatase Content in Sol-Gel-Synthesized Titanium Dioxide Nanoparticles. *Journal of Physical Chemistry B* **2006,** 110, (31), 15134-15139.

12. Gong, X.-Q.; Selloni, A., First-principles study of the structures and energetics of stoichiometric brookite TiO$_2$ surfaces. *Physical Review B: Condensed Matter and Materials Physics* **2007,** 76, (23), 235307/1-235307/11.

13. Aguedach, A.; Brosillon, S.; Morvan, J.; Lhadi, E. K., Photocatalytic degradation of azo-dyes Reactive Black 5 and Reactive Yellow 145 in water over a newly deposited titanium dioxide. *Applied Catalysis, B: Environmental* **2005,** 57, (1), 55-62.

14. Snoswell, D. R. E.; Duan, J.; Fornasiero, D.; Ralston, J., Colloid stability of synthetic titania and the influence of surface roughness. *Journal of Colloid and Interface Science* **2005,** 286, (2), 526-535.

15. Hoffmann, M. R.; Martin, S. T.; Choi, W.; Bahnemann, D. W., Environmental Applications of Semiconductor Photocatalysis. *Chemical Reviews (Washington, D. C.)* **1995,** 95, (1), 69-96.

16. Pelton, R.; Geng, X.; Brook, M., Photocatalytic paper from colloidal TiO$_2$-fact or fantasy. *Advances in Colloid and Interface Science* **2006,** 127, (1), 43-53.

17. Sato, S., Effects of surface modification with silicon oxides on the photochemical properties of powdered titania. *Langmuir* **1988,** 4, (5), 1156-9.

18. Wiese, G. R.; Healy, T. W., Coagulation and electrokinetic behavior of titanium dioxide and aluminum oxide colloidal dispersions. *Journal of Colloid and Interface Science* **1975,** 51, (3), 427-33.

19. Yotsumoto, H.; Yoon, R. H., Application of extended DLVO Theory. I. Stability of rutile suspensions. *Journal of Colloid and Interface Science* **1993,** 157, (2), 426-33.

20. Cornell, R. M.; Posner, A. M.; Quirk, J. P., Titrimetric and electrophoretic investigation of the p.z.c [point of zero charge] and the iep [isoelectric point] of pigment rutile. *Journal of Colloid and Interface Science* **1975,** 53, (1), 6-13.

21. Furlong, D. N.; Parfitt, G. D., Electrokinetics of titanium dioxide. *Journal of Colloid and Interface Science* **1978,** 65, (3), 548-54.

22. Fazio, S.; Guzman, J.; Colomer, M. T.; Salomoni, A.; Moreno, R., Colloidal stability of nanosized titania aqueous suspensions. *Journal of the European Ceramic Society* **2008,** 28, (11), 2171-2176.

23. Mueller, R.; Kammler, H. K.; Wegner, K.; Pratsinis, S. E., OH Surface Density of SiO$_2$ and TiO$_2$ by Thermogravimetric Analysis. *Langmuir* **2003,** 19, (1), 160-165.

24. Seekkuarachchi, I. N.; Tanaka, K.; Kumazawa, H., Dispersion mechanism of nano-particulate aggregates using a high pressure wet-type jet mill. *Chemical Engineering Science* **2008,** 63, (9), 2341-2366.

25. Yaremko, Z. M.; Tkachenko, N. H.; Bellmann, C.; Pich, A., Redispergation of TiO_2 particles in aqueous solutions. *Journal of Colloid and Interface Science* **2006**, 296, (2), 565-571.

26. Bourikas, K.; Stylidi, M.; Kondarides, D. I.; Verykios, X. E., Adsorption of Acid Orange 7 on the Surface of Titanium Dioxide. *Langmuir* **2005**, 21, (20), 9222-9230.

27. Linsebigler, A. L.; Lu, G.; Yates, J. T., Jr., Photocatalysis on TiO_2 Surfaces: Principles, Mechanisms, and Selected Results. *Chemical Reviews (Washington, D. C.)* **1995**, 95, (3), 735-58.

28. Rajeshwar, K., Photoelectrochemistry and the environment. *Journal of Applied Electrochemistry* **1995**, 25, (12), 1067-82.

29. Hagfeldt, A.; Graetzel, M., Light-Induced Redox Reactions in Nanocrystalline Systems. *Chemical Reviews (Washington, D. C.)* **1995**, 95, (1), 49-68.

30. Kavan, L.; Graetzel, M.; Gilbert, S. E.; Klemenz, C.; Scheel, H. J., Electrochemical and photoelectrochemical investigation of single-crystal anatase. *Journal of the American Chemical Society* **1996**, 118, (28), 6716-6723.

31. Fujishima, A.; Honda, K., Electrochemical photolysis of water at a semiconductor electrode. *Nature (London, United Kingdom)* **1972**, 238, (5358), 37-8.

32. Blake, D. M.; Maness, P.-C.; Huang, Z.; Wolfrum, E. J.; Huang, J.; Jacoby, W. A., Application of the photocatalytic chemistry of titanium dioxide to disinfection and the killing of cancer cells. *Separation and Purification Methods* **1999**, 28, (1), 1-50.

33. Nosaka, Y.; Kishimoto, M.; Nishino, J., Factors Governing the Initial Process of TiO_2 Photocatalysis Studied by Means of in-Situ Electron Spin Resonance Measurements. *Journal of Physical Chemistry B* **1998**, 102, (50), 10279-10283.

34. Hirakawa, T.; Nosaka, Y., Properties of O_2^- and OH formed in TiO_2 aqueous suspensions by photocatalytic reaction and the influence of H_2O_2 and some ions. *Langmuir* **2002**, 18, (8), 3247-3254.

35. Schwarz, P. F.; Turro, N. J.; Bossmann, S. H.; Braun, A. M.; Abdel Wahab, A.-M. A.; Duerr, H., A New Method To Determine the Generation of Hydroxyl Radicals in Illuminated TiO_2 Suspensions. *Journal of Physical Chemistry B* **1997**, 101, (36), 7127-7134.

36. Grela, M. A.; Coronel, M. E. J.; Colussi, A. J., Quantitative Spin-Trapping Studies of Weakly Illuminated Titanium Dioxide Sols. Implications for the Mechanism of Photocatalysis. *Journal of Physical Chemistry* **1996**, 100, (42), 16940-16946.

37. Sun, L.; Bolton, J. R., Determination of the Quantum Yield for the Photochemical Generation of Hydroxyl Radicals in TiO$_2$ Suspensions. *Journal of Physical Chemistry* **1996,** 100, (10), 4127-34.

38. Bickley, R. I.; Gonzalez-Carreno, T.; Lees, J. S.; Palmisano, L.; Tilley, R. J. D., A structural investigation of titanium dioxide photocatalysts. *Journal of Solid State Chemistry* **1991,** 92, (1), 178-90.

39. Harada, H.; Ueda, T., Photocatalytic activity of ultrafine rutile in methanol-water solution and dependence of activity on particle size. *Chemical Physics Letters* **1984,** 106, (3), 229-31.

40. Kawahara, K.; Ohko, Y.; Tatsuma, T.; Fujishima, A., Surface diffusion behavior of photogenerated active species or holes on TiO$_2$ photocatalysts. *Physical Chemistry Chemical Physics* **2003,** 5, (21), 4764-4766.

41. Tatsuma, T.; Tachibana, S.-i.; Fujishima, A., Remote Oxidation of Organic Compounds by UV-Irradiated TiO$_2$ via the Gas Phase. *Journal of Physical Chemistry B* **2001,** 105, (29), 6987-6992.

42. Kikuchi, Y.; Sunada, K.; Iyoda, T.; Hashimoto, K.; Fujishima, A., Photocatalytic bactericidal effect of TiO$_2$ thin films: dynamic view of the active oxygen species responsible for the effect. *Journal of Photochemistry and Photobiology, A: Chemistry* **1997,** 106, (1-3), 51-56.

43. Turchi, C. S.; Ollis, D. F., Photocatalytic degradation of organic water contaminants: mechanisms involving hydroxyl radical attack. *Journal of Catalysis* **1990,** 122, (1), 178-92.

44. Brown, R. C.; Wake, D., Air filtration by interception - theory and experiment. *Journal of Aerosol Science* **1991,** 22, (2), 181-6.

45. Farr, S. B.; Kogoma, T., Oxidative stress responses in Escherichia coli and Salmonella typhimurium. *Microbiological reviews* **1991,** 55, (4), 561-85.

46. Watts, R. J.; Kong, S.; Orr, M. P.; Miller, G. C.; Henry, B. E., Photocatalytic inactivation of coliform bacteria and viruses in secondary wastewater effluent. *Water Research* **1995,** 29, (1), 95-100.

47. Bekbolet, M.; Araz, C. V., Inactivation of Escherichia coli by photocatalytic oxidation. *Chemosphere* **1996,** 32, (5), 959-65.

48. Bekbolet, M., Photocatalytic bactericidal activity of TiO$_2$ in aqueous suspensions of E. coli. *Water Science and Technology* **1997,** 35, (11-12, Health-Related Water Microbiology 1996), 95-100.

49. Horie, Y.; David, D. A.; Taya, M.; Tone, S., Effects of light intensity and titanium dioxide concentration on photocatalytic sterilization rates of microbial cells. *Industrial & Engineering Chemistry Research* **1996,** 35, (11), 3920-3926.

50. Matsunaga, T.; Okochi, M., TiO2-Mediated Photochemical Disinfection of Escherichia coli Using Optical Fibers. *Environmental Science and Technology* **1995,** 29, (2), 501-5.

51. Stevenson, M.; Bullock, K.; Lin, W. Y.; Rajeshwar, K., Sonolytic enhancement of the bactericidal activity of irradiated titanium dioxide suspensions in water. *Research on Chemical Intermediates* **1997,** 23, (4), 311-323.

52. Matsunaga, T.; Tomoda, R.; Nakajima, T.; Wake, H., Photoelectrochemical sterilization of microbial cells by semiconductor powders. *FEMS Microbiology Letters* **1985,** 29, (1-2), 211-14.

53. Dandliker, P. J.; Holmlin, R. E.; Barton, J. K., Oxidative thymine dimer repair in the DNA helix. *Science (Washington, D. C.)* **1997,** 275, (5305), 1465-1468.

54. Deisseroth, A.; Dounce, A. L., Catalase: physical and chemical properties, mechanism of catalysis, and physiological role. *Physiological Reviews* **1970,** 50, (3), 319-75.

55. Fridovich, I., Biological effects of the superoxide radical. *Archives of Biochemistry and Biophysics* **1986,** 247, (1), 1-11.

56. http://www.sirinet.net/~jgjohnso/monerans.html

57. http://www.science-art.com/image.asp?id=249&m=52

58. Kubitschek, H. E., Cell volume increase in Escherichia coli after shifts to richer media. *Journal of bacteriology* **1990,** 172, (1), 94-101.

59. Bentley, R.; Meganathan, R., Biosynthesis of vitamin K (menaquinone) in bacteria. *Microbiological reviews* **1982,** 46, (3), 241-80.

60. Hudault, S.; Guignot, J.; Servin, A. L., Escherichia coli strains colonising the gastrointestinal tract protect germfree mice against Salmonella typhimurium infection. *Gut* **2001,** 49, (1), 47-55.

61. Reid, G.; Howard, J.; Gan, B. S., Can bacterial interference prevent infection? *Trends in Microbiology* **2001,** 9, (9), 424-428.

62. Hayashi, T.; Ooka, T.; Ogura, Y.; Asadulghani, Genomic view on the evolution of enterohemorrhagic Escherichia coli. *Evolutionary Biology of Bacterial and Fungal Pathogens* **2008,** 407-419.

63. Lee, S. Y., High cell-density culture of Escherichia coli. *Trends in Biotechnology* **1996,** 14, (3), 98-105.

64. Russo, E., Special Report: The birth of biotechnology. *Nature (London, United Kingdom)* **2003,** 421, (6921), 456-457.

65. Selleck, W.; Tan, S., Recombinant protein complex expression in E. coli. *Current protocols in protein science / editorial board, John E. Coligan ... [et al.]* **2008,** Chapter 5, Unit 5 21.

66. Marques, S.; Ramos, J. L., Transcriptional control of the Pseudomonas putida TOL plasmid catabolic pathways. *Molecular Microbiology* **1993,** 9, (5), 923-9.

67. Ward, P. G.; Goff, M.; Donner, M.; Kaminsky, W.; O'Connor, K. E., A Two Step Chemo-biotechnological Conversion of Polystyrene to a Biodegradable Thermoplastic. *Environmental Science & Technology* **2006,** 40, (7), 2433-2437.

68. Cazorla, F. M.; Duckett, S. B.; Bergstroem, E. T.; Noreen, S.; Odijk, R.; Lugtenberg, B. J. J.; Thomas-Oates, J. E.; Bloemberg, G. V., Biocontrol of avocado dematophora root rot by antagonistic Pseudomonas fluorescens PCL1606 correlates with the production of 2-hexyl 5-propyl resorcinol. *Molecular Plant-Microbe Interactions* **2006,** 19, (4), 418-428.

69. Ghuysen, J. M.; Strominger, J. L.; Tipper, D. J., Bacterial cell walls. *Comprehensive Biochemistry* **1968,** 26A, 53-104.

70. Reaveley, D. A.; Burge, R. E., Walls and membranes in bacteria. *Advances in Microbial Physiology* **1972,** 7, 1-81.

71. Rogers, H. J.; Ward, J. B.; Burdett, I. D. J., Structure and growth of the walls of Gram-positive bacteria. *Symposium of the Society for General Microbiology* **1978,** 28, (Relat. Struct. Funct. Prokaryotic Cell), 139-76.

72. Shockman, G. D.; Barrett, J. F., Structure, function, and assembly of cell walls of gram-positive bacteria. *Annual Review of Microbiology* **1983,** 37, 501-27.

73. Osborn, M. J.; Rick, P. D.; Lehmann, V.; Rupprecht, E.; Singh, M., Structure and biogenesis of the cell envelope of gram-negative bacteria. *Annals of the New York Academy of Sciences* **1974,** 235, 52-65.

74. Bayer, M. E., Structural and functional evidence of cooperativity between membranes and cell wall in bacteria. *International Review of Cytology, Supplement* **1981,** 12, (Membr. Res.: Classic Origins Curr. Concepts), 39-70.

75. Mizushima, S., Structure and function of outer membrane of Escherichia coli: a reconstitution study. **1982,** 113-30.

76. Gottschalk, G., *Biosynthesis of Escherichia coli cells from glucose, Bacterial Metabolism. 2nd Ed.* Springer: New York, 1986; p 359 pp.

77. Saito, T.; Iwase, T.; Horie, J.; Morioka, T., Mode of photocatalytic bactericidal action of powdered semiconductor titanium dioxide on mutans streptococci. *Journal of Photochemistry and Photobiology, B: Biology* **1992,** 14, (4), 369-79.

78. Sunada, K.; Kikuchi, Y.; Hashimoto, K.; Fujishima, A., Bactericidal and Detoxification Effects of TiO_2 Thin Film Photocatalysts. *Environmental Science and Technology* **1998,** 32, (5), 726-728.

79. Dunford, R.; Salinaro, A.; Cai, L.; Serpone, N.; Horikoshi, S.; Hidaka, H.; Knowland, J., Chemical oxidation and DNA damage catalyzed by inorganic sunscreen ingredients. *FEBS Letters* **1997,** 418, (1,2), 87-90.

80. Hidaka, H.; Horikoshi, S.; Serpone, N.; Knowland, J., In vitro photochemical damage to DNA, RNA and their bases by an inorganic sunscreen agent on exposure to UVA and UVB radiation. *Journal of Photochemistry and Photobiology, A: Chemistry* **1997,** 111, (1-3), 205-214.

81. Zempleni, J.; Mock, D. M., Biotin biochemistry and human requirements. *Journal of Nutritional Biochemistry* **1999,** 10, (3), 128-138.

82. Savage, M. D.; Mattson, G.; Desai, S.; Nielander, G. W.; Morgensen, S.; Conklin, E. J., *avidin-biotin chemistry: a hanhbook.* Pierce Chemical Co.: Rockford, 1992.

83. Green, N. M., Avidin. *Advances in Protein Chemistry* **1975,** 29, 85-133.

84. Chaier, L.; Wolf, F. J., The properties of streptavidin, a biotin-binding protein produced by streptomycetes. *Archives of Biochemistry and Biophysics* **1964,** 106, (1), 1-5.

85. Hendrickson, W. A.; Paehler, A.; Smith, J. L.; Satow, Y.; Merritt, E. A.; Phizackerley, R. P., Crystal structure of core streptavidin determined from multiwavelength anomalous diffraction of synchrotron radiation. *Proceedings of the National Academy of Sciences of the United States of America* **1989,** 86, (7), 2190-4.

86. Weber, P. C.; Cox, M. J.; Salemme, F. R.; Ohlendorf, D. H., Crystallographic data for Streptomyces avidinii streptavidin. *Journal of Biological Chemistry* **1987,** 262, (26), 12728-9.

87. Dayhoff, M. O.; Editor, *Atlas of Protein Sequence and Structure, 1972, Vol. 5.* 1972; p 544 pp.

88. Argarana, C. E.; Kuntz, I. D.; Birken, S.; Axel, R.; Cantor, C. R., Molecular cloning and nucleotide sequence of the streptavidin gene. *Nucleic Acids Research* **1986,** 14, (4), 1871-82.

89. McLean, B. W.; Bray, M. R.; Boraston, A. B.; Gilkes, N. R.; Haynes, C. A.; Kilburn, D. G., Analysis of binding of the family 2α carbohydrate-binding module from Cellulomonas fimi xylanase 10A to cellulose: specificity and identification of functionally important amino acid residues. *Protein Engineering* **2000**, 13, (11), 801-809.

90. Pinto, R.; Moreira, S.; Mota, M.; Gama, M., Studies on the Cellulose-Binding Domains Adsorption to Cellulose. *Langmuir* **2004**, 20, (4), 1409-1413.

91. Levy, I.; Shoseyov, O., Cellulose-binding domains. Biotechnological applications. *Biotechnology Advances* **2002**, 20, (3-4), 191-213.

92. Ye, L.; Pelton, R.; Brook, M. A., Biotinylation of TiO_2 nanoparticles and their conjugation with streptavidin. *Langmuir* **2007**, 23, (10), 5630-5637.

93. Brook, M. A.; Brennan, J. D.; Pelton, R.; Voss, R.; Ye, L. Biomolecule compatible silica particles and use for the detection of bacterial pathogens. 2007-CA2106 2008061363, 20071126., 2008.

94. Brook, M. A.; Pelton, R.; Ye, L. Surface modified particles. US Patent (B&P File No. 3244-157), abandoned.

Chapter 2   Biotinylation of TiO₂ Nanoparticles and Their Conjugation with Streptavidin*

2.1   Introduction

The properties of TiO_2, including high refractive index,[1] light absorption/scattering,[2] and photocatalytic activity [3-10] have led to the exploitation of TiO_2 in a variety of fields. Titania has been also widely used in biological applications such as orthopedic [11,12] and dental applications[13] due to its excellent biocompatibility.[14,15] The immobilization of bio-molecules onto TiO_2 substrates has been utilized in bio-recognition templates,[16] bio-separation supports,[17,18] immuno-[19,20] and other biosensors,[21,22] and bio-chips.[23] Thus, there is precedent for linking TiO_2 to specific biological substrates.

Two approaches are typically used to immobilize bio-molecules on oxide surfaces: physisorption,[17-23] and covalent binding.[16,24,25] In most of these applications, biotin-avidin (or streptavidin) complexation is used to bind bio-molecules to TiO_2

---

* This work led to one published paper and two U.S. patents application. One paper concerning this part of work has been published in Langmuir 2007, 23 (10), 5630-5637. Authors include Lu Ye, Robert Pelton and Michael Brook. A US Patent (B&P File No. 3244-166), Biomolecule compatible silica particles, authored by Michael Brook, John Brennan, Robert Pelton, Rebecca Voss, and Lu Ye, has been submitted and is under review. In this patent, the work related to the conjugating biotin to particles was derived from this work described in this thesis. Another US Patent (B&P File No. 3244-157), "Surface modified particles", authored by Michael Brook, Robert Pelton, and Lu Ye, that resulted from this work was filed. However, this patent has been abandoned.

substrates[16,19,20,22] due to the very high affinity ($K_a=10^{15}$ M^{-1})[26,27] between the protein and

the ligand. The physisorptive immobilization of biomolecules onto TiO_2 surfaces has

disadvantages, however, including: 1) lack of the control in the quantity and location of

the immobilized bio-molecules; 2) decreased activity of the immobilized biomolecule; 3)

non-specific adsorption at unmodified sites; and, 4) subtleties in the efficiency of the

adsorption process, which strongly depend on local environmental conditions such as pH

values, temperature, solvent, roughness of the surface of adsorption and hydrophobicity

of the surface of adsorption, making reproducibility difficult.[28,29]

Although covalent binding appears to overcome the above drawbacks, only a few

reports have described the immobilization of biomolecules on TiO_2. Huang[16] showed that

biotin can be directly bound to a TiO_2 surface by coupling the biotin COOH to the titanol

groups in phosphate-buffered saline. The results showed that the surface of the thin

titania coating was fully covered by a biotin monolayer. The group of Dimitrijevic[24] and

Rajh[25] have modified TiO_2 with enediol ligands, typically dopamine, to give terminal

amines, that can react N-hydroxy-succinimide modified biotin. In these cases, dopamine

acts as a ligand to the free surface sites of TiO_2 and to form chemical bonds between the

ligand and TiO_2. We reasoned that improved control in the creation of TiO_2 / biological

composites could be provided by the use of silane coupling agents as linkers.

Silane coupling agents are widely used to modify the surface of mineral oxides

including silica, alumina, titania and others.[30,31] A variety of organic functional groups

can be introduced to the surface using mild conditions. Thus, the traditional silane

coupling agent provides a route to bind biotin molecules to TiO_2 surfaces. Typically, the

inorganic surface is first modified with a silane coupling agent to introduce appropriate functional groups, and then a biotin reagents is tethered to the functional surface.[32,33,34] Finally, the biotin-modified inorganic material is exposed to streptavidin/avidin. Although reports of this type of modification have been reported on silica,[33,34] silicon,[32] gold[35,36] and zeolites[37], we are unaware of reports of analogously prepared biotin-TiO_2. Somewhat surprisingly, with the exception of Dimitrijevic's report, which shows a possibility to control the binding sites of biotin on TiO_2 rod-like nanocrystallates, the covalent binding of biotin to TiO_2 has been limited to TiO_2 films/substrates.

It can be challenging to control the molecular densities of silane agents applied to titania surfaces. The choice of silane coupling agent, humidity, temperature and reaction time all affect the in subtle ways the efficacy of the surface modification.[38,39] Water, in particular, affects the density of surface modification by silane coupling agents on TiO_2 substrates.[40-43] An additional parameter to consider with TiO_2 materials is the crystal habit; TiO_2 can be readily prepared in amorphous form, and as single or mixed crystalline phases (anatase, rutile and Brookite).

Our interest lies in the preparation of biologically modified TiO_2 particles that have photoactivity.[44] Although well defined amorphous titania particles are available from sol-gel processes, the subsequent thermolyses required to convert the TiO_2 into photoactive anatase or rutile play havoc with the colloidal stability of the particles. As a result, the answers to some fundamental problems, such as how many biotin molecules will bind to TiO_2 surfaces under various conditions, the fraction of biotin that remains active to binding, the change in the colloidal stability of biotinylated TiO_2 particles in the presence

of protein, and the role of streptavidin in the flocculation of the biotinylated TiO_2 particles are still unknown.

In this paper, we describe a synthetic route that permits biotin molecules to be covalently bound to an anatase nanoparticle surface using a two-step modification process. The influence of silanization reaction time on the amount of amino groups that become bound to anatase nanoparticles is first described. The efficiency of binding biotin to these attached amino groups is investigated quantitatively, as is the ability to capture streptavidin on these particles surfaces. The changes in colloidal stability of modified TiO_2 particles after the biotinylation, and in the presence of streptavidin, are also described.

2.2   Results and Discussion

2.2.1.   Preparation and Characterization of Biotin modified TiO_2 particles

Commercially available, polydisperse anatase particles were modified with by simple treatment of the particles with a DMSO solution of $H_2N(CH_2)_3Si(OEt)_3$ (Scheme 2-1). Subsequent heating at 120 °C completes the curing process (MOH + EtOSi → MOSi, M = Ti, Si) leading to a silsesquioxane multilayer on the titania surface.[31]   After aminosilanization, the ^{29}Si CPMAS NMR NMR spectrum showed that the T^2: T^3 ratio (T^2 -60.13, T^3 -68.32 ppm, Figure 2-4) was about 1 : 6, which suggests that the efficiency of forming Si-O-Si (and Ti-O-Si) linkages, in a highly condensed coating layer, is high (the ^{13}C and ^{29}Si NMR of the bare particles showed no organic or siliceous materials, see Supplementary Information).   During the initial stages of the surface modification, a

multilayer of silane molecules will form on the TiO$_2$ surface.[40, 43, 45, 46] Although both Ti-O-Si and Si-O-Si bonds will be formed under these conditions, it is difficult to differentiate the two spectroscopically, since the chemical shift in the ^{29}Si NMR of the former is very close to the latter.[47,48]

Biotinylation was performed by dispersing the aminosilanized TiO$_2$ particles in DMSO and capping the amine groups with NHS-ester activated biotin, which is commercially available, and leads to the linkage of the biotin to the surface via amide groups (Scheme 2-2). The chemical shifts of the carbons located at j and a, respectively, clearly show that biotin was attached to the TiO$_2$ surface (Figure 2-4).

The IR spectrum of untreated TiO$_2$ shows a very smooth curve, confirming that no dispersants were present in the TiO$_2$ product, in accordance with the MSDS for the sample. The aminosilanized TiO$_2$ spectrum exhibits a peak at 953 cm^{-1} ascribed to Ti-O-Si,[49,50] along with signals that correspond to the organic fragments of APTS. FT-IR of the biotinylated TiO$_2$ particles demonstrated (new amide peaks at 1702 cm^{-1} (amide I)), and 1547 cm^{-1} ((amide II), Figure 2-1) the grafting of biotin to the surface amino groups had occurred. A comparison of these four IR spectra (Figure 2-1) shows that after the silanization, the APTES moiety was bound to the TiO$_2$ surface and after biotinylation, biotin molecules were linked chemically to the TiO$_2$ surface via amide groups. It should be noted that not all of the surface amino groups were able to react with NHS-biotin (see below).

Silane coupling agents rarely form monolayers on oxide surfaces, particularly those derived from activated silanes such as APTS; monolayers are only observed under

exceptional conditions, including very high vacuum.[31] TEM was used to examine the the thickness of the silane coating multilayer created in the aminosilanization step. As the reaction time increases from 4 - 26 hours, the initially clean TiO_2 surface (Figure 2-2 a) begins to be visibly modified with a surface layer that grows to ~12 nm thickness after 26 hours of aminosilanization. Little further change was observed when these surfaces were biotinylated (Figure 2-2 e, f).

The surface charge of the particles, which will affect their colloidal stability, was established using electrophoretic mobility measurements as a function of the ionic strength and the pH values of the solution. The electrophoretic mobilities of the untreated TiO_2 particles at different pH values in KNO_3 (10^{-3} M) solutions are shown in Figure 2-3. These results are comparable with the mobilities of some commercial TiO_2 samples measured by Gilmar [51] and Furlong [52], and show the presence of surface titanol groups.

After aminosilanization with 26 hours, by contrast, the electrophoretic mobilities of the modified TiO_2 particles were highly positive over a broad pH range due to the ammonium groups attached to the particle surfaces. The biotinylated TiO_2 sample, which was obtained from this aminosilanized TiO_2, still showed positive electrophoretic mobility over a broad pH range, but to a lower degree than the amino-modified material. This indicates that not all of the amino groups were able to react with NHS-biotin.

The variation in the size and size distribution of TiO_2 particles were studied by light diffraction after silylation (over 26 hours) and subsequent biotinylation. The data shows that about 80% of the unmodified TiO_2 particles are in the size range 510-1780 nm (Figure 2-5). However, TEM results indicated that the size of most TiO_2 particles present

in our samples were 50-150 nm in diameter (see Figure 2-2). This inconsistency in sizes from the two measurements indicates that even untreated TiO_2 nanoparticles underwent aggregation in water in spite of their negative surface charge, as has recently been described by Yaremko.[53] In his report, the TiO_2 particles of highest colloidal stability (100-300 nm) were shown to be aggregates consisting of 2-4 particles. In Figure 2-5, it can be seen that the average particle aggregate size of untreated TiO_2 was 890 nm, while that of aminosilanized TiO_2 was 1020 nm. Thus, the particle aggregate size increases as a consequence of silylation. This also confirmed the TEM results described above, which indicated that the thickness of the coating layer can reach ~12 nm. The ability to aggregate the particles is independent of the thickness of the APTS layer: a small fraction of the TiO_2 particles associate to give 4-10 μm aggregates irrespective of the chemistry of the surface layer.

The specific surface area (SSA) of untreated TiO_2 particles, aminosilanized TiO_2 particles and biotinylated TiO_2 particles were measured using nitrogen absorption. The results are shown in Table 2-1. It can be seen that the specific surface area of TiO_2 after aminosilanization decreased significantly, while after biotinylation the value decreased only slightly. The SSA value decreased from 14.1 m^2 g^{-1} to 9.1 m^2 g^{-1} with an increase in the reaction time of the aminosilanization process. The large drop in the SSA of TiO_2 after aminosilanization may be associated with: 1) a silane coating layer that blocks the pores of untreated TiO_2 particles;[54] and/or 2) aggregation of TiO_2 particles by the thick silane coating layer.[55]

2.2.2.   Accessability of Amino Groups on TiO$_2$ particles to Biotin and then to Streptavidin

Based on the nature of two-step modification process, the amount of biotin grafted to the TiO$_2$ surface will be limited by the concentration of available surface amino groups. The quantitative measurement of accessible amino-groups on the TiO$_2$ surface is significant both for understanding the TiO$_2$ surface chemistry and designing the subsequent modification protocols or applications. X-ray Photoelectron Spectroscopy (XPS) was utilized to characterize nitrogen and titanium atomic percentages on untreated TiO$_2$ and aminosilanized TiO$_2$ after reaction times of 4 hours, 16 hours, and 26 hours, respectively, and on a biotinylated surface (starting from the 4 h aminosilanized surface). The samples, as is frequently done for powders, were allowed to adhere to an adhesive film, the excess powder was removed, and the XPS was measured on the exposed particle surface layer. Table 2-1 shows the clean surface of the untreated TiO$_2$, which agrees with the FT-IR spectrum (Figure 2-1). The nitrogen concentration increased from 0.1% up to 10% while the atom% titanium decreased from 15% down to 0.4% with the aminosilanization time. These results were in good agreement with the TEM results. It also suggested that more and more APTS grafted to TiO$_2$ surface as the reaction time was extended. Biotinylation provides a layer that further obscures the underlying titania, and contributes a more nitrogen rich environment.

The total number of amino groups grafted onto the TiO$_2$ surface was measured by conductiometric titration (see Supplementary Material). In combination with the SSA values, the amino group densities can be calculated to be 2.9 nm^{-2}, 26 nm^{-2}, 66 nm^{-2} for

aminosilanized TiO_2 samples obtained after 4 hours, 16 hours and 26 hours reaction time, respectively. The surface amino-group density on the TiO_2 surface was measured using polyelectrolyte titration. In combination with the SSA values, it also can be calculated that the densities of the surface amino-groups were 2.7 nm^{-2}, 10 nm^{-2}, and 17 nm^{-2} for the sample obtained after 4 hours, 16 hours and 26 hours reaction time, respectively. These values are very large if compared with Gamble's reports,[40,41,42] in which the silanized TiO_2 was shown, using surface spectroscopic techniques, to have a monolayer of silane coverage of 1.1 nm^{-2}. However, our conductometric titration results are equivalent in comparison with the result obtained by Kim et al.[56] Kim and his colleagues grafted hyperbranched polymers containing amino groups on an aminosilanized oxide substrate. The surface density of the primary amine functional groups reported in Kim's paper ranged from 3.5 nm^{-2} to 66 nm^{-2}. As shown below, some of the APTS-derived amino groups are unable to bind with biotin. In the highly crosslinked, polycationic silsesquioxane surface layer, it may not be possible to readily titrate all the embedded amino-groups with polyanionic molecules (in this case, potassium polyvinylsulfate), nor to react them with NHS-biotin. However, the conductometric titration can react with all entire amino-groups grafted onto the TiO_2 surface.

2.2.3.   Quantitative Determination of active biotin on TiO_2 particles

The quantity of active biotin on TiO_2 surfaces was measured by Green's method.[57] The density of active biotin on TiO_2 surface can be calculated from the combination of the titration results and the SSA values. Biotin-NHS molecules were reacted to form

covalent bonds with the protruding amino-groups on aminosilane-modified TiO_2 particles modified for 4 hours, 16 hours and 26 hours reaction time to give surface biotin densities of 2.1 nm^{-2}, 7 nm^{-2}, and 11.5 nm^{-2}, respectively.

2.2.4.   Conjugation of streptavidin to biotinylated TiO_2

Biotin molecules were covalently grafted to TiO_2 surfaces, as discussed above. The ability of the attached biotin molecules to conjugate with streptavidin will be key to the exploitation of these compounds. Confocal microscopy images (Figure 2-6) show that biotinylated TiO_2 particles are able to bind to streptavidin-FITC. The fluorescence in Figure 2-6 a is much brighter than that in Figure 2-6 b, consistent with the absence of non-specific adsorption, presumably because the untreated TiO_2 (see Figure 2-3) and streptavidin-FITC [58] are both negatively charged, and therefore that the untreated TiO_2 does not effectively couple to streptavidin-FITC in a pH=9.6 buffer.

From Figure 2-6 a, it can be seen that some of the biotinylated TiO_2 particles flocculate with the addition of streptavidin. This may be because each streptavidin molecule can bind four biotin molecules, or because the charged protein acts as a non-specific locus of aggregation. To address this question, the effect of streptavidin concentration on the aggregation of the biotinylated TiO_2 was studied (Figure 2-7). With increasing concentration of streptavidin, a peak corresponding to aggregates of 5-30 μm diameter first appeared, and then increased in intensity. However, it was also found that the intensity of the peak was always low compared with the main peak at 0.4-5 μm. This suggests that irrespective of the streptavidin concentration only a small fraction of the

biotin binding sites are available to biotinylated TiO_2 particles. This may be because the size of streptavidin is small (5-6 nm)[59] compared with the size of TiO_2 particles used in these experiments, and surface geometry prevents binding of TiO_2 into more than one or two sites on streptavidin (see Figure 2-8). Irrespective, streptavidin molecules did not act as a strong flocculant for the biotinylated TiO_2, although they were readily able to bind to the biotinylated TiO_2 particles, according to the confocal microscopy and active biotin assays. This provides the opportunity to further manipulate the surface of these particles using biotin modified biomolecules that don't suffer from the same geometric constraints[16,60] as the biotin-tethered TiO_2 particles.

The processes described above demonstrate that it is possible to tune the surface characteristics of photoactive TiO_2 particles with respect to the thickness of cationic shells, concentration of active biotin binding groups, and of streptavidin tags. While doing so, colloidal stability can be maintained such that the dispersions of particles can be targeting to accessible (i.e., not particulate) biotin functionalized moieties. Future work will focus on examining the ability to immobilize these particles and exploit their photolytic activity in specific biological environments.

2.3   Experimental Section

2.3.1.   Chemicals

N-hydroxysuccinimido-biotin (*N*-Biotin), biotin, streptavidin-FITC from *Streptomyces avidinii* and 4'-hydroxyazobenzene-2-carboxylic acid (HABA)/avidin reagent were purchased from Sigma and used as received. 3-Aminopropyltriethoxysilane (APTS) and

anhydrous methyl sulfoxide were purchased from Aldrich and used as received. Anatase

nanoparticles, 3.9 g/cm^3, 99+%, were purchased from Aldrich and used as received

(particle size distributions are shown in Figure 2-2; no dispersants were present on the

particles). The reactions were carried out under a nitrogen atmosphere. Streptavidin from

Streptomyces avidinii was purchased from Fluka. Potassium polyvinylsulfate (PVSK)

(MW 19.1 kDa) standard solution was supplied by BTG Mütek. MilliQ water was used

to wash samples and prepare buffers. Sodium bicarbonate buffer (pH=9.6, 25 mM) was

prepared by diluting the mixture of 250 mL sodium bicarbonate solution (0.05 M) and 25

mL NaOH solution (0.1 M) to 500 mL with MilliQ water. Silica particles were prepared

using published routes[61] and were used in this report as a control sample.

2.3.2. Measurements

1. **^{29}Si and ^{13}C CPMAS NMR** were recorded at room temperature on a Bruker AV-300

   spectrometer, which operates at 75.5 MHz for ^{13}C and 59.6 MHz for silicon. The

   samples were in powder form and were packed into 4mm zirconia rotors. The rotors

   were spinning at 10 kHz during the data collection for ^{13}C and 5 kHz for ^{29}Si. Glycine

   was used as an external reference for the ^{13}C spectra and $((CH_3)_3C)_4Si$ was used as a

   reference for the ^{29}Si spectrum.

2. **FT-IR spectra** were collected on a bio-Rad FTS-4 spectrometer (Hercules, CA) using

   conventional transmission. Samples were diluted using dry KBr, pressed into pellets

   and scanned in the range 4000–400 cm^{-1}, with a resolution of 4 cm^{-1}. The spectrum of

   a blank KBr pellet was also measured to allow background subtraction.

3. **Transmission Electron Microscopy (TEM)** of untreated TiO_2, aminosilanized TiO_2 and biotinylated TiO_2 were obtained on a JEOL JEM-1200EX transmission electron microscope. All the TiO_2 samples were dispersed in anhydrous ethanol with ultrasonication for 2 min and then dropped onto the copper grid to dry.

4. **Nitrogen Adsorption** was performed to obtain the specific surface area (SSA) data of the untreated, aminosilanized, and biotinylated TiO_2 on a Quantachrome Nova 2200.

5. **X-ray Photoelectron Spectroscopy (XPS)** was obtained on Leybold Max 200 XPS system equipped with a non-monochromatized Al $K\alpha$ (15 kV, 20 mA) X-ray source. The energy scale was corrected by placing the C1s value for the main C-C component at 285 eV. Spectra were obtained at take-off angle of 90° corresponding to a depth of analysis of about 10 nm, at 2×10^{-9} bar, using a 2×4 mm^2 aperture for measuring the atomic composition on the aminosilanized TiO_2 surface.

6. **Polyelectrolyte Titration,**[62,63] to measure the surface amino-group grafted onto the TiO_2 surface, was performed on a PCD 03 charge titrator (BTG Mütek, Germany). A PVSK standard solution was diluted 50 times before titrating aminosilanized TiO_2 particles. Aminosilanized TiO_2 suspension (0.1 mg mL^{-1}) was made acidic (pH of 3.5) with acetic acid (0.05 N). The reported surface amino group density values represent the mean of three measurements.

7. **Conductometric Titration,** to quantify the total concentration of TiO_2 surface grafted amino-groups, was performed on a Man-Tech PC-Titrate™ Burivar™-I/2 Buret Module (Man-Tech Associates. Inc., Guelph, ON, Canada). Aminosilanized TiO_2 particles obtained by 16 and 26 hours silylation were suspended at a concentration of

0.2 mg/mL in 50 mL of a 1 mM NaCl solution. Aminosilanized TiO$_2$ particles obtained by 4 hours silylation were suspended at 0.4 mg/mL in 250 mL of a 1 mM NaCl solution. The pH was manually lowered to 3.0, and the sample was titrated with 0.1 M NaOH under a N$_2$ atmosphere. A time interval of 120 s between injections was used to ensure full equilibration of the protonation of amino-groups on the TiO$_2$ surface. Titration endpoints were determined by using the standard extrapolation/intersection method. Reported uncertainties indicate approximate ±0.005mL error involved in extrapolating the titration endpoints. The reported amino group density values represent the mean of three measurements.

8. **Electrophoretic Mobility** of TiO$_2$ particles were measured on the ZetaPlus Zeta Potential Analyzer (Brookhaven Instruments Corp.). Measurements were performed in KNO$_3$ (1mM) solution with different pH values for untreated, aminosilanized and biotinylated TiO$_2$. The error bars of the electrophoretic mobilities represent the standard error of the mean value of 10 runs (15 cycles per run). The bars of pH values represent the pH range in which the electrophoretic mobility was tested.

9. **Active biotin density** on the TiO$_2$ surface was measured by titration according to Green's method.[57] HABA exhibits a characteristic absorption band at 500 nm upon binding to avidin. When biotin is introduced in the system, a HABA/avidin complex is converted to a biotin/avidin complex because of the much higher K$_a$ value of the latter (1.3×10^{15} M^{-1}) compared with that of the former (6×10^6 M^{-1}). As HABA is displaced, the absorbance at 500 nm decreases proportionally. The quantity of biotin introduced in the solution was determined by plotting the calibration curve of the

absorbance value of HABA/avidin versus the increasing concentrations of added

biotin. The biotinylated TiO_2 particles were dispersed in MilliQ water to give a known

concentration and then a known volume of the suspension was added to the

HABA/avidin solution. After centrifugation at 10000 rpm for 15 min, the absorbance

at 500 nm of the supernatant liquid was measured. The biotin concentration of

biotinylated TiO_2 sample can be determined by comparison with the calibration curve.

The reported active biotin density values are the average of triplicate measurements.

10.   **Confocal Microscopy** images were obtained on Zeiss LSM 510 Confocal for

streptavidin-FITC immobilized on biotinylated TiO_2 and untreated TiO_2.

11.   **Size and Size distributions** of TiO_2 particles were obtained on Mastersizer 2000

(Malvern Instruments). Untreated TiO_2 (3.6 mg L^{-1}), aminosilanized TiO_2 (6 mg L^{-1})

or biotinylated TiO_2 (6 mg L^{-1}) were dispersed in sodium bicarbonate buffer using

ultrasonication for 5 min. A higher concentration of the aminosilanized and

biotinylated TiO_2 solutions was used because of their lower refractive index than that

of the TiO_2 starting material. Sodium bicarbonate buffer was filtered with 0.2μm filter

disc to remove the dust before use.

2.3.3.   Sample preparation

Aminosilanization of TiO_2 particles

A 500 mL flask was degassed with pure and dry N_2 and charged with TiO_2 (0.3 g,

3.756 mmol) and anhydrous DMSO (210 mL). The particles were dispersed in the

anhydrous DMSO using ultrasonication for 10 min. Afterwards, APTS (1.5 mL, 6.346

mmol) was injected in the flask. After stirring at 85 °C for a specified time (4 h, 16 h, 26 h, respectively), the solid particles were deposited by centrifugation, and then washed with anhydrous DMSO (3×180 mL). The TiO_2 particles were dispersed in anhydrous DMSO (100 mL) using ultrasonication for 10 min and then were cured under a nitrogen stream at 120 °C for 20 h. After thermal cure, the TiO_2 particles were washed with anhydrous DMSO (3×180 mL). Finally, an aliquot of these particles was dried *in vacuo* at 65 °C for characterization. The remaining sample was reserved for the second modification step.

The ^{29}Si NMR spectrum (see Supplementary Material) showed signals at δ=-60.13 ppm (T^2)[64] and δ= -68.32 ppm (T^3). FT-IR spectra (Figure 2-1) showed low intensity peaks consistent with a grafted APTS layer. SSA, XPS and charge titration results are shown in Table 2-1. TEM images of the untreated and aminosilanized TiO_2 are shown in Figure 2-2 a-d, and electrophoretic mobility of the untreated and aminosilanized TiO_2 in Figure 2-3.

Biotinylation of TiO_2 particles

N-Hydroxysuccinimidobiotin (1.0 g, 2.9 mmol) was dissolved in anhydrous DMSO (5 mL). A 250 mL round-bottomed flask was degassed with dry N_2 and charged with amino-modified TiO_2 (0.15 g, 1.878 mmol) and the above DMSO solution (125 μL) which contained *N*-hydroxysuccinimidobiotin (25 mg, 0.073 mmol) using a micropipette. Finally, DMSO (80 mL) was added to the round-bottom flask. The mixture was sonicated for 2 min. After stirring at room temperature for 3 h, the solid particles were deposited by centrifugation, and then washed with anhydrous DMSO (90 mL×3 times),

followed by MilliQ water (3×90 mL), and then dried *in vacuo* at 50 °C to remove the residual solvents. The same processes of aminosilanization and biotinylation were performed to modify SiO_2 particles as a control.

The ^{13}C NMR spectrum (Figure 2-4) shows peaks at δ=173 (*j*), 165 (*a*), 61, 58, 55 (cluster of 4 peaks, *c, b, e* and *n*), 41, 38, 36 (cluster of 3 peaks, *k, d* and *i*), 28, 26, 20, 18 (cluster of 5 peaks, *f, g, h, l* and *o*) and 10 ppm (*m*). Key peaks in the FT-IR spectra (Figure 2-1) include 3435 (-NH_2 and H_2O), 2921 (C-H), 1702 (amide I), 1648 (-NH_2), 1547 (amide II), 1459 (C-H), 1200-1000 (Si-O-Si) and 957 (Ti-O-Si) cm^{-1}.

TEM images of the biotinylated TiO_2 are shown in Figure 2-2 e,f. Electrophoretic mobilities of the biotinylated TiO_2 are shown in Figure 2-3. The specific surface area values of the biotinylated TiO_2 are shown in Table 2-1. The active biotin assay, combined with the SSA value, gave densities for active biotin on the TiO_2 surface of 2.1 nm^{-2}, 7.0 nm^{-2} and 11.5 nm^{-2} for the biotinylated TiO_2 samples obtained from aminosilanization reaction times of 4 h, 16 h and 26 h, respectively. The size and size distribution of TiO_2 particles after aminosilanization and biotinylation are shown in Figure 2-5.

1) Conjugation of streptavidin to biotinylated TiO_2 particles

Biotinylated TiO_2 particles (0.1 g) were dispersed in sodium bicarbonate buffer (pH=9.6, 25mM, 100 mL) using ultrasonication for 5 min. 1 mL of the suspension was mixed with streptavidin-FITC (1 mg) in 9 mL of the same buffer for 2 h in the dark. After incubation, all the solid particles were deposited by centrifugation, and washed with the same buffer (3×40 mL) to remove the excessive free streptavidin-FITC. The same

procedure was performed following the reaction of untreated TiO_2 samples with streptavidin-FITC in the same buffer. Confocal microscope images are shown in Figure 2-6.

In a sodium bicarbonate buffer (pH=9.6, 25 mM), the biotinylated TiO_2 suspension (100 mL) was prepared at a concentration of 6 mg L^{-1}, to give 9.7×10^{-4} mmol L^{-1} of active biotin in the solution. In the same buffer, streptavidin solution was prepared at the concentration of 1 mg mL^{-1}. Following each addition of an aliquot of the streptavidin solution (30 μL) to the biotinylated TiO_2 solution, the system was mixed for 10 min, and then particle sizes and size distributions were measured. Each addition of the streptavidin solution increased the concentration of streptavidin in the system by 5×10^{-6} mmol L^{-1}. Sodium bicarbonate buffer was filtered with a 0.2 μm filter disc to remove dust before use. The aggregation of the biotinylated TiO_2 particles in the present of streptavidin was measured and the results are shown in Figure 2-7. The size distribution curve shows a new peak of 5-30 μm which increases in intensity with each aliquot of streptavidin until 1860 μL streptavidin solution was added to the solution, after which no further changes observed. The concentration of streptavidin at the end point of the titration was 3.1×10^{-4} mmol L^{-1}.

2.4   Conclusions

Biotin can be covalently bound to TiO_2 particles using a silane coupling agent to link biotin to the inorganic TiO_2 surface. The quantity of attached biotin molecules depended on the thickness of the aminopropylsilsequioxane layer moiety attached to the TiO_2

particle surface: longer silanization time led to thicker layers and reached a maximum in these studies of 11.5 nm^{-2}. However, this represents only about 1/6 of the available amino groups in the silane shell and about 60% of the surface amino groups present. The tethered biotin groups are accessible for binding with streptavidin. Although each streptavidin molecule can bind to four biotin molecules, streptavidin did not act as a strong flocculent in our biotinylated TiO$_2$ particles. Thus, the streptavidin modified particles have residual biotin binding sites that are geometrically constrained: they are not accessible to large particles. They should, however, be accessible to small molecules, which would permit the assembly of more complex biotargeting TiO$_2$ particles

	Untreated TiO$_2$	TiO$_2$ after aminosilanization for		
		4 hours	16 hours	26 hours
NH$_2$ density on TiO$_2$ surface (nm^{-2}) measured by polyelectrolyte titration	0	2.7	10	17
Measured by conductometric titration	0	2.9	26	66

	Untreated TiO$_2$	Aminosilanization		
		4 hours	16 hours	26 hours
SSA (m^2 g^{-1})	16.0	14.1	10.2	9.1
		Biotinylation (3 hours)		
		13.4	9.1	8.4

		Untreated TiO$_2$	Aminosilanization			Biotinylated[a] TiO$_2$ 3 h
			4 hours	16 hours	26 hours	
XPS	N%	0.1	2.7	6.2	10.0	8.4
	Ti%	15	8.7	3.7	0.4	5.0

[a] The surface was aminosilanized for 4 h, then biotinylated for 3 h.

Table 2-1 XPS, charge titration results and SSA of the untreated, aminosilanized and biotin modified TiO$_2$
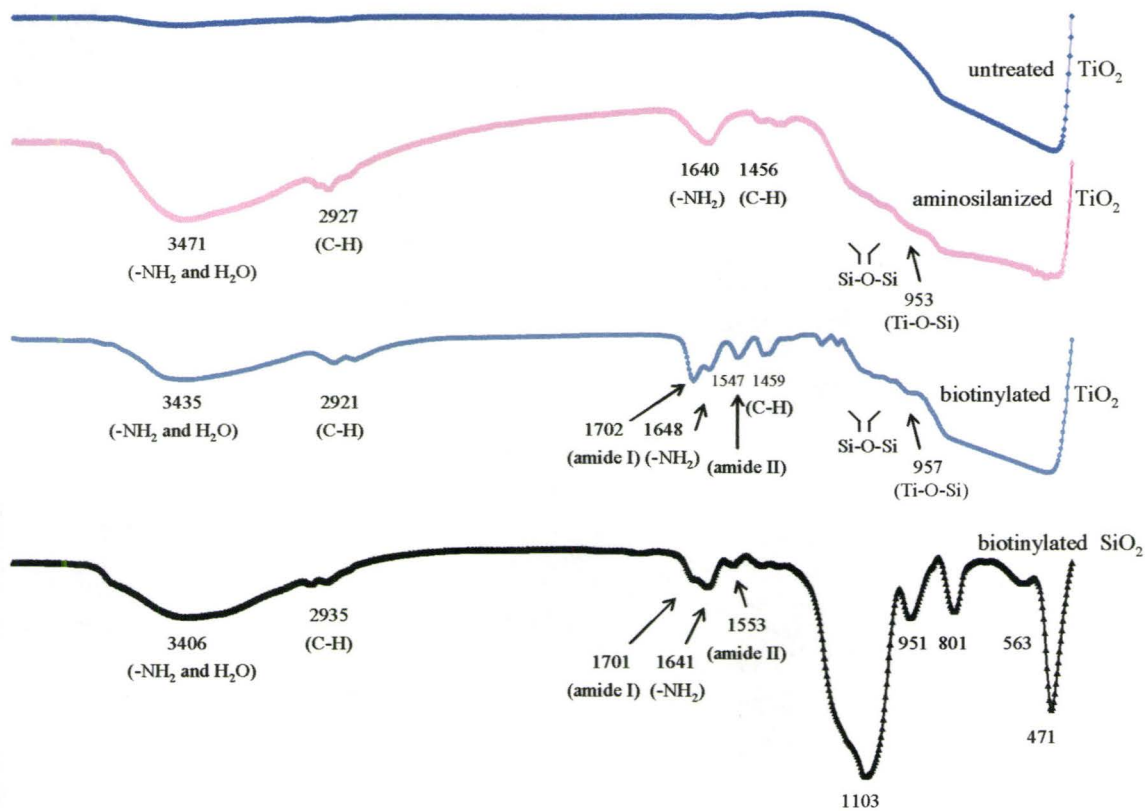
Figure 2-1 FT-IR spectra of untreated TiO₂, aminosilanized TiO₂, biotinylated TiO₂ and biotinylated SiO₂
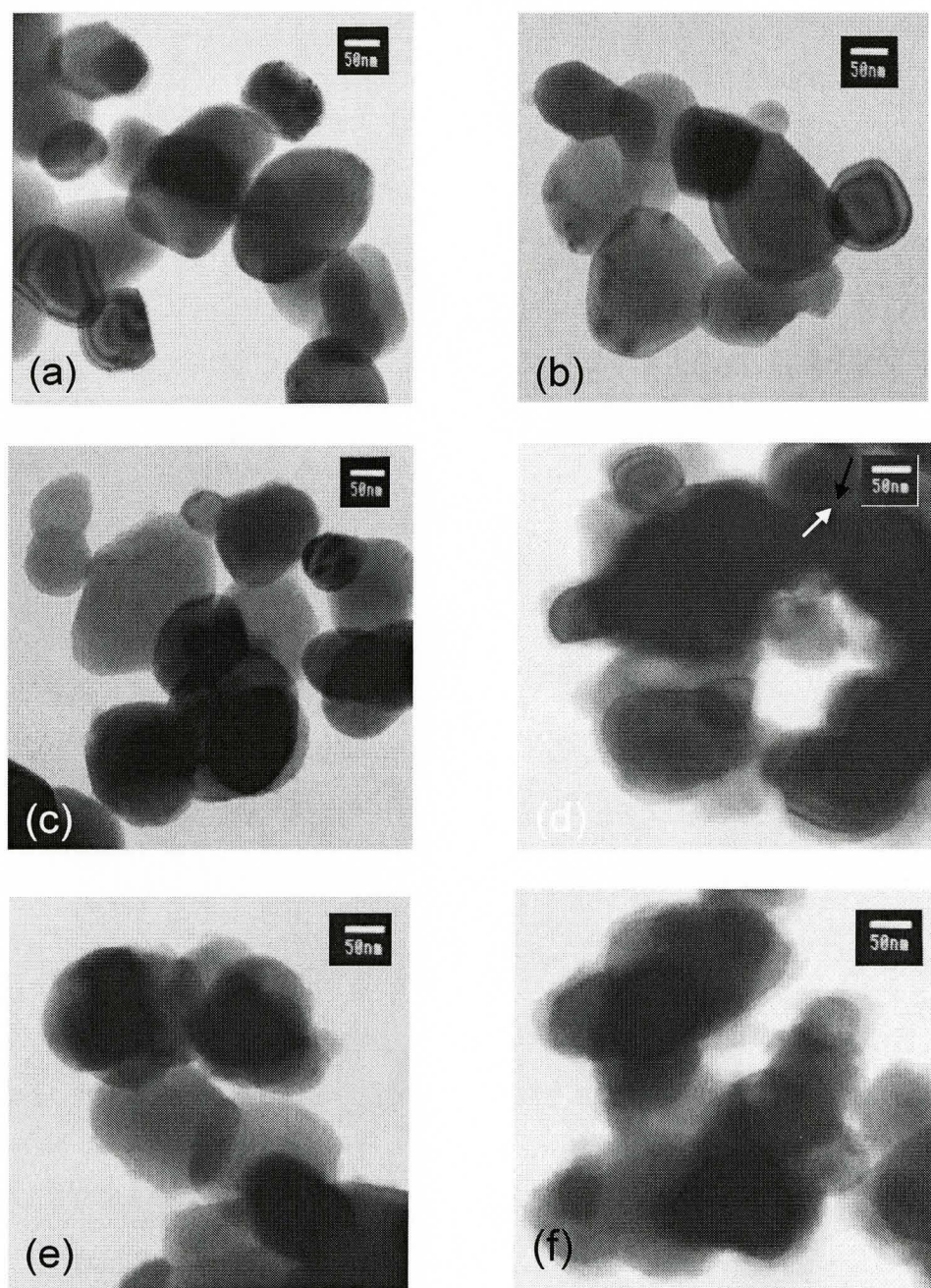
Figure 2-2 TEM images for (a) untreated TiO_2, aminosilanized TiO_2 after (b) 4 hours; (c)

16 hours; (d) 26 hours, biotinylated TiO_2 after aminosilanization (e) 16 hours (3(c)); (f)

26 hours (3(d)). The scale bar in all images is 50 nm
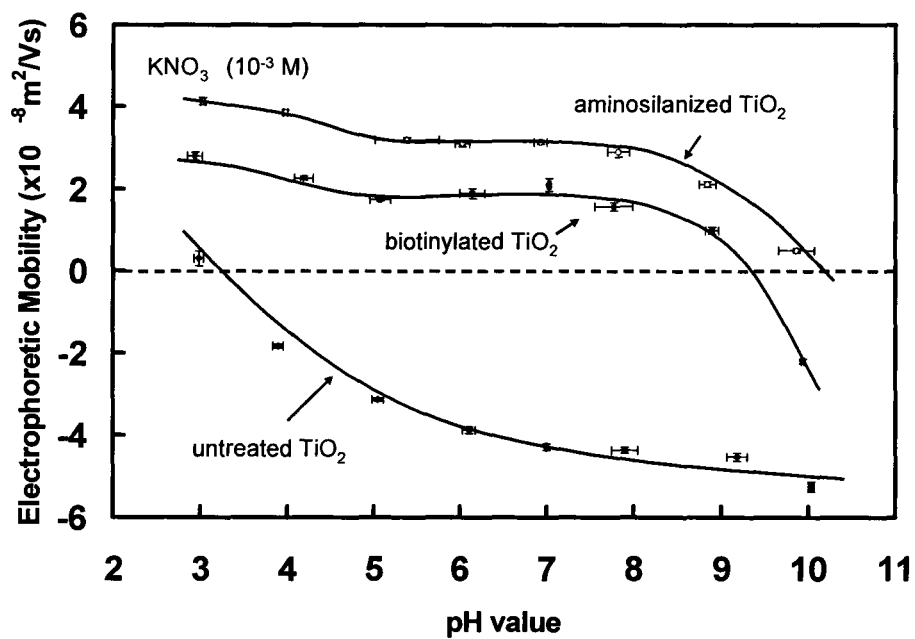
Figure 2-3 Electrophoretic mobilities of untreated, aminosilanized and biotinylated TiO$_2$
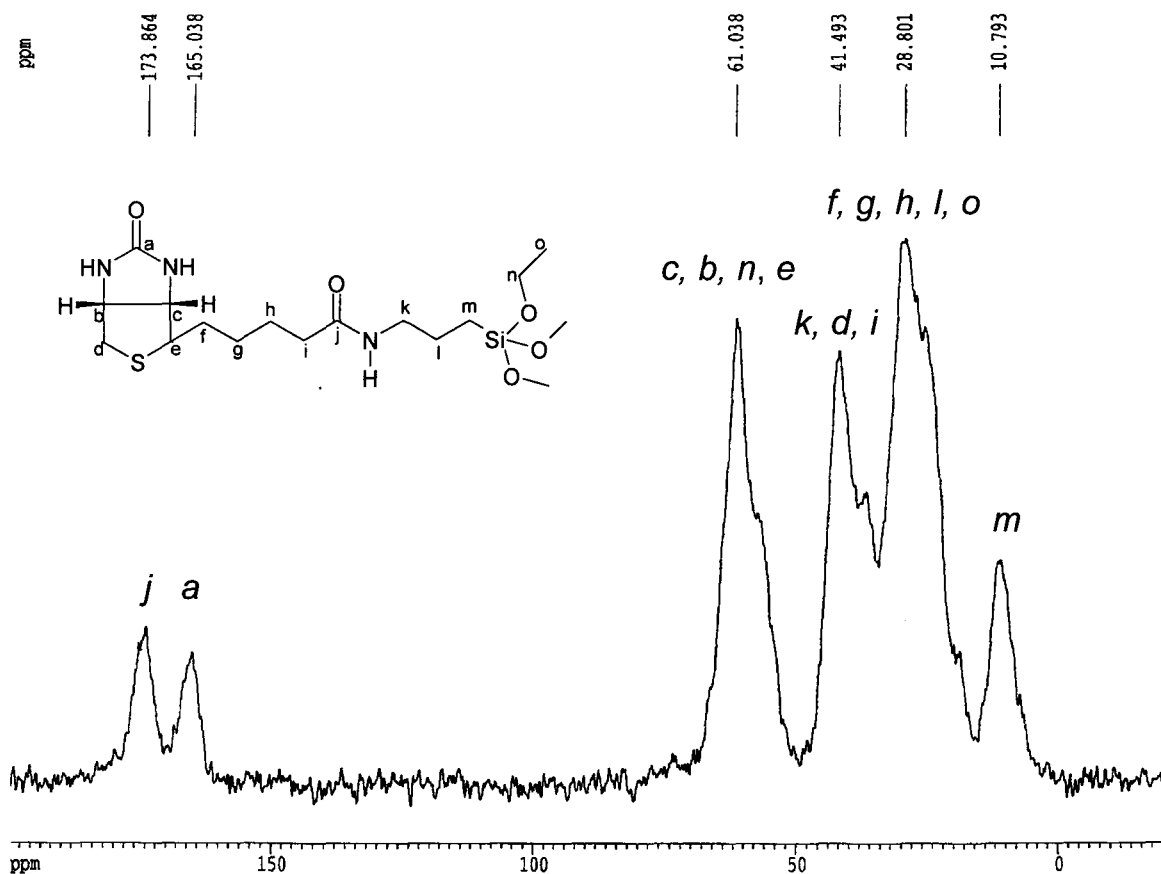
particles

Figure 2-4 ^{13}C CPMAS NMR spectrum for the biotinylated TiO$_2$ particles
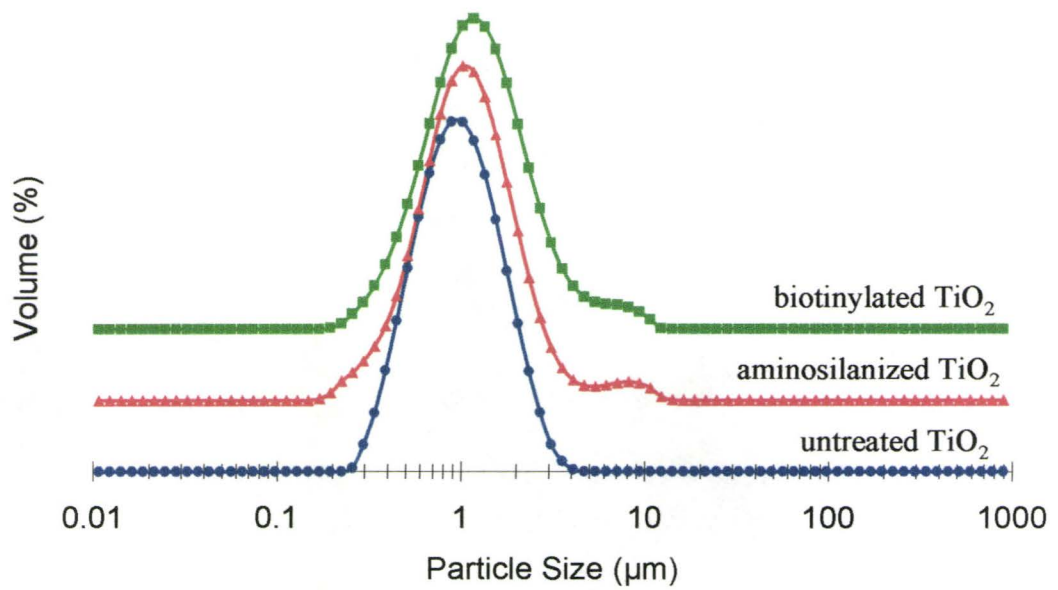
Figure 2-5 Sizes and size distributions of untreated, aminosilanized and biotinylated TiO_2
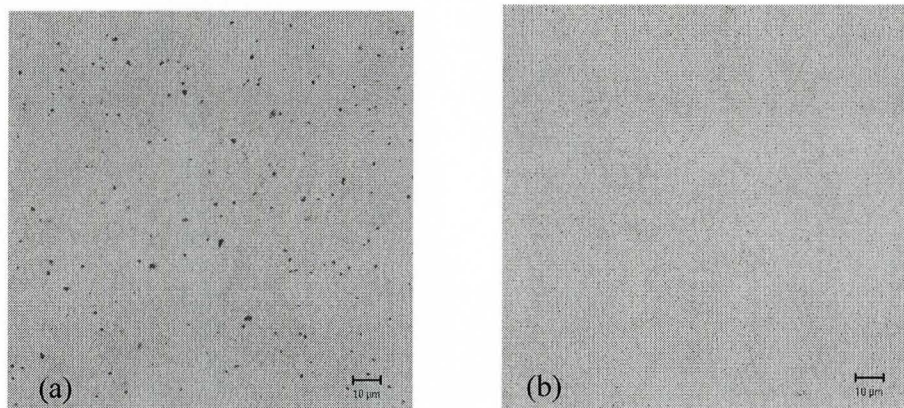
nanoparticles

Figure 2-6 Confocal images of streptavidin-FITC in sodium bicarbonate buffer (pH=9.6, 25mM) with (a) biotinylated TiO_2, (b) untreated TiO_2 (scale bar=10 μm).
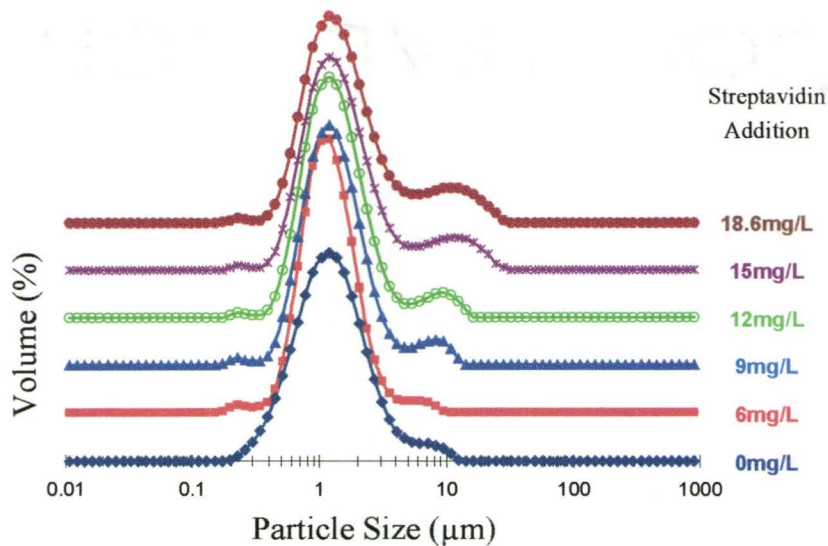
Figure 2-7 Size distribution of biotinylated TiO_2 particles with the addition of streptavidin. The concentration of biotinylated TiO_2 is 6 mg L^{-1}. The concentrations of streptavidin are 0 mg L^{-1} (--◆--), 6 mg L^{-1} (--■--), 9 mg L^{-1} (--▲--), 12 mg L^{-1} (--○--), 15 mg L^{-1} (--∗--), 18.6 mg L^{-1} (--●--),
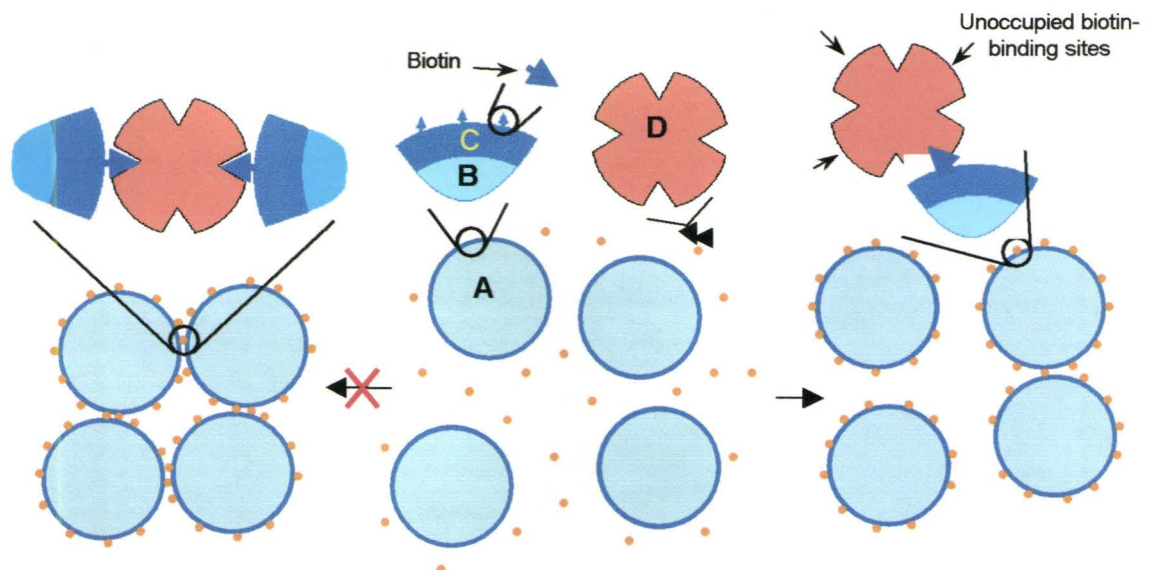
Figure 2-8 Model showing the conjugation of streptavidin with the biotinylated TiO₂

particles. A: biotinylated TiO₂ particle; B: TiO₂ bulk; C: APTS gel layer; D: streptavidin.
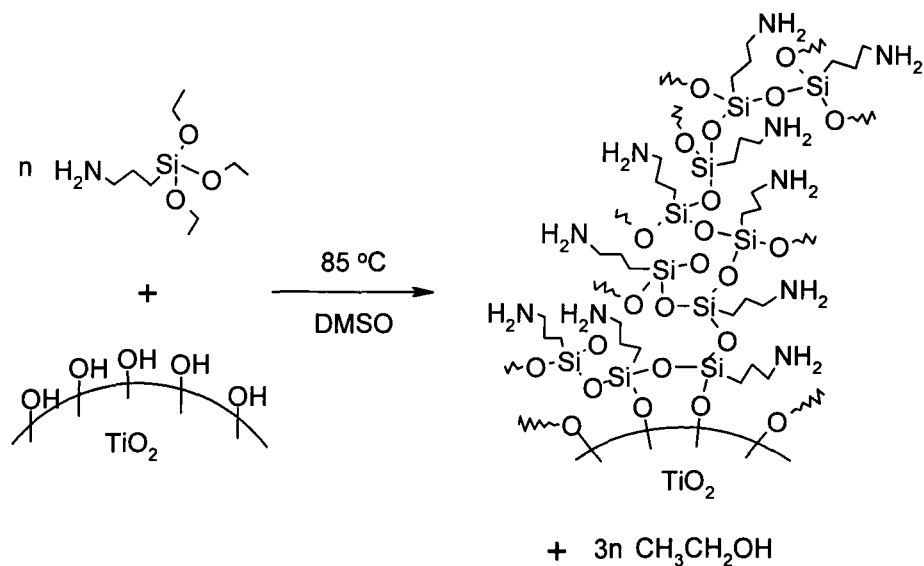
Scheme 2-1   Silanization reaction of TiO$_2$ with APTS
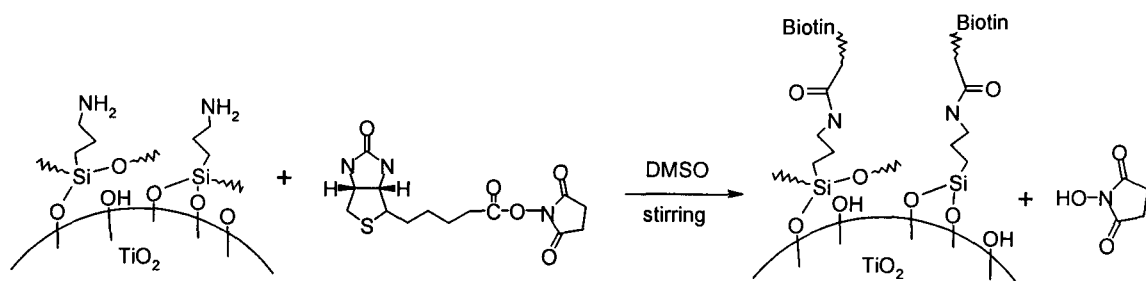
Scheme 2-2   Biotinylation reaction of amino-TiO$_2$ with biotin-NHS

2.5   Reference

[1] a) Braun, J. H.; Baidins, A.; Marganski, R. E. *Prog. Org. Coat.* **1992**, *20*, 2, 105-38. b) Schmidt, C.; Delp, T.; Schoen, S. *U.S. Pat. Appl. Publ.* **2005**, US 2005176850

[2] Brand, R. M.; Pike, J.; Wilson, R. M.; Charron, A. R. *Toxicol. Ind. Health* **2003**, *19*, 9-16.

[3] Legrini, O.; Oliveros, E.; Braun, A. M. *Chem. Rev.* **1993**, *93*, 671-698.

[4] Paz, Y.; Heller, A. *J. Mater. Res.,* **1997**, *12*, 2759-2766.

[5] Linsebigler,, A. L.; Lu, G.; Yates, J. T., Jr. *Chem. Rev.* **1995**, *95*, 735-58.

[6] Chen, C. C.; Lei, P. X.; Ji, H. W.; Ma. W. H.; Zhao, J. C. *Environ. Sci. Technol.* **2004**, *38*, 329-337.

[7] Hashimoto, K.; Irie, H.; Fujishima, A. *Jpn. J. Appl. Phys. Part 1*, **2005**, *44*, 8269-8285.

[8] Hoffmann, M. R.; Martin, S. T.; Choi, W.; Bahnemann, D. W. *Chem. Rev.* **1995**, *95*, 69-96.

[9] Blake, D. M.; Maness P.-C.; Huang, Z.; Wolfrum, E. J.; Huang, J.; Jacoby, W. A. *Sep. Purif. Methods* **1999**, *28*, 1-50.

[10] Hirakawa, K.; Mori, M.; Yoshida, M.; Oikawa, S.; Kawanishi, S. *Free Radical Res.* **2004**, *38*, 439-447.

[11] Milella, E.; Cosentino, F.; Licciulli, A.; Massaro, C. *Biomaterials* **2001**, *22*, 1425-1431.

[12] Oh, S.-H.; Finõnes, R. R.; Daraio, C.; Chen, L. H.; Jin, S. *Biomaterials* **2005**, *26*, 4938-4943.

[13] Rupp, F.; Geis-Gerstorfer, J.; Geckeler, K. E. *Adv. Mater.* **1996**, *8:3*, 254-257.

[14] Lee, S. H.; Kim, H. W.; Lee, E. J.; Li, L. H.; Kim, H. *J. Biomater. Appl.* **2006**, *20*, 195-208.

[15] Wu, J. M.; Hayakawa, S.; Tsuru, K.; Osaka, A. *Thin Solid Films* **2002**, *414*, 283-288.

[16] Huang, J. G.; Ichinose, I.; Kunitake T. *Angew. Chem. Int. Ed.* **2006**, *45*, 1-5.

[17] André, L.M. P.; Flávia, C.; Silvio, L.P. D.; Inés, J.; Yoshitaka, G.; José, A.R. R.; Paulo, J.S. M.; Gilson, P. M.; Anita, J. M. *J. Mol. Catal. B: Enzym.* **2002**, *19-20*, 327-334.

[18] Chen, Y.; Yi, Y.; Brennan, J. D.; Brook, M. A., *Chemistry of Materials* **2006**, 18, (22), 5326-5335.

[19] Stamm, C. Lukosz, W. *Sens. Actuators B* **1996**, *31*, 203-207.

[20] Clerc, D.; Lukosz, W. *Sens. Actuators B* **1997**, *40*, 53-58.

[21] Zhang, Y.; He, P. L.; Hu, N. F. *Electrochimica Acta* **2004**, *49*, 1981-1988.

[22] André, B.; Hans, R. B. *Eur. J. Biochem.* **1995**, *230*, 416-423.

[23] Li, Q. W.; Luo, G. A.; Feng, J.; Zhou, Q.; Zhang, L.; Zhu, Y. F. *Electroanalysis* **2001**, *13*, 5, 413-416.

[24] Dimitrijevic, N. M.; Saponjic, Z. V.; Rabatic, B. M.; Rajh, T. *J. Am. Chem. Soc.* **2005**, *127*, 1344-1345.

[25] Garza, L. de la. Saponjic, Z. V.; Dimitrijevic, N. M.; Thurnauer, Marion. C.; Rajh, T. *J. Phys. Chem. B*; **2006**, *110*, 680-686.

[26] Chaiet, L.; Wolf, F. J. *Arch. Biochem. Biophys.* **1964**, *106*, 1-5.

[27] Green, N. M. *Advances in Protein Chemistry,* Academic Press, New York, (Eds. Anfinsen, C.B.; Edsall, J.T.; Richards, F. M.) **1975**, *29*, 85-133.

[28] Bhaduri, A.; Das, K. P. *J. Dispersion Sci. Technol.* **1999**, *20*, 1097-1123.

[29] Talbot, J.; Tarjus, G.; Van Tassel, P. R.; Viot, P. *Colloids Surf., A* **2000**, *165(1-3)*, 287-324.

[30] Brinker, C. J.; Scherer, G. W. *Sol-Gel Science - The Physics and Chemistry of Sol-Gel Processing,* New York, Academic Press, **1990**

[31] Plueddemann, E. P. *Silane Coupling Agents,* 2nd ed.; Plenum Press: New York, **1991**

[32] Aamer, A.; Chris, B.; Tejal, A. D. *Biomed. Microdevices* **2001**, *3:2*, 89-96.

[33] Weisser, M.; Tovar, G.; Mittle-Neher, S.; Knoll, W.; Brosinger, F.; Freimuth, H.; Lacher, M.; Ehrfeld, W. *Biosens. Bioelectron.* **1999**, *14*, 405-411.

[34] Orth, R. N.; Clark, T. G.; Craighead, H. G.; *Biomed. Microdevices* **2003**, *5:1*, 29-34.

[35] Wagner, P.; Zaugg, F.; Kernen, P.; Hegner, M.; Semenza, G. *J. Vacuum Sci. Technol. B* **1996**, *14*, 1466-1471.

[36] Zaugg, F. G.; Wagner, P.; Kernen, P.; Vinckier, A.; Groscurth, P.; Spencer, N. D.; Semenza, G. *J. Mater. Sci. Mater. Med.* **1999**, *10*, 1-9.

[37] Soong, H. U.; Goo, S. L.; Yun-Jo, L.; Kee-Kahb, K.; Chongmok, L.; Kyung, B. Y. *Langmuir* **2002**, *18*, 4455-4459.

[38] Parikh, A. N., Allara, D. L., Azouz, I. B.; Rondelez, F. *J. Phys. Chem.* **1994**, *98*, 7577-7590.

[39] Combes, J. R., White, L. D.; Tripp, C. P. *Langmuir* **1999**, *15*, 7870-7875.

[40] Gamble, L.; Jung, L. S.; Campbell, C.T. *Langmuir* **1995**, *11*, 4505-4514.

[41] Gamble, L.; Hugenschmidt, M.B.; Campbell, C. T.; Jurgens, T. A.; Rogers, J. W. *J. Am. Chem. Soc.* **1993**, *115*, 12096-12105.

[42] Gamble, L.; Henderson, M. A.; Campbell, C. T. *J. Phys. Chem. B* **1998**, *102*, 4536-4543.

[43] Trummer, N.; Adányi, N.; Váradi, M.; Szendrö, I. *Fresenius J Anal. Chem.* **2001**, *371*, 21-24.

[44] Pelton, R.; Geng, X.; Brook, M. *Adv. Colloid Interface Sci.*, in press and references cited therein.

[45] Vrancken, K.C.; Possemiers, K.; Van Der Voort, P.; Vansant, E. F. *Colloids Surf. A* **1995**, *98*, 235-241.

[46] Wayne, Y.; Robert, P. C.; Jeng-D., J.; Yoram, C. *Langmuir* **2001**, *17*, 5882-5888.

[47] Dagobert, H.; Manfred, N.; Helmut, S. *J. Sol-Gel Sci. Tech.* **1998**, *13*, 37-43.

[48] Dirken, P. J.; Smith, M. E.; Whitfield, H. J. *J. Phys. Chem.* **1995**, *99*, 395-401.

[49] Méndez-V., J.; Mendoza-S., R. Gómez-L., J.; Gaviño, R. *J. Sol-Gel Sci. Technol.* **1997**, *8*, 235-241.

[50] Beghi, M.; Chiurlo, P.; Costa, L.; Palladino, M.; Pirini, M. F. *J. Non-Cryst. Solids* **1992**, *145*, 175-179.

[51] Gilmar de, A. G.; Julien, F. C.; Braz, B. *J. Braz. Chem. Soc.* **1999**, *10*, 2, 92-96.

[52] Furlong, D. N.; Parfitt, G. D. *J. Colloid Interface Sci.* **1978**, *65*, 548-554.

[53] Yaremko, Z.M.; Tkachenko, N.H.; Bellmann, C.; Pich, A. *J. Colloid Interface Sci.* **2006**, *296*, 565-571.

[54] Andrzejewska, A.; Krysztafkiewicz, A.; Jesionowski, T. *Dyes Pigments* **2004**, *62*, 121-130.

[55] Teofil J.; Andrzej, K. *Appl. Surf. Sci.* **2001**, *172*, 18-32.

[56] Kim, H. J.; Moon, J. H.; Park, J. W. *J. Colloid Interface Sci.* **2000**, *227*, 247-249.

[57] Green, N. M. *Biochem. J.* **1965**, *94*, 23c-24c.

[58] Savage, M.D.; Mattson, G.; Desai, S.; Nielander, G.W.; Morgensen, S.; Conklin, E. J. *Avidin-biotin chemistry: a handbook.* **1992**, Rockford, II: Pierce Chemical Co.

[59] Hendrickson, W. A.; Pähler, A.; Smith, J. L.; Satow, Y.; Merritt, E. A.; Phizackerley. *Proc. Natl. Acad. Sci. USA.* **1989**, *86*, 2190- 2194.

[60] Leon, G.; Adina, N; *J. Chromatography,* **1990**, *510*, 23-39.

[61] Costa, C. A. R.; Leite, C. A. P.; Galembeck, F. *J. Phys. Chem. B* **2003**, *107*, 4747-4755.

[62] Terayama, H., *J. Polym. Sci.* **1952**, *8:2*, 243-253.

[63] Tanaka, H.; Sakamoto, Y. *J. Polym. Sci., Part A: Polym. Chem.* **1993**, *31:11*, 2687-2691.

[64] Nomenclature follows the sol gel literature; T^0 = RSi(OR')$_3$, or RSi(OH)$_3$, T^1 = RSi(OSiZ$_3$)(OR')$_2$, or RSi(OSiZ$_3$)(OH)$_2$, etc.: see Brook, M. A. Silicon in Organic, Organometallic, and Polymer Chemistry, Wiley: New York, **2000**, Chap. 1.

Chapter 2 - Appendix 1
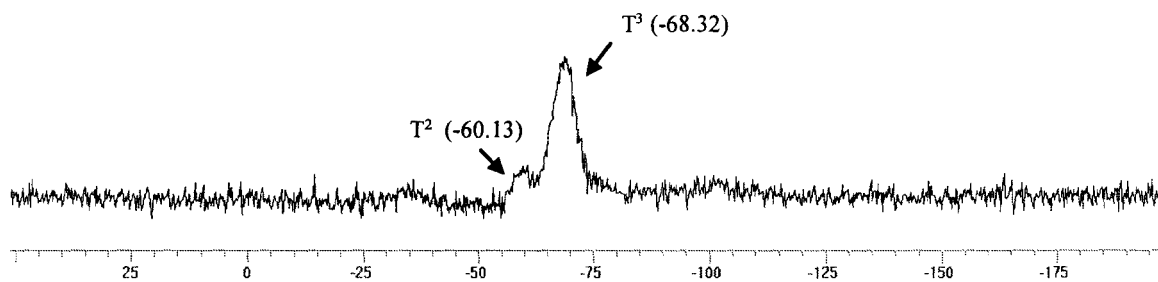
Figure 2A1-1 ^{29}Si CPMAS NMR spectrum for the aminosilanizated TiO_2 particles
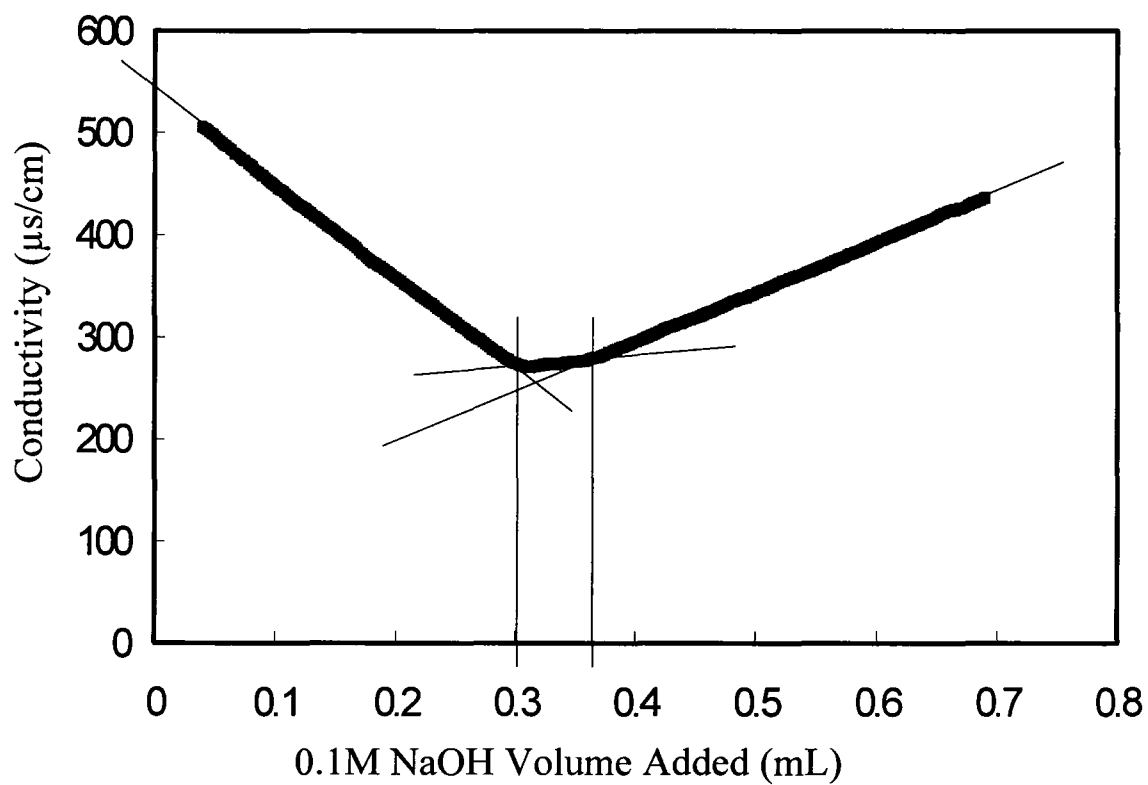
Figure 2A1-2 Conductometric titration curve for aminosilanized TiO_2 sample after 4 hours of reaction time
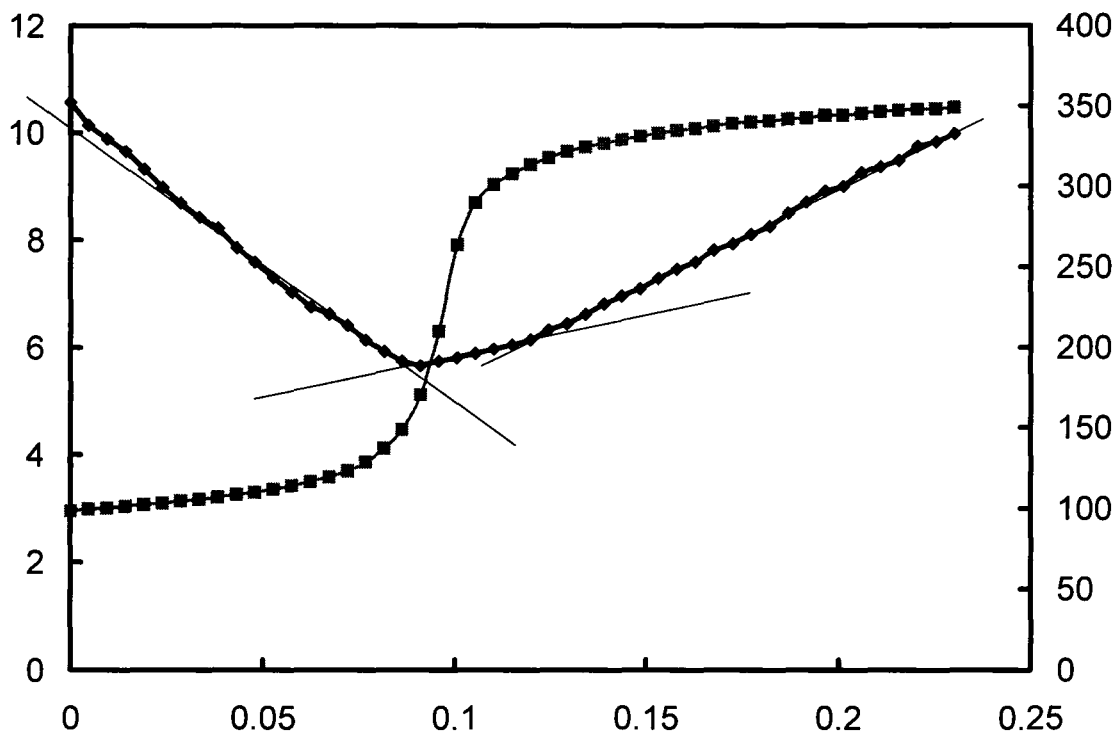
Figure 2A1-3 Conductometric titration curve for aminosilanized TiO_2 sample after 16

hours of reaction time
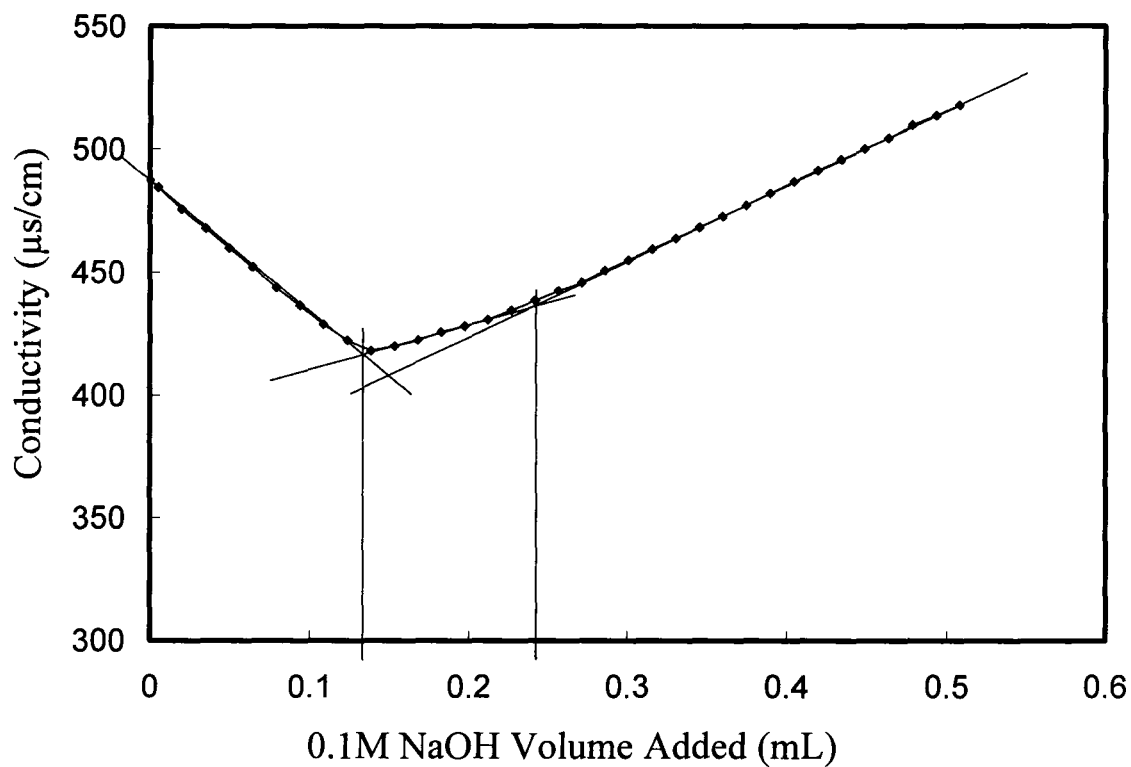
Figure 2A1- 4 Conductometric titration curve for aminosilanized TiO$_2$ sample after 26 hours of reaction time

2.A.1.1 Calculation of the densities of amino groups on TiO$_2$ surfaces with different aminosilanization time, data were obtained by conductometric titration

Equation: $D_{NH_2}{}^c = \dfrac{V_{NaOH} \times C_{NaOH} \times N_{av}}{m_{TiO_2}{}^c \times SSA}$

$D_{NH2}{}^c$: density of amino groups on TiO$_2$ surfaces calculated by the result measured by conductometric titration

V_{NaOH}: the volume of NaOH solution consumed for titration

C_{NaOH}: the concentration of NaOH solution

N_{av}: Avogadro's number

$m_{TiO2}{}^c$: the mass of TiO$_2$ used in conductometric titration

SSA: the specific surface area of TiO$_2$

For the TiO$_2$ particles aminosilanized for 4h:

$m_{TiO2}{}^c$ =100 mg

V_{NaOH} =0.068 mL

SSA =14.12 m^2/g

$D_{NH2}{}^c$ =2.9 nm^{-2}

For the TiO$_2$ particles aminosilanized for 16h:

$m_{TiO2}{}^{c}$ =10 mg

V_{NaOH} =0.045 mL

SSA =10.19 m^2/g

$D_{NH2}{}^{c}$ =26.594 nm^{-2}

For the TiO$_2$ particles aminosilanized for 26h:

$m_{TiO2}{}^{c}$ =10mg

V_{NaOH} =0.1 mL

SSA =9.087 m^2/g

$D_{NH2}{}^{c}$ =66.272 nm^{-2}

2.A.1.2 Calculation of the densities of amino groups on TiO$_2$ surfaces with different aminosilanization time, data were obtained by polyelectrolyte titration

The standard PVSK solution was diluted by 50-fold for titration. Therefore the concentration of PVSK for titration is 2×10^{-5} N

Equation: $D_{NH_2}{}^{P} = \dfrac{V_p \times C_p \times N_{av}}{m_{TiO_2}{}^{P} \times SSA}$

D_{NH2}^{P}: density of amino groups on TiO_2 surfaces calculated by the result measured by polyelectrolyte titration

V_{NaOH}: the volume of PVSK solution consumed for titration

C_{NaOH}: the concentration of PVSK solution (2×10^{-5} N)

N_{av}: Avogadro's number

m_{TiO2}^{P}: the mass of TiO_2 used in polyelectrolyte titration

SSA: the specific surface area of TiO_2

For the TiO$_2$ particles aminosilanized for 4h:

$m_{TiO2}^{P} = 1$ mg

$V_p = 3.16$ mL

SSA $= 14.12$ m^2/g

$D_{NH2}^{P} = 2.695$ nm^{-2}

For the TiO$_2$ particles aminosilanized for 16h:

$m_{TiO2}^{P} = 1$ mg

$V_p = 8.72$ mL

SSA $= 10.19$ m^2/g

$D_{NH2}^{P} = 10.307$ nm^{-2}

For the TiO$_2$ particles aminosilanized for 26h:

$m_{TiO2}^{P} = 0.7$ mg

V_p =8.94 mL

SSA =9.087 m^2/g

D_{NH2}^p =16.928 nm^{-2}

2.A.1.3 Calculation of the densities of active biotin on TiO$_2$ surfaces with different aminosilanization time, data were obtained by Green's method

Equation: $$D_b = \frac{V_b \times C_b \times N_{av}}{m_b \times V_{TiO_2} \times C_{TiO_2} \times SSA}$$

D_b: density of active biotin on TiO$_2$ surfaces calculated by the result measured by Green's method

V_b: the volume of biotin solution required for titrating the HABA/avidin solution to the same absorbance change of solution that caused by the addition of biotinylated TiO$_2$ suspension

C_b: the concentration of free biotin solution (0.122155mg/mL)

V_{TiO2}: the volume of TiO$_2$ suspension used for titration (15.3 µL)

C_{TiO2}: the concentration of TiO$_2$ suspension (0.5 mg/mL)

N_{av}: Avogadro's number

M_b: the molecular weigh of biotin (244.31 g/mol)

SSA: the specific surface area of TiO$_2$

For the TiO$_2$ particles aminosilanized for 4h:

V$_b$ = 0.709 μL

SSA=13.41 m^2/g

D$_b$= 2.081 nm^{-2}

For the TiO$_2$ particles aminosilanized for 16h:

V$_b$ = 1.619 μL

SSA= 9.134 m^2/g

D$_b$= 6.977 nm^{-2}

For the TiO$_2$ particles aminosilanized for 26h:

V$_b$ = 2.449 μL

SSA= 8.417 m^2/g

D$_b$= 11.451 nm^{-2}

2.A.1.4   Calculation of the equivalent spherical diameter of the TiO$_2$ particles based on the specific surface area data

Equation: $D = \dfrac{6}{\rho \times SSA}$

D: diameter of the equivalent spherical diameter

ρ: density of TiO$_2$ used in the work (3.895 g/L)

SSA: the specific surface area of TiO$_2$

For untreated TiO$_2$:

SSA= 16.05 m^2/g

D= 95.977 nm

For aminosilanized TiO$_2$:

4h: SSA= 14.12 m^2/g   D= 109.096 nm

16h: SSA= 10.19 m^2/g   D= 151.171 nm

26h: SSA= 9.087 m^2/g   D= 169.521 nm

For biotinylated TiO$_2$:

Obtained from 4h silylation: SSA= 13.41 m^2/g   D= 114.872 nm

Obtained from 16h silylation: SSA= 9.134 m^2/g   D= 168.649 nm

Obtained from 26h silylation: SSA= 8.417 m^2/g   D= 183.015 nm

2.A.1.5 Calculation of the density of amino groups based on the thickness

of the gel coating on TiO$_2$ surfaces obtained by TEM observation based on

Equation: $D_{NH_2} = \dfrac{T \times N_{av} \times \rho}{M_w}$

D_{NH2}: the density of amino groups

T: the thickness of the gel coating on TiO_2 particles that observed by SEM

N_{av}: Avogadro's number

ρ: density of APTS coating layer (≈ 1 g/mL)

Mw: the molecular weigh of the grafted APTS moiety (110 g/mole)

For the TiO_2 particles aminosilanized for 16h:

T= 5nm D_{NH2}=27.373 nm^{-2}

For the TiO_2 particles aminosilanized for 26h:

T= 12nm D_{NH2}=65.696 nm^{-2}

Chapter 2 - Appendix 2   The Synthesis of Biotinyltriethoxysilane

Experimental Section

Chemicals and Measurements

N-hydroxysuccinimido-biotin (N-Biotin), 98%, was purchased from Sigma, 3-Aminopropyltriethoxysilane (APTS), 99%, and anhydrous methyl sulfoxide were purchased from Aldrich and used as received. Diethyl ether and dichloromethane were purchased from Aldrich and dried over the Alumina column prior to use. The reaction was carried out in a nitrogen atmosphere. ^{1}H and ^{13}C NMR were recorded at room temperature on a Bruker AC-200 spectrometer. FT-IR spectra were obtained on a Perkin-Elmer 283 spectrometer. Electrospray mass spectra were recorded on a Micromass Quattro LC, triple quadruple MS. The melting point of the synthetic product was measured on Gallenkamp Melting Point Apparatus.

Synthesis

A 50 ml flask was degassed with pure and dry N_2 and charged with N-biotin (0.306g, 0.89 mmol) and DMSO (2 ml). A solution of APTS (0.35ml, 1.48 mmol) in DMSO (10 ml) was added dropwise (Scheme 2A2-1). After stirring at room temperature for 6h, the mixture was concentrated under reduced pressure to remove solvent and unreacted APTS. The residue was washed with diethyl ether, 3 × 50 mL, then extracted with

dichloromethane (2×50 mL). The white solid was filtered off, the combined extracts were

concentrated and dried *in vacuo* to give the product, Biotinyltriethoxysilane, as a white

solid (0.27 g, 67.3% yield, m.p 70°C.)
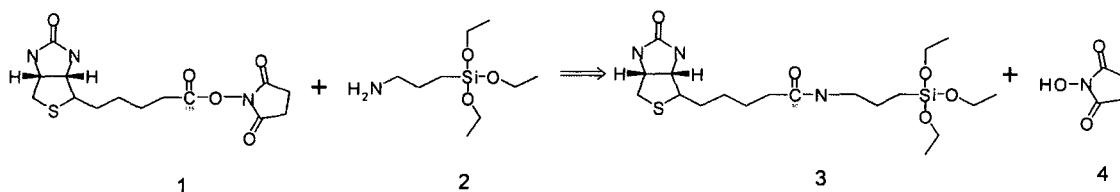
Scheme 2A2-1 The synthesis of biotinyltriethoxysilane

Results and Discussion:

The ^{1}H-NMR and ^{13}C-NMR spectra:

(a)
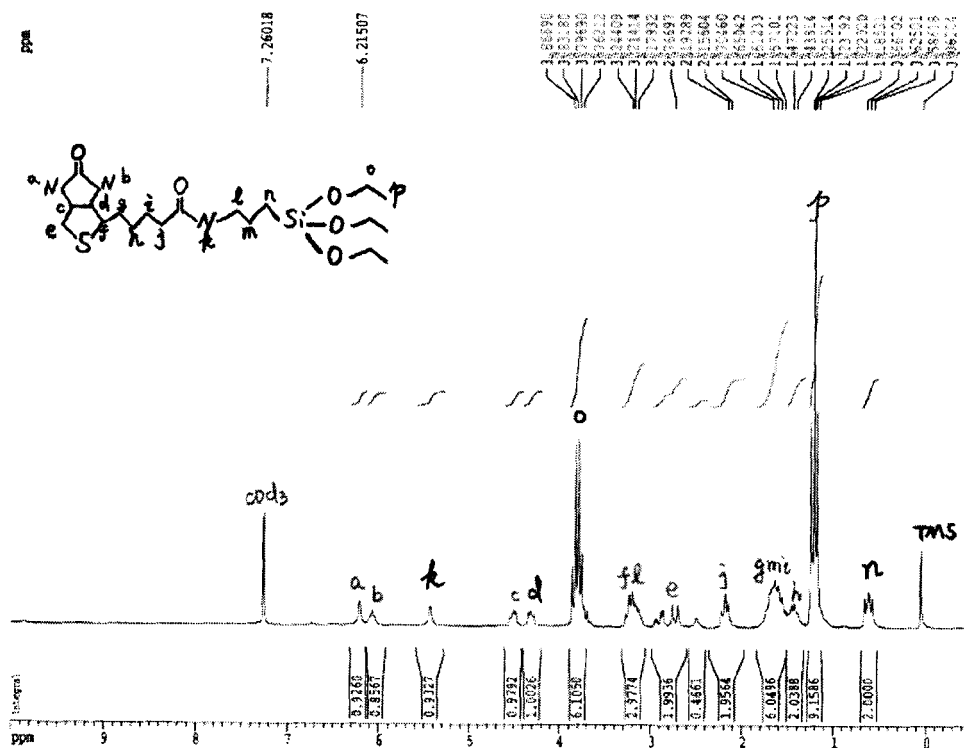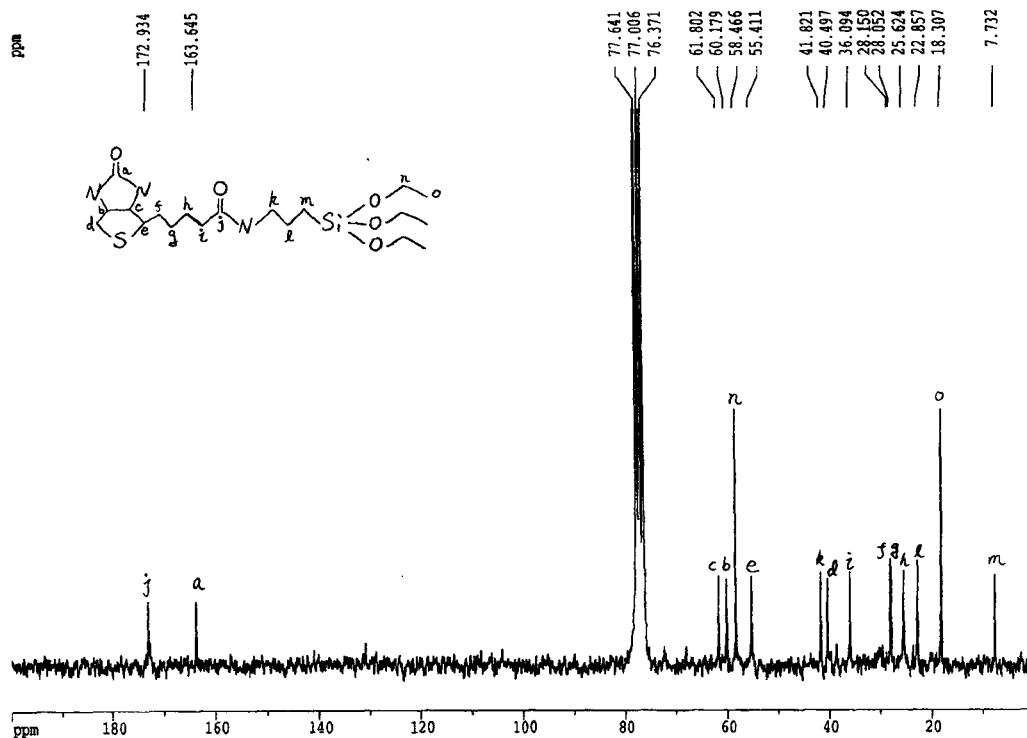
(b)

Figure 2A2-1 (a) The ^{1}H-NMR spectra of biotinyltriethoxysilane in CDCl$_3$ with 1%TMS;

(b) The ^{13}C-NMR spectra of biotinyltriethoxysilane in CDCl$_3$ with 1%TMS

^{1}H NMR (200.2 MHz, CDCl$_3$):

δ=0.62(t, J=8.1Hz, 2H, H$_n$), 1.22(t, J=7Hz, 9H, H$_p$), 1.44(m, 2H, H$_h$), 1.57~1.70(m, 2H,

H$_g$, 2H, H$_m$, 2H, H$_i$), 2.19(t, J=7.3Hz, 2H, H$_j$), 2.82(m, 2H, H$_e$), 3.10~3.28(m, 1H, H$_f$, 2H,

H$_l$), 3.81(dd, J=7Hz, J=14Hz, 6H, H$_o$), 4.32(m, 1H, H$_d$), 4.51(m, 1H, H$_c$), 5.43(1H, H$_k$),

6.07(1H, H$_b$), 6.22(1H, H$_a$) ppm

^{13}C NMR (50.3 MHz, CDCl$_3$):

δ=7.732(C$_m$), 18.307(C$_o$), 22.857(C$_l$), 25.624(C$_h$), 28.052(C$_g$), 28.150(C$_f$), 36.094(C$_i$),

40.497(C$_d$), 41.821(C$_k$), 55.411(C$_e$), 58.466(C$_n$), 60.179(C$_b$), 61.802(C$_c$), 163.645(C$_a$),

172.934(C$_j$) ppm

Analyses for ^{1}H NMR:

Hydrogen atom location	Chemical Shift (ppm)	integral area (number of H atoms)
a	6.22	0.9260
b	6.07	0.8567
c	4.51	0.9792
d	4.32	1.0026
e	2.82	1.9936
f+l	3.10~3.28	2.9774
g+m+i	1.57~1.70	6.0496
h	1.44	2.0388
j	2.19	1.9564
k	5.43	0.9327
n	0.62	2.0000
o	3.81	6.1050
p	1.22	9.1586

Table 2A2-1 Each peak with the corresponding chemical shift and integral area of the

1H-NMR spectra

^{29}Si NMR (300 MHz, CDCl$_3$):
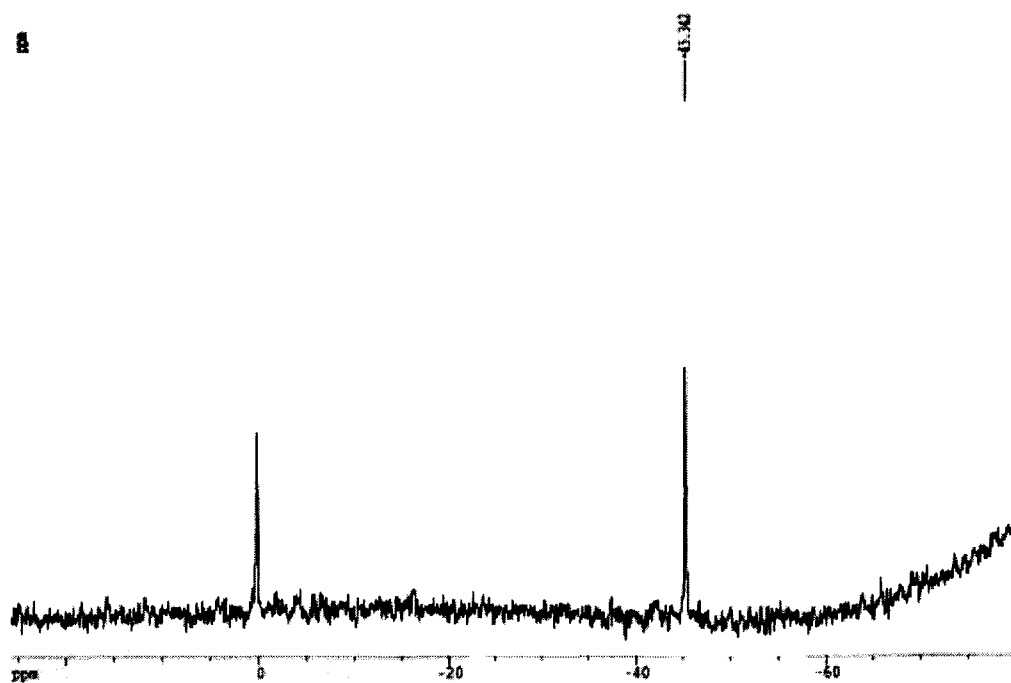
Figure 2A2-2 ^{29}Si-NMR spectrum of biotinyltriethoxysilane in CDCl$_3$
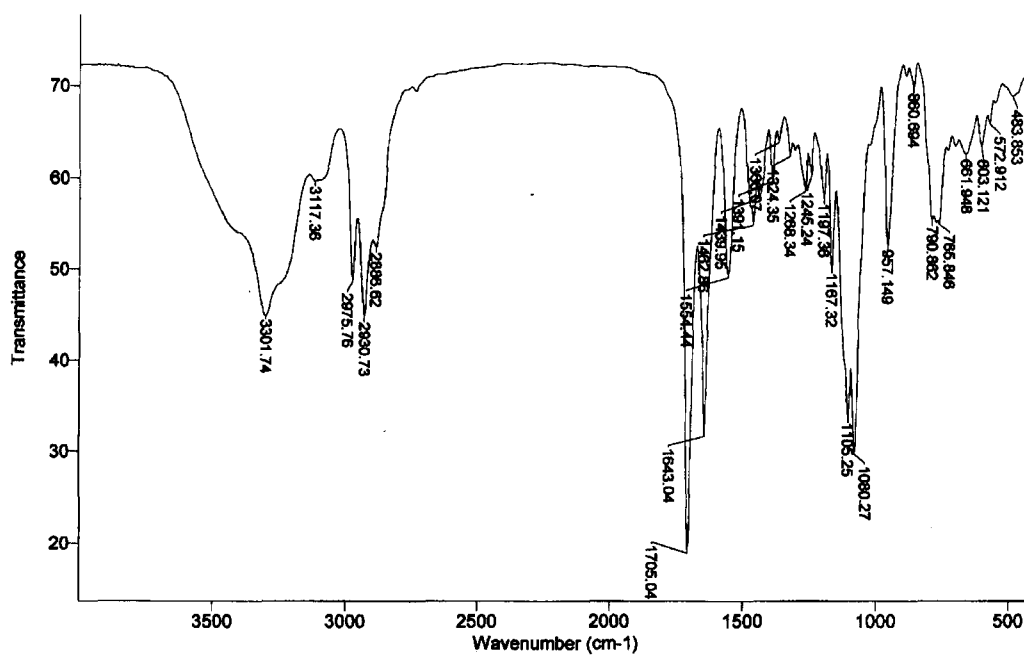
Figure 2A2-3 FT-IR spectrum of the biotinyltriethoxysilane in solid state

δ=-45.342(Si(OEt)$_3$), 0(TMS, internal reference) ppm

Fourier Transform Infrared spectra (Figure 2A2-3, KBr, cm^{-1}):

-CONH-:1680 cm^{-1}~1630 cm^{-1}

The LR-MSI spectrum assignment:

MS (LR-ESI):

m/z = 470.4 (M+Na, 100); 402.4 (M- OCH$_2$CH$_3$, 50); 448.4(M+H, 41);

917.6(2M+Na, 43); 895.6(2M+H, 9); 465.4(M+NH$_4$, 19); 486.4(M+Na+NH$_4$-2H, 8);

806.5(2M-2(OCH$_2$CH$_3$), 4); 359.3(M-2(OCH$_2$CH$_3$)+2H, 12);

207.0(CH$_3$CH$_2$CH$_2$Si(OCH$_2$CH$_3$)$_3$+H, 5); 115.0(CH$_2$CH$_2$CH$_2$SiOCH$_2$CH$_3$, 7);

82.4(2(CH$_2$CH$_3$)+Na+H, 10);
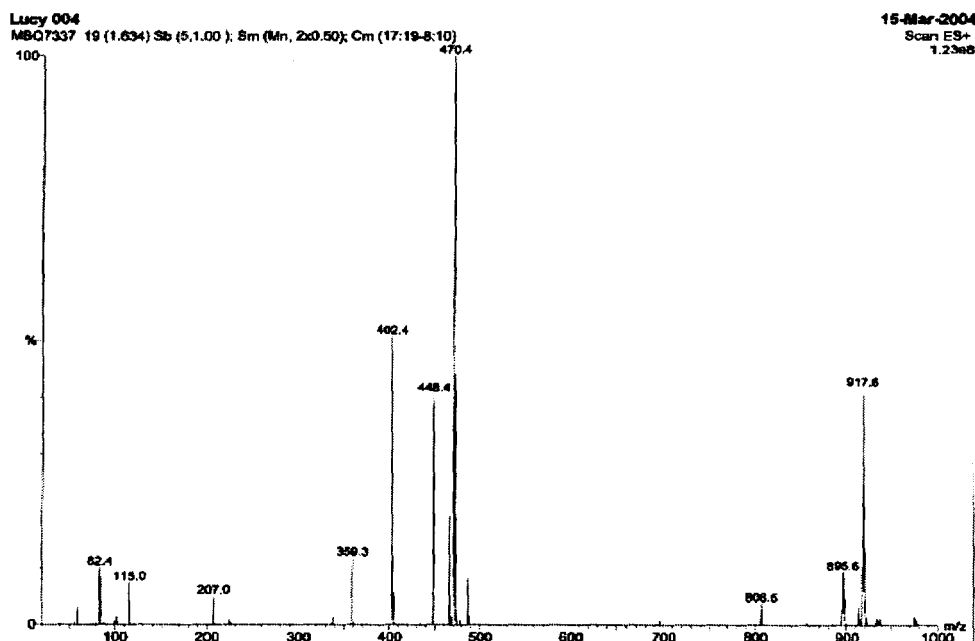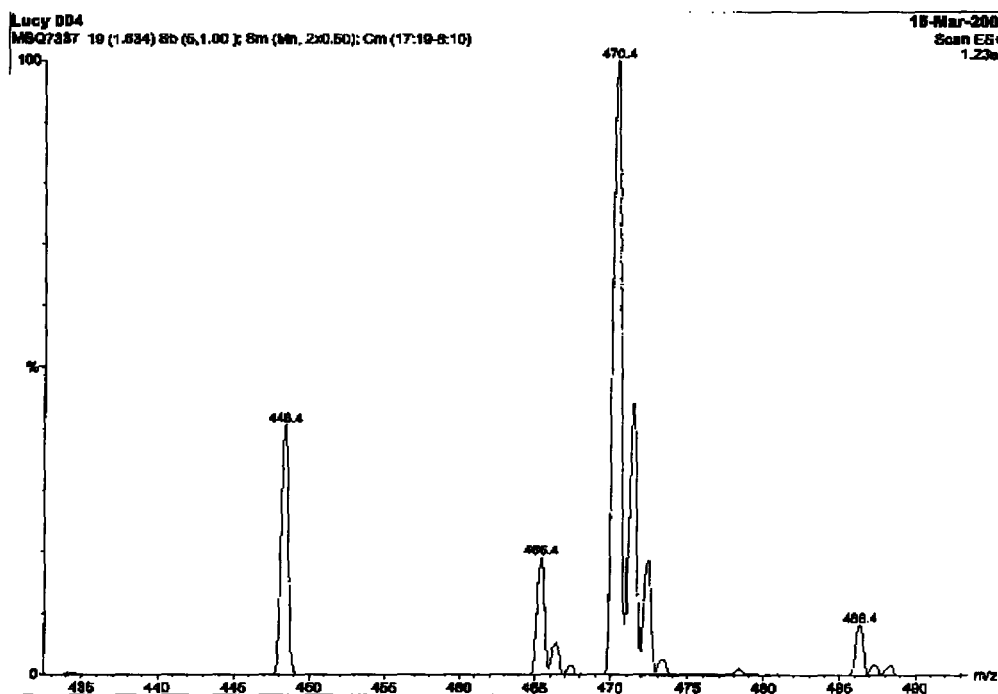
Figure 2A2-4 The electrospray of biotinyltriethoxysilane with low resolution

m/z	Proposed fraction	Proposed formula	Calculated m/z
84.2	$2(CH_2CH_3)+Na+H$	$C_4H_{11}Na$	82.1
115.0	$CH_2CH_2CH_2SiOCH_2CH_3$	$C_5H_{11}OSi$,	115.1
207.0	$CH_3CH_2CH_2Si(OCH_2CH_3)_3+H$	$C_9H_{23}O_3Si$	207.1
359.3	$M-2(OCH_2CH_3)+2H$	$C_{15}H_{29}N_3O_3SSi$	359.2
402.4	$M-OCH_2CH_3$	$C_{17}H_{32}N_3O_4SSi$	402.2
448.4	$M+H$	$C_{19}H_{38}N_3O_5SSi$	448.2
465.4	$M+NH_4$	$C_{19}H_{41}N_4O_5SSi$	465.3
470.4	$M+Na$	$C_{19}H_{37}N_3NaO_5SSi$	470.2
486.4	$M+Na+NH_4-2H$	$C_{19}H_{39}N_4NaO_5SSi$	486.2
806.5	$2M-2(OCH_2CH_3)$	$C_{34}H_{70}N_6O_8S_2Si_2$	806.4
895.6	$2M+H$	$2(C_{19}H_{39}N_3NaO_5SSi)+H$	895.5
917.6	$2M+Na$	$2(C_{19}H_{39}N_3NaO_5SSi)+Na$	917.4

Table 2A2-2 Each peak with the corresponding proposed fraction and formula

MS (HR-ESI):

$C_{19}H_{37}N_3NaO_5SSi$: calcd. 470.2121 (M+Na,100), found 470.2128 (HR-ESI)
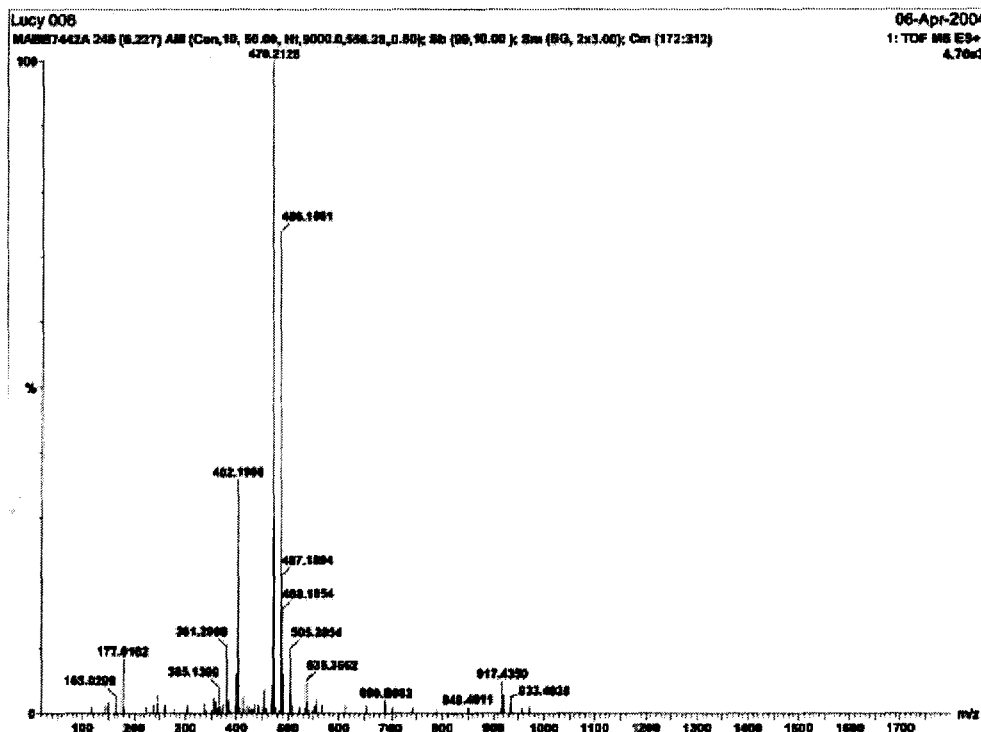
(a)
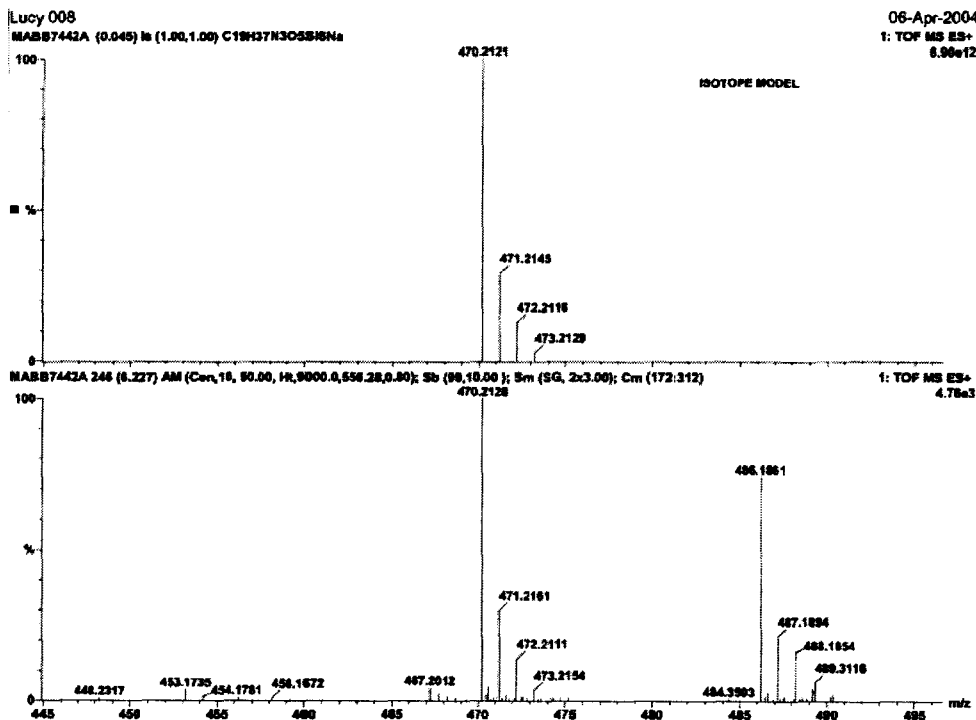
(b)
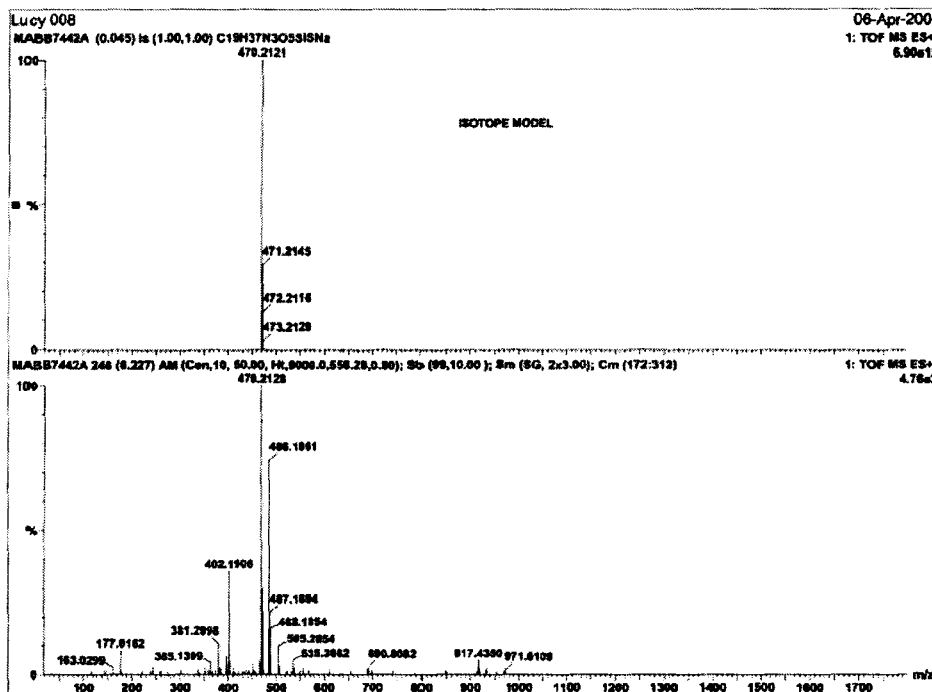
(c)

Elemental Composition Report   **Page 1**

Single Mass Analysis
Tolerance = 10.0 PPM / DBE: min = -1.5, max = 50.0
Isotope cluster parameters: Separation = 1.0   Abundance = 1.0%

Monoisotopic Mass, Odd and Even Electron Ions
476 formula(s) evaluated with 10 results within limits (all results (up to 1000) for each mass)
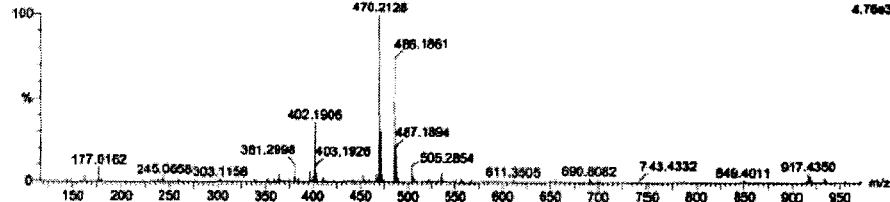
Mass	Calc. Mass	mDa	PPM	DBE	Score	Formula						
470.2128	470.2123	0.4	1.0	3.5	2	C20	H37	N3	O4	Na	S2	
	470.2121	0.7	1.4	3.5	1	C19	H37	N3	O5	Na	S	Si
	470.2114	1.3	2.8	4.5	10	C19	H33	N3	O9	Na		
	470.2146	-1.8	-3.9	-0.5	8	C15	H37	N3	O10	Na	Si	
	470.2148	-2.1	-4.4	-0.5	9	C16	H37	N3	O9	Na	S	
	470.2155	-2.7	-5.7	-1.5	3	C16	H41	N3	O5	Na	S2	Si
	470.2096	3.1	6.7	-1.0	7	C17	H39	N2	O7	Na	S2	
	470.2094	3.4	7.1	-1.0	4	C16	H39	N2	O8	Na	S	Si
	470.2089	3.8	8.1	8.5	5	C21	H33	N3	O4	Na	S	
	470.2087	4.0	8.6	8.5	6	C22	H33	N3	O5	Na	Si	

Minimum: -1.5
Maximum: 10.0   10.0   50.0

(d)

Figure 2A2-5 The electrospray of biotinyltriethoxysilane with high resolution

m/z	Proposed fraction	Proposed formula	Calculated m/z
177.0162	3(OCH$_2$CH$_3$)+Na+H+NH$_4$	C$_6$H$_{20}$NNaO$_3$	177.1341
245.0658	NH$_2$CH$_2$CH$_2$CH$_2$Si(OCH$_2$CH$_3$)$_3$+Na+H	C$_9$H$_{24}$NNaO$_3$Si	245.1423
303.1158	M+2H+CH$_2$CH$_3$+OCH$_2$CH$_3$-NHCH$_2$CH$_2$CH$_2$Si(OCH$_2$CH$_3$)$_3$	C$_{14}$H$_{27}$N$_2$O$_3$S	303.1742
381.2998	M+Na+H-2(OCH$_2$CH$_3$)	C$_{15}$H$_{28}$N$_3$NaO$_3$SSi	381.1518
402.1906	M-OCH$_2$CH$_3$	C$_{17}$H$_{32}$N$_3$O$_4$SSi	402.1906
403.1926	M-OCH$_2$CH$_3$+H	C$_{17}$H$_{33}$N$_3$O$_4$SSi	403.1961
470.2128	M+Na+NH$_4$-H	C$_{19}$H$_{40}$N$_4$NaO$_5$SSi	487.2386
486.1861	M+Na+NH$_4$-2H	C$_{19}$H$_{39}$N$_4$NaO$_5$SSi	486.2308
487.1894	M+Na+NH$_4$-H	C$_{19}$H$_{40}$N$_4$NaO$_5$SSi	487.2386
505.2854	M+2(CH$_2$CH$_3$)	C$_{23}$H$_{47}$N$_3$O$_5$SSi	505.3006
611.3505	M+3(OCH$_2$CH$_3$)+CH$_2$CH$_3$	C$_{27}$H$_{57}$N$_3$O$_8$SSi	611.3636
690.8082	M+Na+NHCH$_2$CH$_2$CH$_2$Si(OCH$_2$CH$_3$)$_3$	C$_{28}$H$_{59}$N$_4$NaO$_8$SSi$_2$	690.3490
743.4332	2M+Na+H+OCH$_2$CH$_3$-NHCH$_2$CH$_2$CH$_2$Si(OCH$_2$CH$_3$)$_3$	C$_{31}$H$_{58}$N$_5$NaO$_8$S$_2$Si	743.3394
849.4011	2M-OCH$_2$CH$_3$	C$_{36}$H$_{69}$N$_6$O$_9$S$_2$Si$_2$	849.4106
917.4350	2M+Na	C$_{38}$H$_{78}$N$_6$Na$_2$O$_{10}$S$_2$Si$_2$+Na	917.4344

Table 2A2-3 Each peak with the corresponding proposed fraction and formula

The reaction of N-hydroxysuccinimido-biotin and 3-Aminopropyltriethoxysilane in DMSO under room temperature gave a good yield of biotinyltriethoxysilane. The NMR (^{1}H NMR and ^{13}C NMR) data as well as high resolution mass spectra (ESI) and IR confirmed the structure of 3 as illustrated in assignments of the spectra in Table 2A2-1 to Table 2A2-3 along with Figure 2A2-1 to Figure 2A2-4, respectively.

Biotinyltriethoxysilane is a white solid with moderate moisture sensitivity. In wet CDCl$_3$ solution the white precipitate was observed during NMR measurement. The colour turns to pale yellow when it exposes to air.

Conclusion:

1) The yield of this synthesis is ~67.3%.

2) Biotinyltriethoxysilane becomes yellow when it adsorbs moisture.

3) The melting point of biotinyltriethoxysilane is ~70°C.

Chapter 3   Photo-flocculation of TiO$_2$ Microgel Mixed Suspensions[*]

3.1   Introduction

The controlled aggregation of colloidal suspensions is important in many technologies. For example, antibody mediated latex aggregation [1] is an established technology in bio-sensing. More recently, there have been many reports of bioassays that exploit colloidal gold aggregation.[2-7] For bio-sensing, a specific target triggers visible particle aggregation. In other applications such as papermaking, pigment manufacture, and water treatment, controlling colloidal aggregation is important and there are advantages in having a trigger that can turn off colloidal stability, initiating flocculation. Traditionally, the trigger is use of simple electrolytes; increasing salt concentration above the critical coagulation concentration induces rapid flocculation. However, many processes cannot tolerate high

---

[*] This work has led to one published paper in Langmuir 2008, 24, 9341-9343. This paper, Photoflocculation of TiO$_2$ Microgel Mixed Suspensions, was authored by Lu Ye, Chuanwei Miao, Michael Brook and Robert Pelton. In this publication, the polymeric microgel was prepared and provided by Chuanwei Miao, otherwise, all the research work was undertaken by me.

electrolyte loadings.   Other common aggregation triggers include, pH change [8], temperature change [9] and addition of polymeric flocculants. [10]

There are very few reports of using light to trigger nanoparticle aggregation. A number of reports from Eastoe's group describe the light triggered aggregation of emulsions [11], colloidal gold [12], vesicle suspensions [13] and most recently silica [14]. In each case, their colloidal dispersions were stabilized by a surfactant that decomposed with irradiation.

In this communication, we report a new light-triggered system we call photo-flocculation.   Our work exploits the photocatalytic properties of anatase (TiO_2). Fujishima and Honda showed that wet anatase generates hydroxyl, peroxy radicals and other reactive oxygen species when irradiated with UV.[15-17] These extremely aggressive radical species efficiently oxidize organic entities, including simple hydrocarbons, ultimately into CO_2. The photocatalytic properties of anatase have been exploited to give self-cleaning windows and antibacterial surfaces.[18]   Herein, we describe the use of photocatalysis to trigger colloidal or nanoparticle aggregation by changing TiO_2 from a positively charged to a negatively charged colloidal particle.

3.2   Results and Discussion

A commercial photocatalytic TiO_2 (Degussa P25) was derivatized with a DMSO solution of $H_2N(CH_2)_3Si(OEt)_3$ to give an aminosilane coating.[19] P25 is comprised of 80% anatase, 20% rutile [20] in the form of 0.1 μm aggregates of ~30 nm primary particles,

giving a nonporous solid with a specific surface area of 55±15 m^2 g^{-1}.[16] The TiO$_2$ particles were characterized before and after aminosilane treatment. Table 3-1 summarizes the electrophoretic mobility, particle size and surface composition (x-ray photoelectron spectroscopy) of TiO$_2$. Before derivatization, the titania was negatively charged with low nitrogen and no silicon contamination. Derivatization increased the surface silicon and nitrogen content due to the amino silane coating; our previous work showed that these conditions give an amino group density of 16 nm^{-2} when measured by polyelectrolyte titration and is 19 nm^{-2} when measured by conductometric titration, emphasizing the three dimensional nature of the amino silane treated surfaces. [19] In addition, the derivatization process gave a more complete dispersion of the TiO$_2$ particles as evidenced by lower average particle size. Finally, UV irradiation removed most of the nitrogen and about half of the silicon.

Electrophoresis measurements were used to follow changes in the surface composition. Initially negatively charged titania was rendered positive by the amino silane but reverted to negative when the surface amino groups were removed by reactive oxygen species.

The photodecomposition of the amino silane surface layer was rapid. Figure 3-1 shows electrophoretic mobility and average particle sizes of the amino-TiO$_2$ as a function of exposure time. Within 20 seconds exposure to UV, the sign of the electrophoretic mobility changed from positive to negative. There appeared little further change in the TiO$_2$ surface after 60 seconds of irradiation. The corresponding average particle size results, also shown in Figure 3-1, suggests some aggregation occurs as the particles

crossed the isoelectric point. Untreated TiO_2 is an electrostatically stabilized colloid in water that will aggregate near the isoelectric point.[21, 22] The absence of large-scale aggregation reflects the rapid transition through the isoelectric point from cationic to anionic particles.

The photocatalytic removal of the amino groups was used to initiate flocculation of mixed suspensions. Figure 3-2 shows a series of images from an experiment in which a mixed dispersion of amino-TiO_2 and poly(vinylamine) (PVAm) microgels was irradiated with UV. The microgels are water swollen, crosslinked PVAm particles; their properties are summarized in the experimental section.[23] Like the amino-TiO_2 particles, the microgels are positively charged due to a very high content of amino groups. The initial mixed cationic suspension was colloidally stable, whereas catastrophic flocculation was observed after 300 s irradiation (see Figure 3-2) due to the transformation of positive TiO_2 into negatively charged TiO_2 particles which aggregated the positively charged PVAm microgel particles. As a control experiment, PVAm microgel without TiO_2 did not aggregate with UV irradiation.

Finally from a colloid science perspective, the results in Figure 3-2 are an example of a heteroflocculation due to the electrostatic attraction between oppositely charged particles. The major features of electrostatic heteroflocculation are well documented from both theoretical [24] and experimental [25 26] perspectives. The novel feature of our work was that cationic particles were converted into anionic particles *in situ* by light.

3.3   Experimental

AEROXIDE® TiO$_2$ P 25 was donated by Degussa Corporation (Parsippany, NJ, USA). 3-Aminopropyltriethoxysilane (APTS), hexamethyldisilazane, chlorotrimethylsilane, anhydrous methyl sulfoxide and anhydrous N,N-dimethylformamide were purchased from Aldrich and used as received. Potassium nitrate solution (1.0 mM, pH=7.4±0.2) was prepared by dissolving 0.1011 g KNO$_3$ in 1L MilliQ water. MilliQ water was used to wash samples and to prepare the buffer.

PVAm microgel was prepared by precipitation polymerization of N-vinylformamide in methyl ethyl ketone followed by hydrolysis in an alkali condition. Further details have been published elsewhere.[23] At pH 7 in 5 mM NaCl, the gels had an average diameter of 1.5 μm, a dispersity (D90-D10/D50) of 3.14 and a water content of 96 wt%.

TiO$_2$–NH$_2$ preparation. A 500 mL flask was degassed with pure, dry N$_2$ and charged with TiO$_2$ (0.3 g, 3.756 mmol) and anhydrous DMSO (200 mL). The particles were dispersed in anhydrous DMSO using ultrasonication for 10 min. Afterward, APTS (1.5 mL, 6.346 mmol) was injected into the flask. After stirring at 85 °C for 16 h, the solid particles were deposited by centrifugation and then washed with anhydrous DMSO (3 × 180 mL). The TiO$_2$ particles were dispersed in anhydrous DMF (150 mL) using ultrasonication for 5 min and then were cured in the presence of 100 μL hexamethyldisilazane and 10 μL chlorotrimethylsilane in a nitrogen stream at 120 °C for 2 h. After curing, the TiO$_2$ particles were washed with anhydrous DMF (3 × 180 mL) and

then MilliQ water (3 × 180 mL). Finally, the particles were dried in vacuo at 65 °C for the measurements.

UV Irradiation. A Black-Ray® XX-15BLB UV Bench Lamp (365 nm) was applied as the light source in the photodegradation of aminosilanized TiO_2 nanoparticles assay. The intensity of UV irradiation was measured by a Traceable® Ultra Violet Light Meter (VWR). An incident intensity of 23 W m^{-2} to the surface of the TiO_2 suspension was controlled by adjusting the position of the light source. 1.5 mL of untreated TiO_2 suspension (0.5 mg/mL) or aminosilanized TiO_2 (0. 5 mg/mL) in KNO_3 solution (1mM, pH = 7.4 ± 0.2) were placed in a sealed quartz 3.5 mL cuvette containing a magnetic stirring bar. The stirred sample was exposed to short periods (5s, 10s, 15s, etc.) of UV illumination. After each exposure, samples were removed for particle size and electrophoresis measurements. The pH value of the solution did not change as a consequence UV illumination.

Electrophoretic mobilities were measured with a ZetaPlus Zeta Potential Analyzer (Brookhaven Instruments Corp.) using the phase analysis light scattering mode. The samples were dispersed in KNO_3 solution (1mM, pH = 7.4 ± 0.2) at a concentration of 0.04 mg/mL. The error bars of the electrophoretic mobilities represent the standard error of the mean value of 10 runs (15 cycles per run).

Particle size distributions were measured with a Mastersizer 2000 (Malvern Instruments). Samples were dispersed in KNO_3 solutions (1 mM, pH = 7.4 ± 0.2) that were filtered with a 0.2 μm filter disc prior to use to remove dust.

For the heteroflocculation experiments, 2.5 mL of mixed suspension of TiO_2-NH_2 (0.2 mg/mL) and PVAm microgel 0.2mL (0.34 wt%) dispersed in 1m M KNO_3 at pH 7.4, was irradiated (23 W m.$^{-2}$) in a quartz cuvette. The irradiation was interrupted at 1 min intervals and photographs were taken.

	Electrophoretic mobility ($\times 10^{-8}$ m^2/ Vs) in 1 mM KNO$_3$ pH 7.4 $\pm$ 0.2	Size (volume weighted mean diameter μm)	XPS result (Atom %)		
			N	Si	Ti
Untreated P25 TiO$_2$	-1.04 $\pm$ 0.17	4.65	0.5	0	26.4
Aminosilanized P25 TiO$_2$	3.18 $\pm$ 0.09	1.61	3.5	3.2	21.1
Aminosilanized P25 TiO$_2$ after UV illumination	-1.61$\pm$ 0.11	4.01	0.4	1.8	25.3

Table 3-1 Properties of untreated, aminosilanized P25 TiO$_2$ and aminosilanized P25 TiO$_2$ after 5 min UV illumination
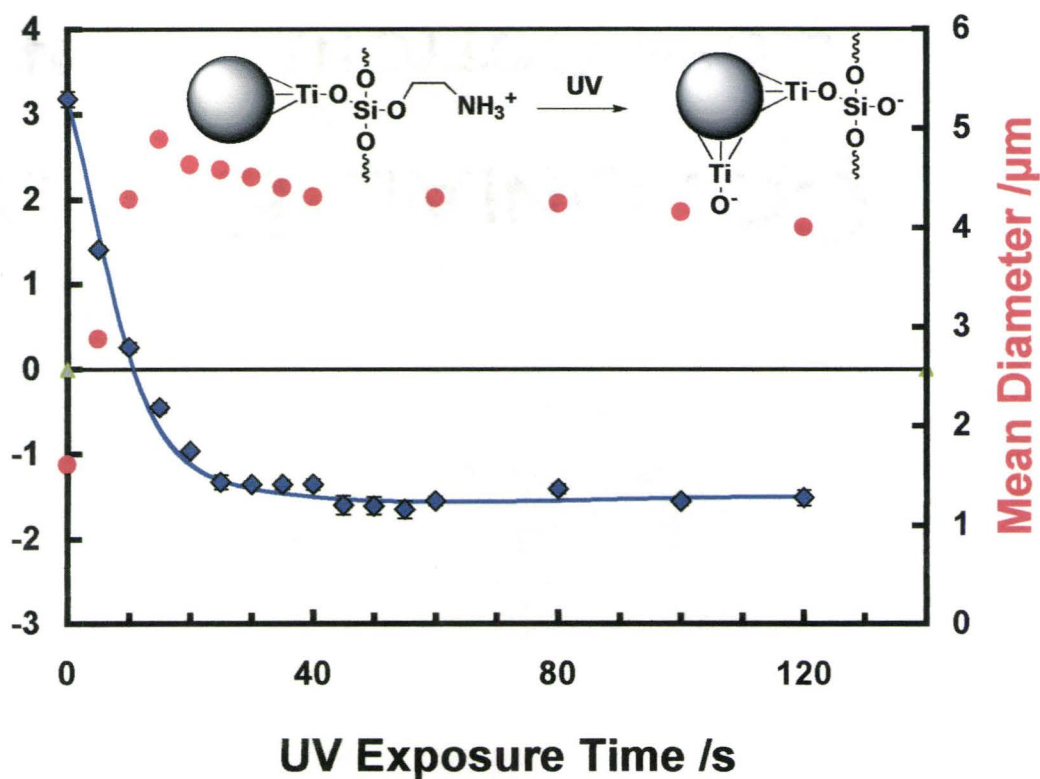
Figure 3-1　Electrophoretic mobility and particle size of titania treated with amino silane as a function of UV irradiation time.
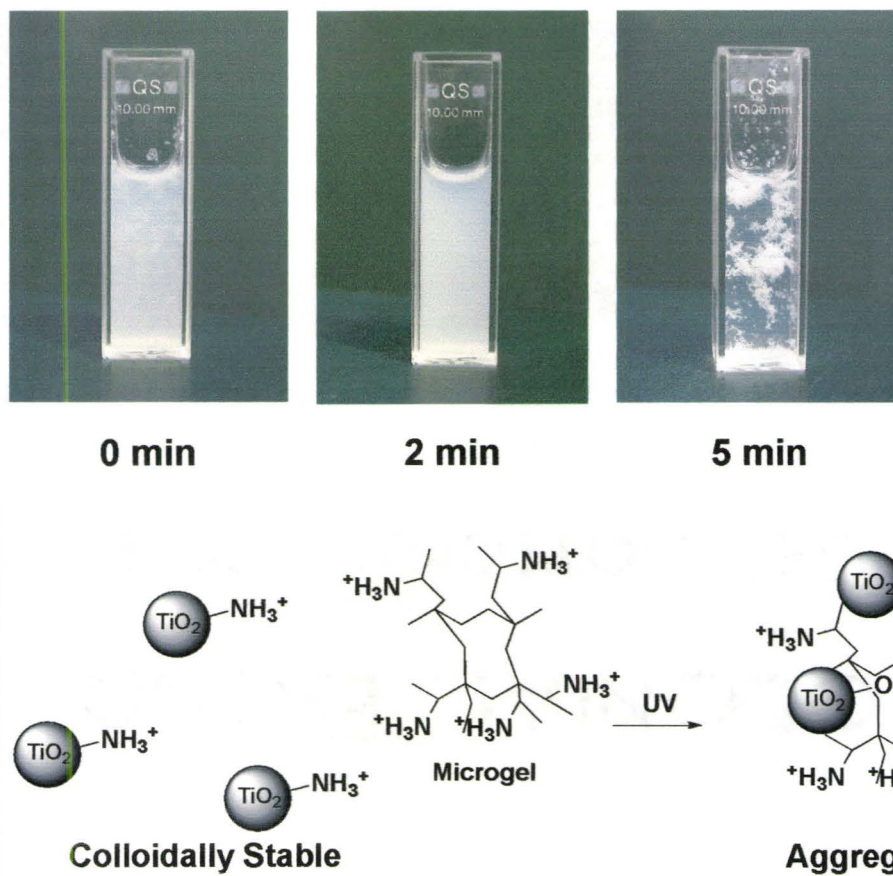
Figure 3-2   Photograph of mixed suspension of TiO_2 –NH_2 and PVAm microgel before and after UV irradiation.

3.4   References

1.   Pichot, C., Surface-functionalized latexes for biotechnological applications. *Current Opinion in Colloid & Interface Science* **2004**, 9, (3-4), 213-221.

2.   Huang, S.-H., Gold nanoparticle-based immunochromatographic test for identification of Staphylococcus aureus from clinical specimens. *Clinica Chimica Acta* **2006**, 373, (1-2), 139-143.

3.   Beermann, B.; Carrillo-Nava, E.; Scheffer, A.; Buscher, W.; Jawalekar, A. M.; Seela, F.; Hinz, H. J., Association temperature governs structure and apparent thermodynamics of DNA-gold nanoparticles. *Biophysical Chemistry* **2007**, 126, (1-3), 124-131.

4.   Wang, Z. X.; Levy, R.; Fernig, D. G.; Brust, M., Kinase-catalyzed modification of gold nanoparticles: A new approach to colorimetric kinase activity screening. *Journal of the American Chemical Society* **2006**, 128, (7), 2214-2215.

5.   Xu, C.; Wang, H.; Peng, C.; Jin, Z.; Liu, L., Colloidal gold-based immunochromatographic assay for detection of diethylstilbestrol residues. *Biomedical Chromatography* **2006**, 20, (12), 1390-1394.

6.   Shim, W. B.; Yang, Z. Y.; Kim, J. Y.; Choi, J. G.; Je, J. H.; Kang, S. J.; Kolosova, A. Y.; Eremin, S. A.; Chung, D. H., Immunochromatography using colloidal gold-antibody probe for the detection of atrazine in water samples. *Journal of Agricultural and Food Chemistry* **2006**, 54, (26), 9728-9734.

7.   Zhao, W.; Chiuman, W.; Lam, J. C. F.; McManus, S. A.; Chen, W.; Cui, Y.; Pelton, R.; Brook, M. A.; Li, Y., DNA Aptamer Folding on Gold Nanoparticles: From Colloid Chemistry to Biosensors. *Journal of the American Chemical Society* **2008**, 130, (11), 3610-3618.

8.   Sawai, T.; Yamazaki, S.; Ikariyama, Y.; Aizawa, M., pH-Responsive swelling of the ultrafine microsphere. *Macromolecules* **1991**, 24, (8), 2117-18.

9.   Deng, Y. L.; Xiao, H. N.; Pelton, R., Temperature-sensitive flocculants based on poly(N-isopropylacrylamide-co-diallyldimethylammonium chloride). *Journal of Colloid and Interface Science* **1996**, 179, (1), 188-193.

10.   Smith-Palmer, T.; Pelton, R., Flocculation of Particles In *Encyclopedia of Surface and Colloid Science*, Marcel Dekker: 2002; pp 2207-2224.

11.   Eastoe, J.; Dominguez, M. S.; Cumber, H.; Wyatt, P.; Heenan, R. K., Light-sensitive microemulsions. *Langmuir* **2004**, 20, (4), 1120-1125.

12.   Vesperinas, A.; Eastoe, J.; Jackson, S.; Wyatt, P., Light-induced flocculation of gold nanoparticles. *Chemical Communications* **2007**, (38), 3912-3914.

13.   Eastoe, J.; Vesperinas, A.; Donnewirth, A. C.; Wyatt, P.; Grillo, I.; Heenan, R. K.; Davis, S., Photodestructible vesicles. *Langmuir* **2006**, 22, (3), 851-853.

14. Salabat, A.; Eastoe, J.; Vesperinas, A.; Tabor, R. F.; Mutch, K. J., Photorecovery of Nanoparticles from an Organic Solvent. *Langmuir* **2008,** 24, (5), 1829-1832.

15. Fujishima, A.; Honda, K., Electrochemical photolysis of water at a semiconductor electrode. *Nature* **1972,** 238, (5358), 37-8.

16. Hoffmann, M. R.; Martin, S. T.; Choi, W.; Bahnemann, D. W., Environmental Applications of Semiconductor Photocatalysis. *Chemical Reviews (Washington, D. C.)* **1995,** 95, (1), 69-96.

17. Hashimoto, K.; Irie, H.; Fujishima, A., TiO2 photocatalysis: A historical overview and future prospects. *Japanese Journal of Applied Physics, Part I: Regular Papers and Short Notes* **2005,** 44, (12), 8269-8285.

18. Maness, P.-C.; Smolinski, S.; Blake, D. M.; Huang, Z.; Wolfrum, E. J.; Jacoby, W. A., Bactericidal activity of photocatalytic TiO2 reaction: toward an understanding of its killing mechanism. *Applied and Environmental Microbiology* **1999,** 65, (9), 4094-4098.

19. Ye, L.; Pelton, R.; Brook, M. A., Biotinylation of TiO2 nanoparticles and their conjugation with streptavidin. *Langmuir* **2007,** 23, (10), 5630-5637.

20. Wold, A., Photocatalytic properties of TiO_2. *Chem. Mater.* **1993,** 5, 280-283.

21. Furlong, D. N.; Parfitt, G. D., Electrokinetics of titanium dioxide. *Journal of Colloid and Interface Science* **1978,** 65, (3), 548-54.

22. Snoswell, D. R. E.; Duan, J. M.; Fornasiero, D.; Ralston, J., Colloid stability of synthetic titania and the influence of surface roughness. *Journal of Colloid and Interface Science* **2005,** 286, (2), 526-535.

23. Miao, C.; Chen, X.; Pelton, R., Adhesion of Poly(vinylamine) Microgels to Wet Cellulose. *Industrial & Engineering Chemistry Research* **2007,** 46, (20), 6486-6493.

24. Hogg, R.; Healy, T. W.; Fuerstenau, D. W., Mutual Coagulation of Colloidal Dispersions. *Transactions of the Faraday Society* **1966,** 62, 1638-1651.

25. Bleier, A.; Matijevic, E., Heterocoagulation. I. Interactions of monodispersed chromium hydroxide with polyvinyl chloride latex. *Journal of Colloid and Interface Science* **1976,** 55, (3), 510-524.

26. Luckham, P.; Vincent, B.; Hart, C. A.; Tadros, T. F., The Controlled Flocculation of Particulate Dispersions Using Small Particles of Opposite Charge .1. Sediment Volumes and Morphology. *Colloids and Surfaces* **1980,** 1, (3-4), 281-293.

Chapter 4   Selective flocculation and killing of *Escherichia coli* with antibody coated photocatalytic TiO₂[*]

4.1   Introduction

The use of photocatalytic TiO_2 for killing pathogens has been extensively studied since the first work done by Matsunaga, Tomada, Nakajima and Wake in 1985.[1] Under near UV irradiation (<380nm), TiO_2 generates reactive oxygen species (ROS).[2-4] These ROS are extremely aggressive, being capable of oxidizing cell membranes[5] or damaging DNA/RNA molecules[6,7] to lead to the death of pathogens. However, the short lifetime of ROS[3,8] results in short effective diffusion lengths and low pathogen killing efficiency. Kawahara and Tatsuma's experimental results suggested that ROS can diffuse as far as 50-70 μm through the vapor phase.[9,10] However, in Kikuchi's report, it is also pointed

---

[*] This work will result in one paper, entitled, Selective flocculation and killing of *Escherichia coli* with antibody coated TiO₂, authored by Lu Ye, Robert Pelton, Carlos Filipe, Hai Wang, Luba Brovko, and Michael Brook. The paper is currently being prepared, and will be published soon. In this paper, knowledge related to *Pseudomonas putida* was provided by Hai Wang and Luba Brovko. This contribution makes them co-authors. The treatment of bacteria was guided by Carlos Filipe, which makes him a coauthor. While the research benefitted from the information provided by these researchers, all the research was undertaken by me.

out that 50 μm was too far for hydroxyl radicals to travel and they thus concluded that the active long-range bactericidal disinfection agent was H_2O_2 generated by the coupling of hydroxyl radicals.[11] Therefore, reducing the distance between the photocatalytic TiO_2 and the target bacteria is the key to improve the photodisinfection efficiency of UV-TiO_2 system.

TiO_2 has been reported to be an effective disinfection agent to kill a variety of microorganisms including viruses, bacteria, protozoa, and fungi.[12] However, depending on the application, it is not always wise to kill all the microorganisms around us because some microorganisms are beneficial to humans. For instance, *Pseudomonas putida* (*P. putida*), which lives in soil, can clean up the pollutants in soil[13, 14] and even protect some plants from certain plant diseases.[15] That is to say, humans cannot survive without certain microorganisms. On the other hand, we need to remove or kill many pathogens in our environment. Therefore, there is a need to achieve selective disinfection of certain microorganism, while keeping others alive. However, selective photodisinfection of bacteria using TiO_2 has rarely been reported. This is probably due to the difficulty of effectively delivering TiO_2 to the targeted microorganisms, in another words, there are no biological, chemical or physical interactions between TiO_2 and microorganisms that can be used to control the selectivity of disinfection. We hypothesized that coupling targeting biomolecules (for instance, antibodies that are responsible for specific binding to the target bacteria) to photocatalytic TiO_2 surfaces, promotes the specific binding of catalyst to the target bacteria, and leads to selective photodisinfection under band-gap irradiation.

There are two main challenges involved in this work. One lies in effectively attaching antibodies to photocatalytic TiO_2 surfaces. Although many studies on the fabrication and applications of antibody conjugated particles, such as SiO_2,[16] gold,[17, 18] silver,[19] magnetic nanoparticles,[20, 21] and latex,[22] have been reported, very few samples about antibody conjugated TiO_2 particles have been explored except the work done by Xu.[23] In her report, antibodies were physisorbed to TiO_2 nanoparticles and these modified TiO_2 nanoparticles showed a high efficiency of killing cancer cells, depending on the recognition effect of antibodies on TiO_2 surfaces. However, the physisorptive method for the preparation of biomolecules coated particles has some disadvantages: 1) some undesired molecules may occupy parts of the particle surfaces due to the nonspecific adsorption; 2) electrostatic force can deform the spatial structure of the biomolecules, which is important in maintaining the biofunctions of biomolecules; 3) the strong dependence of the physisorptive process on local environmental conditions such as pH values, salt concentrations, temperature and agitation results in limited applications and poor reproducibility.[24, 25]

Our solution is to use streptavidin/biotin complexation ($K_a=10^{15}$ M^{-1}) [26, 27] to couple biotinylated *E. coli* antibody with biotinylated photocatalytic TiO_2 colloidal particles. Biotinylated *E. coli* antibody is commercial product. Streptavidin/biotin complexation is well known for their super stable binding, being able to withstand high temperatures (up to 132 °C), extreme changes in pH (2-13), organic solvents and even some denaturing agents such as 8M guanidine-HCl.[26, 28] This work is base on our previous work, in which biotinylated TiO_2 particles have been obtained by treating TiO_2 nanoparticles first with 3-

aminopropyltriethoxysilane and then with *N*-hydroxysuccinimidobiotin and the bioconjugation of streptavidin with biotinylated TiO_2 has been demonstrated and studied.[29] In this work, biotinylated *E. coli* antibodies were conjugated with streptavidin-biotinylated TiO_2 particles to prepare antibodies coated photocatalytic TiO_2 particles.

The other challenge is identification of different bacteria in a mixed bacterial suspension. In the selective photodisinfection experiments, two classes of bacteria are used: *E. coli* K12 as the target bacteria and *P. putida* as the control bacteria. These two classes of bacteria are similar in their appearances. We adopted a special culture medium, *E. coli/Coliform* count plate (Petrifilm[TM], 3M[TM]),[30] to identify *E. coli* from other non-*E. coli/*Coliform bacteria such as *P. putida*. On these plates, after the bacteria are cultured at 37 °C for 48 h, only those *E. coli* colonies will grow with visible trapped bubbles, whereas non-*E. coli/Coliform* bacteria such as *P. putida* colonies will not grow with bubbles. Thereby, *E. coli* colonies can be identified simply by this characteristic.

In the present work, we report a strategy for the selective flocculation and disinfection of bacteria for the first time by using photocatalytic titania conjugated with a special targeting antibody. Two elements are required: the preparation of antibody conjugated TiO_2 nanoparticles and their application in a mixed bacterial suspension containing the targeted bacteria and the control bacteria. The antibody attached to TiO_2 surfaces is expected to promote deposition of the TiO_2 particles onto the surface of the target bacteria. Our work revealed the feasibility of using explicit antibody conjugated TiO_2 nanoparticles to selectively kill the targeted bacteria using UV while keep other bacteria alive.

4.2 Experimental Section

4.2.1   Materials

TiO$_2$ particles (anatase, 3.9×10^3 kg/m^3, 99+ %) were purchased from Aldrich and used as received. The anatase particles have been characterized in our previous work [29]. The specific surface area (SSA) of TiO$_2$ particles, which is 16.0×10^3 m^2/kg, was obtained on a Quantachrome Nova 2200 by nitrogen absorption. Biotinylated TiO$_2$ nanoparticles were prepared by treating TiO$_2$ nanoparticles with 3-aminopropyltriethoxysilane (APTS) in anhydrous DMSO, followed by reaction with N-hydroxysuccinimidobiotin (Scheme 4-1), as described in our previous work.[29] Streptavidin from *Streptomyces avidinii* and atto-610-streptavidin were purchased from Fluka and used as received. Biotin was purchased from Sigma and used as received. Biotinylated *E. coli* antibody (ab20640) was purchased from Abcam. Plasmid pCA24N carries the gene coding for a green fluorescent protein (GFP) variant, which has enhanced excitation at 488nm.[31] *Escherichia coli* (*E. coli*) K12 stain DH5α (Invitrogen, Burlington, Canada) was cultured according to the standard protocol. Luria-Bertani (LB), used as the media for *E. coli* culture, contains 10 g of tryptone (EMD), 5 g of yeast extract (EMD), and 10 g of NaCl (Aldrich) per liter. Antibiotic chloramphenicol was purchased from Fluka and prepared at a concentration of 34μg/mL in dry ethanol. Isopropyl β-D-1-thiogalactopyranoside (IPTG) (Fermentas, Burlington, ON, Canada) was used to induce expression of green fluorescent protein in *E. coli*. *Pseudomonas putida* (*P. putida*) strain LV 2-4 (culture: CRIFS C852) was kindly provided by Dr. Luba Brovko from the Univeristy of Guelph. Phosphate Buffered Saline

(PBS) buffer (137 mM NaCl, 2.7 mM KCl, 4.2 mM Na_2HPO_4, 1.4 mM KH_2PO_4, pH 7.0) was autoclaved before use. MilliQ grade water (equipment) was used for preparing all the aqueous solutions. *E. coli/coliform* count plates (Petrifilm[TM]) were purchased from 3M[TM] company and used according to the manufacturer's instructions.

4.2.2   Experiments

1) Cell culture

E. coli K-12 stain DH5α (Invitrogen, Burlington, Canada) was transformed with plasmid pCA24N, and inoculated into fresh sterilized autoclaved Luria-Bertani (LB) media supplemented with 0.1% chloramphenicol solution (34μg/ml) from a single colony and grown up aerobically (37 °C, 180rpm) to get an OD_{600} of 1.0. For the case in which green fluorescent protein (GFP) is needed, IPTG was added, with a final concentration of 0.5mM, into the media to induce expression of GFP, when OD_{600} reached 0.6-0.8.

P. putida LV 2-4 (culture: CRIFS C852) was kindly provided by Dr. Luba Brovko from the University of Guelph. *P. putida* was cultured in the same conditions as *E. coli* except that the temperature was set at 30 °C.

Phosphate Buffered Saline (PBS) buffer (137 mM NaCl, 2.7 mM KCl, 4.2 mM Na_2HPO_4, 1.4 mM KH_2PO_4, pH 7.2) was autoclaved before use. After culture, both bacteria were collected separately by centrifugation at 8500 rpm for 10min. The harvested cell pellet was dispersed in PBS buffer and centrifuged again. This wash process was repeated 3 times, for completely removal of the culture broth. Finally the two resulting pellets were separately resuspended and diluted to cell density of 3.8×10^8

colony forming units per mL (CFU/mL) in sterile PBS buffers. These culture solutions were stored at 4°C for the further use in the photodisinfection experiments. The colony forming unit counts per mL were tested by spread plate method using regular *E. coli* LB-agar media.

2) Preparation of *E. coli* antibody conjugated TiO$_2$ colloidal particles (EA TiO$_2$) and control particles including untreated TiO$_2$ colloidal particles and streptavidin-biotinylated TiO$_2$ colloidal particles

(a) Biotinylated TiO$_2$ preparation.

A 500 mL flask was degassed with pure, dry N$_2$ and charged with TiO$_2$ (12 mg, 0.15 mmol) and anhydrous DMSO (50 mL). The particles were dispersed in anhydrous DMSO using ultrasonication for 10 min. Afterward, APTS (0.1 mL, 0.423 mmol) was injected into the flask. After stirring at 85 °C for 5 h, the solid particles were deposited by centrifugation and then washed with anhydrous DMSO (3 × 180 mL) to remove the excess APTS. After washing, the particles were dispersed in anhydrous DMSO (50 mL) again and cured in a nitrogen stream at 120 °C for 8 h. After curing, the TiO$_2$ particles were allowed to react with *N*-hydroxysuccinimidobiotin at room temperature for 3 h. Finally, the solid particles were washed with anhydrous DMSO (3×180mL), followed by MilliQ water (3×180mL), and then dried in vacuo at 65 °C to remove the residual solvents.

(b) EA TiO2 and streptavidin-coated TiO2 preparation.

The biotinylated TiO_2 particles (1.2 mg) were dispersed in 3 mL of PBS buffer (pH 7)

through ultrasonication (Bransonic Ultrasonic cleaner Model: 3510R-DTH, Branson

Ultrasonic Corporation USA) for 2 min. Streptavidin solution at a concentration of 0.5

g/L was prepared by dissolving lyophilized streptavidin in the same PBS buffer as

described above. The streptavidin solution (2mL) and the biotinylated TiO_2 suspension

(3mL) were then mixed and agitated at room temperature for 1 h in dark. After that, the

particles were deposited by centrifugation at 12000rpm for 10 min. The absorbance value

of the supernatant liquid was tested at 282nm using a UV-vis spectrum. Then the

particles were washed according to a fixed procedure: 1) disperse particles in 3mL PBS

buffer by ultrasonication for 2 min; 2) deposit particles by centrifugation at 12000rpm for

10 min; and 3) test the absorbance value of the supernatant liquid at 282nm, and remove

the supernatant liquid. The washing process was repeated until the absorbance value

reached the baseline (±0.0005), the absorbance of the blank PBS buffer, indicating that

the unbound streptavidin molecules had all been washed off from the biotinylated TiO_2

colloidal particles. After that, the preparation of streptavidin-biotinylated TiO_2 colloidal

particles was complete (Figure 4-1). The density of the attached streptavidin on TiO_2

surfaces could be calculated using Equation 1.

The streptavidin-coated TiO_2 colloidal particles (1.2 mg) were then mixed with

biotinylated *E. coli* antibody (60 μg) in 1mL PBS buffer at pH 7 for 1 h in dark to prepare

E. coli antibody conjugated TiO_2 colloidal particles (EA TiO_2) (Figure 4-1). The ratio of

streptavidin-coated TiO_2 colloidal particles to biotinylated *E. coli* antibody for EA TiO_2

preparation was determined by an experiment, described as below. First, 1.2 mg

streptavidin-coated TiO_2 colloidal particles were dispersed in 1 mL of PBS buffer through ultrasonication for 2 min. Then, following each addition ($3\mu L$, 4 g/L) of biotinylated *E. coli* antibody solution to the streptavidin-coated TiO_2 colloidal particles suspension, the system was agitated for 20 min in dark, and then centrifuged at 12000rpm for 10 min. The absorbance value of the supernatant liquid was then tested at 280nm. The process of addition-agitation-centrifugation-testing was repeated until the absorbance value was higher than 0.004, indicating the addition of biotinylated *E. coli* antibody was slightly overdosed (3 μg biotinylated *E. coli* antibody in the supernatant liquid of the solution) for coupling with 1.2 mg streptavidin-coated TiO_2 in 1mL PBS buffer. This experimental results showed that 60 ± 14 μg of biotinylated *E. coli* antibody was an appropriate dose for conjugating with 1.2 mg streptavidin-coated TiO_2 particles to prepare 1.2 mg EA TiO_2 particles.

In the present work, both untreated TiO_2 particles and streptavidin-coated TiO_2 particles were used as the control TiO_2 specimens. Furthermore, during the preparation of EA and streptavidin-coated TiO_2 particles, atto-610-streptavidin could be used instead of streptavidin to allow the particles enable to be excited at wavelength of 610nm therefore to emit red fluorescence light.

3) Binding of bacteria with EA TiO_2 or control TiO_2

All suspensions, including *E. coli* at $OD_{600}\approx1$, *P. putida* at $OD_{600}\approx0.1$ and all TiO_2 specimens (at a concentration of 0.4 g/L), were prepared in PBS buffer (140mM, pH 7.0)

for the binding and control experiments. The materials used in the binding and control

experiments were summarized in Table 4-1.

The binding experiment

1 mL of *E. coli* suspension and 1 mL of EA TiO_2 suspension were mixed on a shaking

table (Barnstead/ Lab-Line USA Model No. 4633) at a speed of 120 rpm for 1 h in dark.

The mixed suspension was then observed under a confocal microscope and scanning

electron microscopy. After keeping the mixture untouched for 2 h, the supernatant liquid

was observed under an optical microscope, while the sediments were also observed under

both optical microscope and scanning electron microscope.

The control experiments

There are five control experiments using different TiO_2 specimens or different

bacteria (Table 4-1). All of these controls were done and tested exactly as above, except

that the omitting of the confocal microscopy observation for the control 1, 3-5, in which

either *P. putida* was used instead of *E. coli* or untreated TiO_2 was used instead of EA or

streptavidin-coated TiO_2.

4) Photodisinfection experiments.

All photodisinfection experiments were carried out in a laminar airflow hood after

proper sterilization at room temperature. The various mixtures contain *P. putida* (0.1mL,

3.8×10^8 CFU/mL), *E. coli* (0.1mL, 3.8×10^8 CFU/mL), and TiO_2 (0.1mL, 0-0.4 mg/mL)

(Table 4-2). The initial concentrations of bacteria suspensions were roughly controlled

by diluting the bacterial suspension to the desired OD_{600} values. The corresponding

OD_{600} values for *E. coli* and *P. putida* at a concentration of $\sim 3.8 \times 10^8$ (CFU/mL) are ~ 1.0 and ~ 0.1, respectively. In each batch of experiments, a control experiment for indicating the initial concentrations of viable bacteria were carried out. By the plate counting method, the initial concentrations of viable bacteria were obtained and then adjusted to be 3.8×10^8 (CFU/mL) to enable all of data on bacterial concentrations comparable from the same original concentration.

The mixtures were mixed completely and then placed separately in each well of 48 wells (multiwell cell culture plate, BD Falcon™) and lidded. A Black-Ray® XX-15BLB UV Bench Lamp (365 nm) was provided as the light source in the photodisinfection experiments. The light was given from top with an incident intensity of 5.8 W m^{-2} to the surface of the mixtures. The intensity of UV irradiation was measured by a Traceable® Ultra Violet Light Meter (VWR). These mixtures were exposed to UV irradiation for certain time (0, 1, 2 h), without or with agitation. After each exposure, samples were diluted with sterile PBS buffer with appropriate dilution multiples (dilution multiples vary from 10^4-10^7, depending on the extent of killing) for easily and clearly numbering the subcultured bacterial colonies on plates). From each diluted solution, an aliquot (0.1mL) of the solution was inoculated into *E. coli* LB-agar medium plates and another aliquot (1 mL) into the *E. coli/coliform* count plates (Petrifilm™, 3M™). The solution on each plate was spread, and then the inoculum was kept for colony growth at 37 °C for 48 h. After 48 h, *E. coli* colonies on *E. coli/coliform* count plates were identified and numbered (as E) by the characteristics of trapping with bubbles, according to the manufacturer's instructions. The total colonies of *E. coli* and *P. putida* on *E. coli* LB-agar medium plates

were also numbered and the data were multiplied with 10 to represent the total colonies of

E. coli and *P. putida* (as T). The difference between these two data represents the number

of *P. putida* colonies (as P, P=T-E). Multiplication with the dilution folds, the cell

densities (CFU/mL) of both of *E. coli* and *P. putida* after photodisinfection in the

mixtures were obtained.

4.2.3 Measurements

The size and size distribution of TiO_2 particles were obtained on a Mastersizer 2000

(Malvern Instruments). EA TiO_2 (6 mg L^{-1}), untreated TiO_2 (3.6 mg L^{-1}), or streptavidin-

coated TiO_2 (6 mg L^{-1}) was dispersed in PBS buffer (140mM, pH 7) using ultrasonication

for 2 min before measurements. A higher concentration was used for EA and

streptavidin-coated TiO_2 suspensions because their refractive indices are lower than that

of TiO_2 starting material. PBS buffer was filtered with a 0.22 μm filter disc to remove

dust before use.

UV-vis absorbances of samples were measured on a UV-vis spectrum (Beckman

Coulter DU800 Spectrohotometer, Software version 2.0). For quantifying the

concentration of streptavidin, the extinct coefficient value was obtained (3.4 L/g) by

plotting the absorbance values at 282 nm wavelength vs. the known concentration of

streptavidin.

Scanning electron microscopy (SEM) images were obtained on a JEOL JSM-7000F

scanning electron microscope. All specimens were washed then diluted by MilliQ water.

After drying on aluminum stubs, samples were sputter-coated with gold and observed.

Confocal microscopy images of GFP *E. coli*, EA and streptavidin-coated TiO_2 (both labeled with atto-610-streptavidin) in PBS buffer were obtained on Zeiss LSM 510 confocal microscope.

Electrophoretic mobilities of bacteria, all TiO_2 specimens were measured on a ZetaPlus zeta potential analyzer (Brookhaven Instruments Corp.) operating in phase analysis light scattering mode. Measurements were performed in PBS buffer (140 mM, pH 7). The mean and standard deviation (see Table 4-3) were calculated from 10 runs (15 cycles per run).

Optical microscopy images were obtained on a Zeiss EL-Einsatz microscope equipped with a QICAM QImaging camera.

4.3 Results

TiO_2 is well known to generate ROS proximal to the particle.[3, 8, 32] We therefore hypothesized that exposure to UV would lead to the effective and preferential killing of those bacteria directly tethered to the TiO_2 particle. By contrast, other bacteria present should not be affected except by adventitious proximity. To examine this proposal, we prepared a series of targeted TiO_2 particles and examined the specificity of binding and killing in bacterial mixtures in the presence of UV light.

EA TiO_2, i.e. *E. coli* antibodies coated photocatalytic TiO_2 particles, were fabricated by a novel method developed in the present work. First, biotinylated TiO_2 nanoparticles were obtained by treating TiO_2 with $H_2N(CH_2)_3Si(OEt)_3$ and then *N*-

hydroxysuccinimidobiotin in a DMSO solution.[29] These biotinylated TiO_2 nanoparticles were bioconjugated first with streptavidin and then biotinylated *E. coli* antibody in PBS buffer to give an *E. coli* antibody coating (Figure 4-1). During this modification process, streptavidin-coated TiO_2 was also prepared, if coupling biotinylated *E. coli* antibody is omitted. In this work, EA TiO_2 was used as the biofunctionalized catalyst, while both of untreated TiO_2 and streptavidin-coated TiO_2 were used as the control TiO_2 particles. Two classes of bacteria, *Escherichia coli (E. coli)* K-12 stain DH5α and *P. putida* LV 2-4, were employed in this work. The former was used as the target bacteria and the latter was the control. All of the TiO_2 samples and bacteria were characterized in their surface biomolecules densities (only for EA and streptavidin-coated TiO_2), surfaces charges and sizes.

Characterization of TiO_2 specimens (EA TiO_2, untreated TiO_2 and streptavidin-coated TiO_2) and bacteria (*E. coli* and *P. putida*)

1. Densities of streptavidin on streptavidin-coated TiO_2 and *E. coli* antibody on EA TiO_2

The density of *E. coli* antibodies on EA TiO_2 surfaces plays a significant role in promoting the binding and killing of the target bacteria, as *E. coli* antibody molecules are responsible for recognizing and binding to the antigen, *E. coli*. The density of antibodies, however, depends on the density of streptavidin on streptavidin-coated TiO_2 surfaces.

In the preparation of streptavidin-coated TiO_2 colloidal particles, large excesses streptavidin molecules were added to the biotinylated TiO_2 colloidal suspension to

achieve the maximum attachment. Then the unbound streptavidin molecules were removed in the washing process. By measuring the residual streptavidin in the solution, the quantity of bioconjugated streptavidin was obtained and the density of bioconjugated streptavidin on streptavidin-coated TiO_2 was calculated to be ~0.02/nm^2 (Equation 1).

For the preparation of EA TiO_2 particles, biotinylated *E. coli* antibody molecules were added to streptavidin-coated TiO_2 colloidal solution with many discontinuous tiny doses to meet the maximum attachment. Addition of antibody was stopped when the presence of antibody was detected by testing the UV absorbance of the supernatant liquid, suggesting the added antibody was slightly excessive for coupling with streptavidin-coated TiO_2 colloidal particles in the solution. The accuracy of this test method is limited by the sensitivity of *E. coli* antibody in solution to UV absorbance, however, enough for finding the appropriate amount of antibody for preparing EA TiO_2 in this antibody attachment experiment. Our experimental results showed that 60±14 µg of antibody was appropriate for coupling with 1.2 mg of streptavidin-coated TiO_2 to give 1.2 mg EA TiO_2 particles. The density of conjugated antibody on EA TiO_2 could be then calculated to be ~0.015/nm^2 (Equation 2).

2. Electrophoretic mobilities

The electrophoretic mobilities of EA TiO_2, untreated TiO_2, streptavidin-coated TiO_2, *E. coli* and *P. putida* are $(-1.76 \pm 0.07) \times 10^{-8}$ m^2/Vs, $(-1.82 \pm 0.12) \times 10^{-8}$ m^2/Vs, $(-1.43 \pm 0.22) \times 10^{-8}$ m^2/Vs, $(-1.37 \pm 0.09) \times 10^{-8}$ m^2/Vs and $(-1.49 \pm 0.12) \times 10^{-8}$ m^2/Vs in PBS buffer (140 mM, pH 7), respectively, indicating that TiO_2 specimens and both bacteria used in the present work were all negatively charged (Table 4-3).

3. Sizes

The size and size distribution of TiO_2 specimens were measured by Fraunhofer diffraction. The data showed that the mean size of TiO_2 colloidal particles increased after each step of surface modification including biotinylation, conjugation of streptavidin and conjugation of biotinylated *E. coli* antibody (Figure 4-2). In 140mM PBS buffer at pH 7.0, untreated TiO_2 colloidal particles showed an average size of 1.55 µm and a dispersity (D90-D10/D50) of 1.822. After biotinylation, the average size became 1.592 and the dispersity became 1.938. After streptavidin and then antibody bioconjugations, streptavidin-coated TiO_2 colloidal particles showed an average size of 1.83µm and a dispersity of 1.800, and EA TiO_2 colloidal particles had an average size of 2.88µm and a dispersity of 4.977. However, according to SEM and the MSDS of the sample, the particle size distributions of the TiO_2 used in this work were mainly in the range of 50-200nm (Figure 4-3).

Our SEM observation showed that the size of the majority of *E. coli* K12 bacteria is (0.5-1.0) µm × (1.5-2) µm and *P. putida* LV 2-4 bacteria have a similar size (Figure 4-4).

4. Fluorescence

Fluorescence labeled EA and streptavidin-coated TiO_2 particles in PBS buffer both give red fluorescence (Figure 4-3b and d), while GFP *E. coli* give green fluorescence (Figure 4-4b), observed with confocal microscopy.

Selective binding (flocculation) of EA TiO$_2$ to *E. coli*

EA TiO$_2$ particles, prepared by the above-mentioned method, were mixed with *E. coli* bacteria in PBS buffer to examine the specific adhesion. A series of control experiments, including EA TiO$_2$ mixed with *P. putida*, streptavidin-coated or untreated TiO$_2$ mixed with *E. coli* or *P. putida*, were also performed (Table 4-1). The experimental results showed that only EA TiO$_2$ particles bound to the surfaces of *E. coli* bacteria (Figure 4-5), whereas no binding was found in any of the control experiments (Figure 4-6). Besides the specific binding, it was also found EA TiO$_2$ underwent flocculation with target bacteria, *E. coli* (Figure 4-7a). Through careful observation, it can be roughly estimated that the flocculation will form as the ratio of added EA TiO$_2$ particles to *E. coli* bacteria is over ~50. When this ratio is in excess to ~200, the most of the *E. coli* bacteria in the mixture were flocculated and eventually precipitated with EA TiO$_2$ particles, as evidenced provided by optical microscopy: very few *E. coli* cells were found in the supernatant liquid (Figure 4-7b), whereas in controls, many *E. coli* bacteria were observed in the supernatant liquid and the sediments were found to be consist of mainly TiO$_2$ particcles (Figure 4-7 c-d). Furthermore, the sediments of the mixture of *E. coli* and EA TiO$_2$ in the binding experiment looked quite different from those in the control experiments. The sediments in the binding experiment were light yellowish and inhomogeneous, whereas those in the controls were very white and homogeneous (Figure 4-8).

Bacterial Response to UV

A bacterial mixture containing *E. coli* K-12 (the target bacteria) and *P. putida* LV 2-4 (the control bacteria) was employed in this work. These two different bacteria were both contained in 0.3mL PBS buffer at a same concentration (CFU/mL=3.8×10^8) for easily comparing the efficiency of killing of each bacteria after exposure to UV. The original concentrations of bacteria both can be roughly controlled by diluting the bacterial suspensions (CFU/mL) to certain OD_{600} values, according to the calibration curves plotted by the bacterial concentration against OD_{600} values (Figure 4-9). For CFU/mL of ~3.8×10^8, the corresponding OD_{600} values for *E. coli* and *P. putida* are ~1.0 and ~0.1, respectively. The real original concentrations of bacteria for each experiment were detected by plate counting method and all the data obtained from the same batch experiment were adjusted to be performed from the same original bacterial concentrations.

In photodisinfection experiments, the bacterial mixture was mixed with TiO_2 colloidal particles completely to obtain the specific binding/flocculation before UV irradiation was given. The mixture containing *E. coli*, *P. putida* and EA TiO_2 particles was then exposed to 365nm irradiation at an intensity of 5.8 W/m^2 for certain time period to achieve photodisinfection. The survival numbers of each class of bacteria were then obtained by plate counting method after subculture and compared with the results obtained from the control experiments, in which control TiO_2 specimens were omitted or used instead of EA TiO_2, to examine the preference of photodisinfection. The recipes are summarized in Table 4-2.

Determination of the optimum number ratio of particles to E. coli bacteria

Prior to testing the responses of bacteria to UV in the present of EA TiO_2 particles, a variety of survey experiments were used to optimize the number ratio of particles to *E. coli* bacteria for maximizing photodisinfection selectivity. The impact of the number ratio of particles to *E. coli* (or *P. putida*) bacteria on the selectivity of killing bacteria was studies and the results were shown in Figure 4-10. It can be seen from this figure that EA TiO_2 and control TiO_2 specimens showed a similar low efficiency of killing *P. putida*. Besides, a much larger fraction of *E. coli* was killed than that of *P. putida* even with the control TiO_2 particles (without antibodies on the surfaces), suggesting the more sensitive response of *E. coli* to UV-TiO_2 system than *P. putida*. Considering these characteristics, the efficiency and selectivity of photodisinfection with EA TiO_2 were evaluated based on the deduction of the effects of killing with control TiO_2. Since the photodisinfection experiments were carried out in the bacterial mixture containing *E. coli* and *P. putida* at a same original concentration, the preference of killing *E. coli* over *P. putida* with EA TiO_2 was evaluated by BSE-BSC. Herein, "**BSE**" refers to the preference of **B**acterial **S**urvival with **E**A TiO_2, which was calculated by log(viable *P. putida* bacteria conc. with EA TiO_2/ viable *E. coli* bacteria conc. with EA TiO_2). "**BSC**" refers the preference of **B**acterial **S**urvival with **C**ontrol TiO_2, which was calculated by log (viable *P. putida* bacteria conc. with streptavidin-coated TiO_2/ viable *E. coli* bacteria conc. with streptavidin-coated TiO_2). Viable Bacteria concentration is represented by cell density (CFU/ml - colony forming units per milliliter). When the value of BSE-BSC equals to zero, it shows no difference in preference of killing bacteria with EA TiO_2 and with control TiO_2, i. e. no selectivity at all. Increasing of this value suggests increasing of selectivity.

Figure 4-10 shows that the maximum selectivity could be achieved when the number ratio of particles to *E. coli* bacteria reaches ~26. Further increasing this ratio increased the efficiency of killing of *E. coli*, however, decreased the selectivity.

Influence of agitation on selectivity of photodisinfection

In most of studies and applications related to use TiO_2 particles to kill pathogens in solution, agitation of solution is necessary to maintain stable photocatalytic disinfection because TiO_2 particles precipitate fast.[5, 33-35] In agreement with these reports, we also found that agitation is necessary to maintain stable antibacterial effect in our control experiments, in which there is no specific targeting biomolecule involved. However, in our selective photodisinfection experiments with using EA TiO_2, agitation of solution was found to give a negative effect on the efficiency of killing *E. coli* bacteria. The impact of the speed of agitation on the killing of both bacteria with EA TiO_2 or with the control TiO_2 was studied and the results were shown in Figure 4-11. The modified Reynolds number (*Re*) of the agitated solution was calculated by Equation 3, according to the study on agitation systems done by McCabe et al.[36] It can be seen from Figure 4-11 that agitation did not significantly affect the efficiency of killing *P. putida*. For killing *E. coli*, slight agitation at a low modified Reynolds number (*Re* <12) did not affect the efficiency greatly. However, once *Re* is over 12, the efficiency starts to decrease drastically, and finally reaches the same level of that using the control TiO_2 when *Re* is in excess of ~38. In the photodisinfection experiments, it was also found that agitation did not affect either the efficiency or the selectivity of inactivation if light is not offered (Table 4-4). Finally,

after exposure to UV for 2h with agitation (**Re** >25), the solution was then observed carefully and the flocculation of bacteria and EA particles (as mentioned-above) was found to be disappeared.

UV irradiation time of selective photodisinfection

Two classes of bacteria and EA TiO$_2$ at the optimum ratio (TiO$_2$/*E. coli*≈26) were mixed completely and then exposed to UV light (365 nm, 5.8 W m^{-2}) without agitation for different time periods (0, 1, 2 h). After UV irradiation, the resulting mixtures were diluted with PBS buffer, and then subcultured on LB-agar plates and *E. coli/coliform* count plates (Petrifilm^{TM}, 3M^{TM}). The colonies of *E. coli* were identified on the *E. coli/Coliform* count plates, and the total colonies of *E. coli* and *P. putida* were numbered on LB-agar plates by the regular plate counting method.

Table 4-4 shows that there is no bactericidal effect on either *E. coli* or *P. putida* in the dark in the absence of TiO$_2$ or in the presence of different TiO$_2$ within 2 h in the mixed suspensions. This is not a surprising result since TiO$_2$ is a stable, non-toxic and non-soluble photoactive solid that will generate ROS only if band-gap irradiation is provided. The inactivation of *E. coli* under UV irradiation in the absence of TiO$_2$ is very low (Figure 4-12), suggesting the experimental condition associated with UV light (365nm irradiation at an intensity of 5.8 W/m^2) does not act on killing bacteria effectively alone.

Figure 4-12 also shows the response of the two types of bacteria in the mixtures to UV irradiation as a function of the TiO$_2$ particles present. Particles that possess the *E. coli* antibody are expected to preferentially bind to available *E. coli*, which will then be most

susceptible to oxidative cleavage. By contrast, *P. putida* should be much less affected: these organisms will have not particular affinity for the particles and will only be killed by adventitious proximity during irradiation. The results matched these expectations: *E. coli* cells were killed effectively (from 3.8×10^8 CFU/mL to 6.5×10^6 CFU/mL after 1 h of UV irradiation, and to 3.7×10^4 CFU/mL after 2 h of UV irradiation) only with EA TiO_2 particles. By contrast, the concentrations of surviving *P. putida* were similar to those in the control experiments (from 3.8×10^8 CFU/mL to 3.2×10^8 CFU/mL after 1 h of UV irradiation, and to 1.1×10^8 CFU/mL after 2 h of UV irradiation).

4.4 Discussion

Preparation of EA TiO₂

For the first time, antibody conjugated TiO_2 colloidal particles are prepared by using biotin-streptavidin bioconjugation rather than physisorption. This route of preparing EA TiO_2 nanoparticles represents a general method for fabricating TiO_2 colloidal particles conjugated with a variety of bio-molecules by simply attaching the desired biotinylated bio-molecules to biotinylated TiO_2 surfaces via biotin/streptavidin complexation.

In our previous work, the conjugation of streptavidin with biotinylated TiO_2 colloidal particles has been demonstrated by fluorescence-based observation and the feasibility of attaching other biotinylated biomolecules to the streptavidin-coated TiO_2 colloidal particles has been also revealed.[29] In the present work, streptavidin-coated TiO_2 particles with the diameter within 50-200nm were fabricated. The density of conjugated

streptavidin was tested by the measurement of UV absorbance of the residual streptavidin in solution after washing process to be ~0.02/nm². Huang tested the densities of streptavidin adsorbed on polystyrene latex with a diameter of 272nm and the biotinylated DNA on the streptavidin-coated polystyrene latex by fluorescence-based quantification measurement.[37] In Huang's report, it is showed that streptavidin was adsorbed to polystyrene latex at coverage of 0.048/nm² and biotinylated DNA was bound to streptavidin-coated polystyrene at a density of 0.12 per one streptavidin. Huang's data for the streptavidin adsorption density is really high, if considering the theoretical density value for full monolayer attachment of streptavidin, which is ~0.04/nm² calculated by the size of one streptavidin, ca. 4.5×5.5nm.[38, 39] Our result for the binding of streptavidin to biotinylated TiO_2 particle suggests a coverage of 50%, obtained by comparing our experimental density with the theoretical density of the full attachment (= 0.02 nm^{-2}/0.04 nm^{-2}). Thus, only a half of the surface of particles was covered by streptavidin. This is probably due to the aggregation of TiO_2 particles. Evidences for particles aggregation were obtained from comparing the real size with the size data measured in water. The size of TiO_2 used in this work is 50-200nm, according to the SEM observation (Figure 4-3) and the MSDS provided by the manufacturer. However, the size and size distribution of these colloidal particles in water measured by Fraunhofer diffraction showed to be at least 1.5μm on average and a dispersity of > 1.8, respectively (Figure 4-2). This inconsistency implies that these TiO_2 colloidal particles underwent aggregation in water, though they were stabilized by their negative surface charge [40, 41]. Aggregation of these TiO_2 colloidal particles renders parts of surface inaccessible to streptavidin. Besides, the

efficiency of attaching streptavidin is also affected by the density of biotin on TiO_2 surfaces,[29] surface roughness of particles, and some non-specific adsorptions.

By this fabrication method, EA TiO_2 were also prepared by binding biotinylated *E. coli* antibody to streptavidin-coated TiO_2 and the density of *E. coli* antibody was found to be and ~0.015/nm². As a result, the biotinylated *E. coli* antibody bound to streptavidin-coated TiO_2 particles at a density of 0.75 per one streptavidin. Compared with Huang's result, in which 0.12 bulky biotinylated DNA was bound to one streptavidin that had been absorbed on 272nm polystyrene latex, our data on the binding of biotinylated *E. coli* antibody to streptavidin-coated TiO_2 shows a higher efficiency of conjugation.

Selective binding (flocculation) of EA TiO₂ to E. coli

The *E. coli* antibody (ab20640) used in our experiments is capable of recognizing and binding to all "O" and "K" antigenic serotypes of *E. coli*, according to the product instruction issued by Abcam Company. Therefore, we proposed that the antibody molecule promotes the photocatalytic TiO_2 particles to approach/contact the antigen, *E. coli*, in the presence of other bacteria in the solution. Our binding experimental results matched this proposal: only EA TiO_2 colloidal particles bound to *E. coli* K12, whereas no bindings were found in any of the control experiments, in which either control TiO_2 particles were used instead of EA TiO_2 or *P. putida* was used instead of *E. coli* (Figure 4-4, Figure 4-5 and Figure 4-6). Furthermore, the electrophoretic mobility results showed that all the bacteria and TiO_2 specimens involved in this work were negatively charged in PBS buffer (140mM, pH 7), suggesting that there was no electrostatic attraction among

them (Table 4-3). As a result, the selective binding of EA TiO_2 colloidal particles to *E. coli* was confirmed due to the biorecognition between the antibody (*E. coli* antibody conjugated on the EA TiO_2 surfaces) and the antigen (*E. coli*).

More interesting, except the specific binding displayed by EA TiO_2 to the target bacteria, it was also found that the EA TiO_2 colloidal particles underwent flocculation with *E. coli* bacteria while those control TiO_2 (without the targeting molecule on the surfaces) did not (Figure 4-7). We tried to detect the lowest number ratio of EA TiO_2 to *E. coli* cells required for the formation of flocs by measuring the change of turbidity of the suspension as EA TiO_2 particles were added to the bacterial solution. However, this measurement was strongly interfered by the adhesion of EA TiO_2 to the cuvette wall, therefore, hardly gave precise data on flocculation. Nevertheless, through careful observation, the number ratio of EA TiO_2 particles to *E. coli* bacteria to induce flocculation can be roughly estimated to be ~50. Furthermore, it was also found that most *E. coli* bacteria in the suspension were flocculated (Figure 4-7 a) and precipitated with particles to give a relatively clear supernatant liquid (Figure 4-7 b) and form large visible sediments (Figure 4-8), when this number ratio is over ~200. This ratio is only a quarter of the full monolayer coverage of a typical *E. coli* bacterium, which is 863, calculated by dividing the surface area of one *E. coli* cell (~5.52 μm^2, assuming the size of one cell is ~0.8μm×~1.8μm) by the surface area of one particle (~6.4×10^{-3} μm^2, assuming the diameter of one particle is ~80nm).

Our EA TiO_2 colloidal particles acted as a strong flocculating agent in the bacterial suspension depending on the bioconjugation between antibodies and antigens. Tuning

solution pH to give TiO_2 a positive surface charge to attract negatively charged pathogens probably is another method to improve the contact. However, flocculation of TiO_2 colloidal particles with bacteria based on electrostatic attraction has been rarely reported.

In addition, the sediments consisting of EA TiO_2 particles and *E. coli* cells were light yellow and inhomogeneous, whereas the sediments of control experiments, in which either control TiO_2 particles were used instead of EA TiO_2 or *P. putida* was used instead of *E. coli*, mainly consisting of TiO_2 particles, were very white and homogeneous (Figure 4-8). The flocculation and the special appearance of the sediments of the binding experiment with using EA TiO_2 colloidal particles can be easily detected by eye, which may provide us a simple method for detecting the presence of specific bacteria in water without the need of any detective instruments or skillful technicians, although the sensitivity is not an advantage. This is probably useful in some developing countries and districts, where poor living conditions and terrible bio-contamination are threatening humans whereas instruments and technicians are lacking.

Selective photodisinfection

In selective photodisinfection experiments, *E. coli* bacterial suspension and *P. putida* bacterial suspension were mixed. In the mixture, the concentrations of these two classes of bacteria are same, i.e. 3.8×10^8 CFU/mL. This bacterial mixture was then mixed with TiO_2 suspension completely before exposure to UV irradiation. The recipes for photodisinfection experiments are summarized in Table 4-2. It was found that the ratio of

particles to bacteria and agitation of solution both affect the efficiency and selectivity of

killing.

From Figure 4-10, it can be seen that the number ratio of one particle to one *E. coli*

bacterium showed low efficiency and no bio-selectivity of killing.   However, the

preference of killing *E. coli* bacteria is enhanced rapidly with the increasing of this ratio,

and reaches the maximum when the ratio is ~26. This number ratio, if compared with the

one required for the full coverage, which is 863 as calculated above, suggests a low

coverage of ~3%. Thus, the most effective preference of killing of *E. coli* over *P. putida*

via biorecognition, can be achieved at only ~3% coverage of EA TiO$_2$ particles on *E. coli*

bacteria. Using more EA TiO$_2$, though increases the efficiency of killing, but not as much

as with using control TiO$_2$, displays a negative effect on the bio-selectivity. This result,

combined with the number ratios for forming flocculation (~50 for inducing flocculation

and ~200 for totally flocculating with *E. coli* bacteria in solution), suggests the specific

binding of EA TiO$_2$ to *E. coli* promotes the selectivity, while flocculation does not. This

is probably because flocs prevents UV light from penetrating the interiors to kill bacteria

effectively. According to Nosaka's report, the penetration depth of adsorbed light into

TiO$_2$ is only ~25nm.[33] However, the penetration depth of UV irradiation into the flocs

consisting of *E. coli* and EA TiO$_2$ colloidal particles in water is still unknown. What we

have known is that, from a colloid science perspective, a large number of TiO$_2$ particles

and bacteria inside the flocs with a macro level size (Figure 4-8), are inaccessible to UV

irradiation, therefore, the interior bacteria are not killed as effectively as those outside the

flocs.

Agitation of solution, commonly used in disinfection of pathogens with photo-irradiated TiO_2 in water to prevent precipitation of catalyst, in this work, however, decreased the selectivity of photodisinfection dramatically (Figure 4-11). According to McCabe et al., the flow is laminar when agitator Reynolds number is smaller than 10 and turbulent when *Re* is greater than 10,000.[36] In the photodisinfection experiments in this thesis, gentle agitation, or laminar flow, did not apparently affect the selectivity. While stirring at agitator *Re* (the modified Reynolds number, calculated by Equation 3) in excess of 12, the selectivity was dropped rapidly and disappeared completely until agitator *Re* reached ~38 (Figure 4-11). It is also found that agitation affects selectivity of disinfection only when UV irradiation is given. These results suggested that the multi-linker bioconjugation (cells-antibody-biotin-streptavidin-biotin-TiO_2) was probably destroyed by ROS generated from UV-TiO_2 system. The damage to the bioconjugating linker could lead to the detachment of TiO_2 from cells surface, and turbulent agitation of the solution promotes the detachment. Evidences for this explanation were obtained by careful observation: flocculation could not be found in the solution after 2h of UV irradiation with agitator *Re* of ~25. Besides, our previous work suggested the bio/chem coating on the TiO_2 nanoparticles can be destroyed by ROS under UV irradiation.[42]

In light-TiO_2 system, the active agents for the inactivation of pathogens are reactive oxygen species (ROS), generated from TiO_2 surfaces [2-7]. These ROS are very short lifetime therefore can not diffuse long distance in solution [3, 8]. The effective diffusion lengths of ROS in water are still unknown, however, in some reports, it was pointed out that 50 μm was too far for certain ROS such as hydroxyl radicals to travel [11]. The surface

charge of most bacteria and TiO_2 in water are both negative generally (Table 4-3), which prevents TiO_2 from approaching to bacteria. Therefore, the space between TiO_2 and bacteria is the main cause to inactivate most ROS before they can reach the target pathogens.

An alternative way is to use the attraction force from opposite surfaces charges of TiO_2 and bacteria to reduce the space between them in water.[35] Most bacteria display greater negative surface charge than positive charge in water.[43] Positive surface charge of TiO_2 can be given by adjusting pH of solution to allow particles to approach/contact bacteria. In the work reported by Gumy and his colleagues, 13 different commercial TiO_2 powders with different isoelectric points (IEP) from 3 to 7.5 were studied for their efficiency of killing *E. coli* K12 bacteria.[34] Their results showed that except the case with using Degussa P25 TiO_2,[34, 44] surface charge of TiO_2 particles could be tuned to be positive or negative via simply adjusting pH of solution and positively charged TiO_2 showed a stronger bactericidal effect on *E. coli* than negatively charged TiO_2. The author explained that identical surface charge repulsed the TiO_2 from *E. coli* therefore decreased the efficiency of killing, and vice versa. Although controlling surface charge of TiO_2 particles could be a tool to allow the contact/approaching to the target bacteria to achieve effective photodisinfection, which might be weakened by the instable adhesion of particles to bacteria due to the shear force from flowing in water. Furthermore, the application of this method for selective photodisinfection is hardly expected except some very rare examples in which the target bacteria and the non-target bacteria display

opposite surface charge in the same solution, even in this case, the application is limited by the pH of solution.

The effect of proximity could be clearly seen from Figure 4-12. In control experiments with TiO_2 that possessed no special targeting molecules or without TiO_2, the efficiency of killing either *E. coli* or *P. putida* in solution was low. However, EA TiO_2 killed the target *E. coli* bacteria very effectively, whereas played a similar antibacterial effect on *P. putida* as the control TiO_2 specimens. We have shown this is because our EA TiO_2 can bind to the surface of *E. coli* cells, therefore avoids the long travelling of ROS to reach the target cells. This can be regarded as an evidence of improving killing efficiency of UV-TiO_2 system by reducing the distance between TiO_2 and targeted bacteria. In our photodisinfection experiments, EA TiO_2 was proved to be capable of killing 99.99% *E. coli* cells (from 3.8×10^8 to 3.7×10^4) after 2h of UV irradiation, suggesting the promising applications of this method for removing or killing most of the undesired bacteria.

4.5 Conclusions

1. EA TiO_2 colloidal particles can specifically bind to *E. coli*, depending on the biorecognition between *E. coli* antibody (on EA TiO_2 surfaces) and the antigen (*E. coli*).

2. EA TiO$_2$ can selectively and effectively kill the targeted bacteria, while leaving other bacteria alive.

3. The density of streptavidin on streptavidin-coated TiO$_2$ surfaces is ~0.02/nm^2 and the coverage is ~50%. The density of biotinylated *E. coli* antibody on EA TiO$_2$ surfaces is ~0.015/nm^2, suggesting 75% of streptavidin is accessible for binding to biotinylated *E. coli* antibody.

4. When the number ratio of EA TiO$_2$ particles to *E. coli* bacteria reaches ~50, large visible flocs consisting of particles and *E. coli* cells are formed. When this number ratio is over ~200, equaling to ~¼ of the number required for the full coverage of bacteria, relatively complete flocculation of *E. coli* bacteria with EA TiO$_2$ particles can be obtained.

5. Maximum bio-selectivity of photodisinfection can be achieved by controlling the number ratio of recognition biomolecule-coated particles to the target bacteria at ~26, which equals to a coverage of ~3%.

6. We propose that the sheer sensitivity of the selective photodisinfection reflects weak bacteria-EA-TiO$_2$ adhesion, resulting from photocatalytic decomposition of the antibody linkage.

(a)
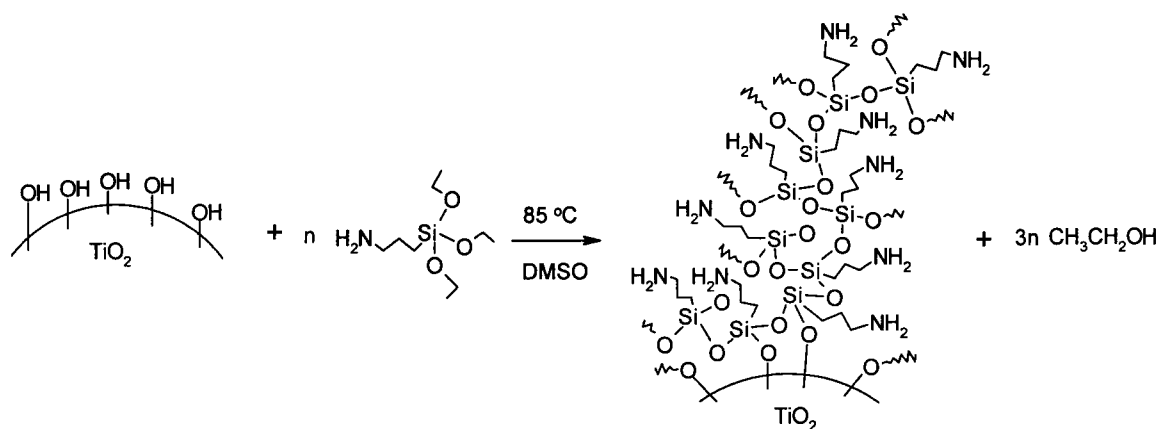
(b)
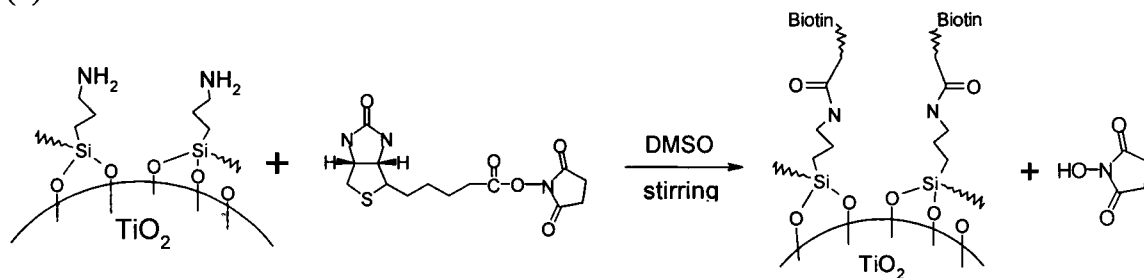
Scheme 4-1   (a) Silanization Reaction of TiO₂ with APTS; (b) Biotinylation Reaction of Amino-TiO₂ with Biotin-NHS
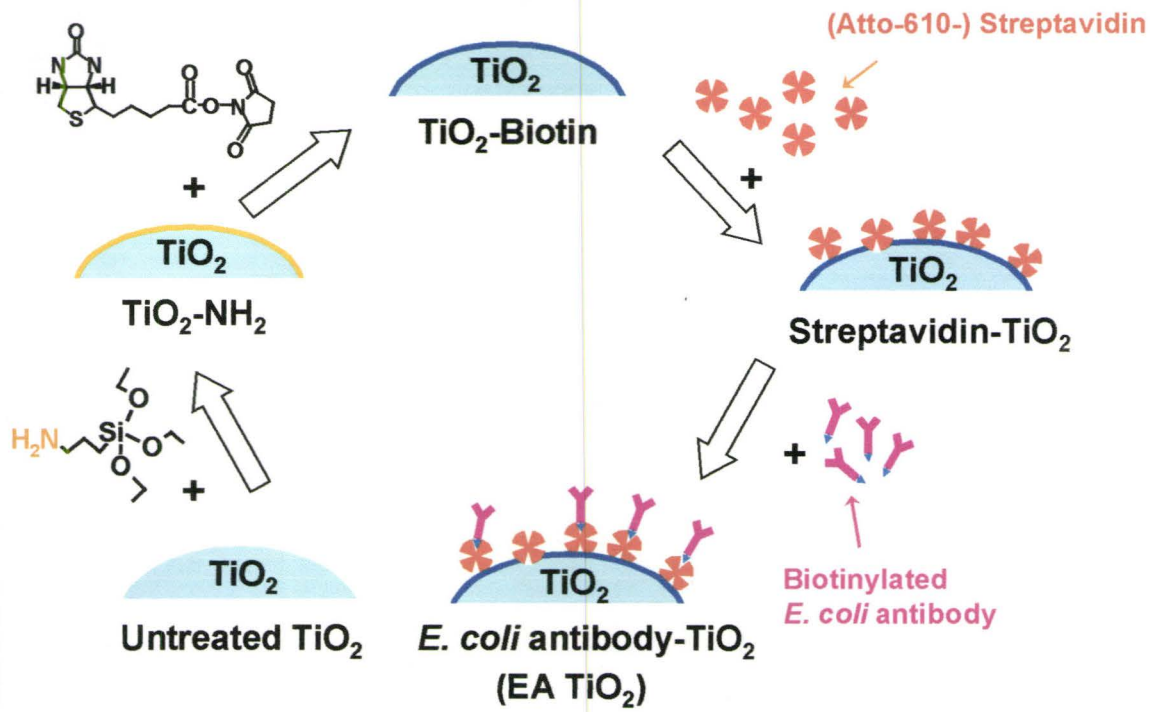
Figure 4-1 The preparation of streptavidin-coated TiO_2 and EA TiO_2

		Bacteria		TiO$_2$ specimens		
		GFP *E. coli*	*P. putida*	EA TiO$_2$	Control TiO$_2$	
					Untreated TiO$_2$	Streptavidin-coated TiO$_2$
Binding experiment		Applied	Not applied	Applied	Not applied	Not applied
Control experiments	Control-1	Applied	Not applied	Not applied	Applied	Not applied
	Control-2	Applied	Not applied	Not applied	Not applied	Applied
	Control-3	Not applied	Applied	Applied	Not applied	Not applied
	Control-4	Not applied	Applied	Not applied	Applied	Not applied
	Control-5	Not applied	Applied	Not applied	Not applied	Applied

Table 4-1 The materials used in the binding experiments

	P. putida	*E. coli*	TiO$_2$
Photodisinfection experiment	0.1mL 3.8×10^8 CFU/mL	0.1mL 3.8×10^8 CFU/mL	EA TiO$_2$ 0.1mL 0-0.4 g/L
Control-1	0.1mL 3.8×10^8 CFU/mL	0.1mL 3.8×10^8 CFU/mL	No TiO$_2$ applied
Control-2	0.1mL 3.8×10^8 CFU/mL	0.1mL 3.8×10^8 CFU/mL	Untreated TiO$_2$ 0.1mL 0-0.4 g/L
Control-3	0.1mL 3.8×10^8 CFU/mL	0.1mL 3.8×10^8 CFU/mL	Streptavidin-coated TiO$_2$ 0.1mL 0-0.4 g/L

Table 4-2 Recipes of photodisinfection experiments

	Electrophoretic mobility ($\times 10^{-8}$ m^2/Vs)	Std. error	Conductance (μS)
P. putida LV 2-4	-1.49	0.12	26073
E. coli K12 DH5α	-1.37	0.09	21662
EA TiO$_2$	-1.76	0.07	26804
Untreated TiO$_2$	-1.82	0.12	26280
Streptavidin-coated TiO$_2$	-1.43	0.22	26753

Table 4-3 Electrophoretic mobility tests for *P. putida* LV 2-4, *E. coli* K12 DH5α, EA

TiO$_2$, untreated TiO$_2$, and streptavidin-coated TiO$_2$ nanoparticles in PBS buffer (140mM,

pH 7)
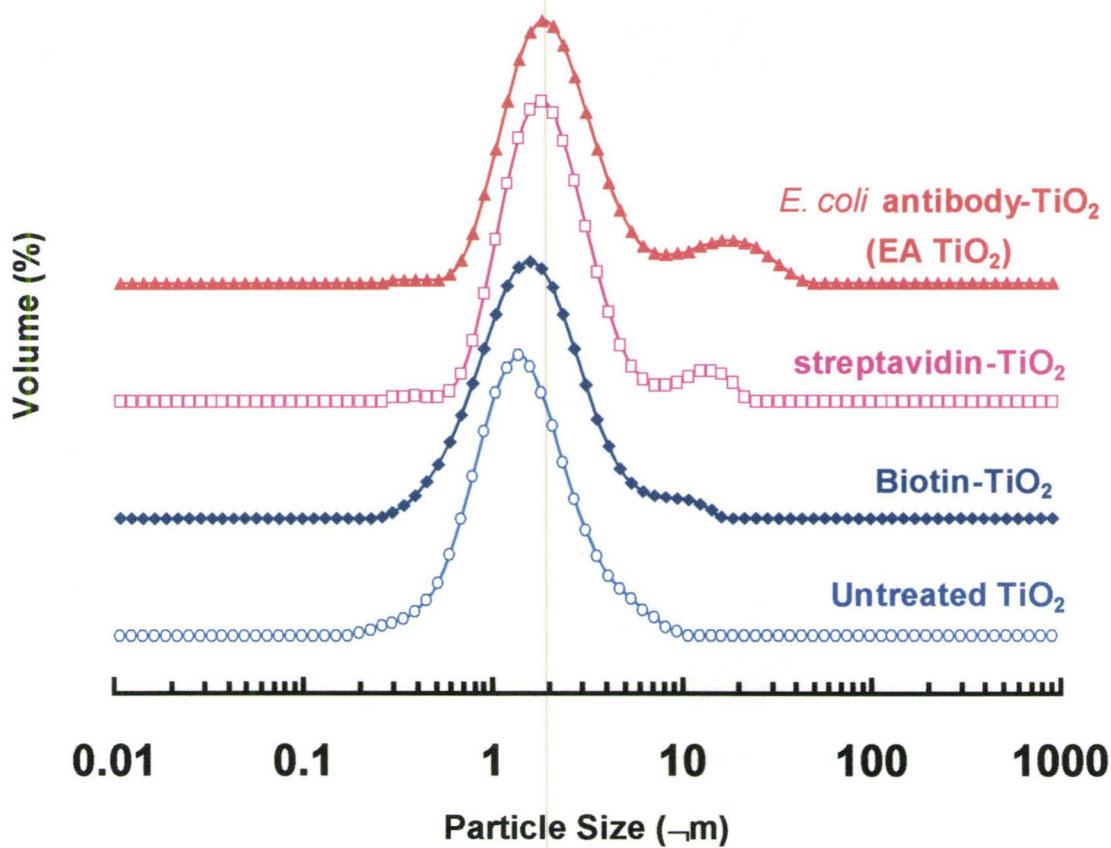
Figure 4-2   Size and size distribution of untreated, biotinylated, streptavidin-coated and

EA TiO$_2$ colloidal particles in PBS buffer at pH 7.0
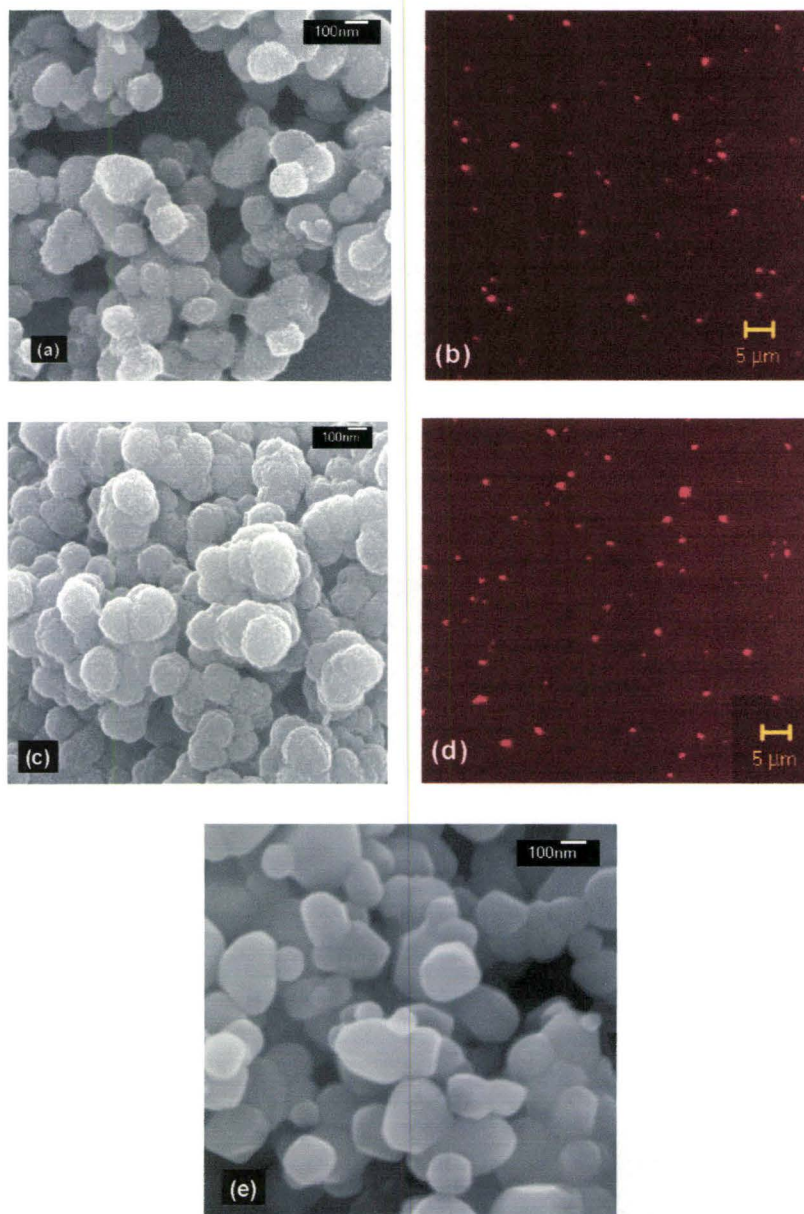
Figure 4-3 (a) A SEM image of EA TiO_2; (b) a confocal image of EA TiO_2 in PBS buffer at pH 7.0; (c) a SEM image of streptavidin-coated TiO_2; (d) a confocal image of streptavidin-coated TiO_2 in PBS buffer at pH 7.0; (e) a SEM image of untreated TiO_2
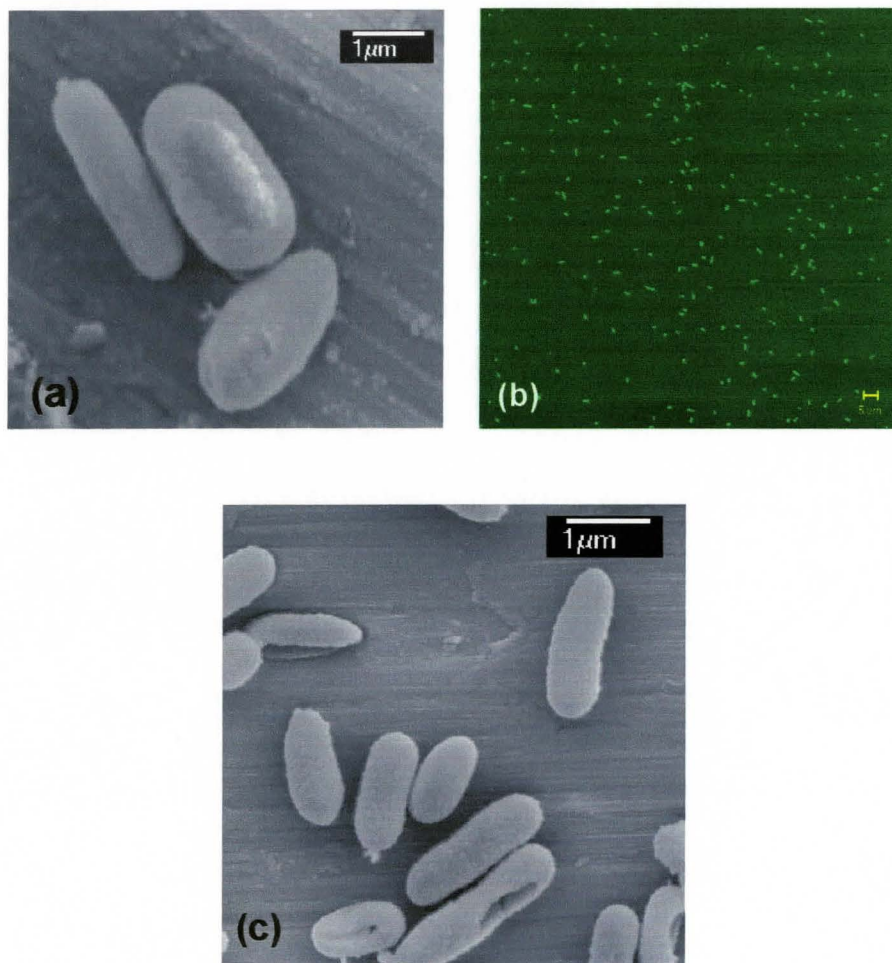
Figure 4-4   (a) A SEM image of GFP *E. coli*; (b) a confocal microscopy image of GFP *E. coli* under the green wavelength excitement; (c) a SEM image of *P putida*
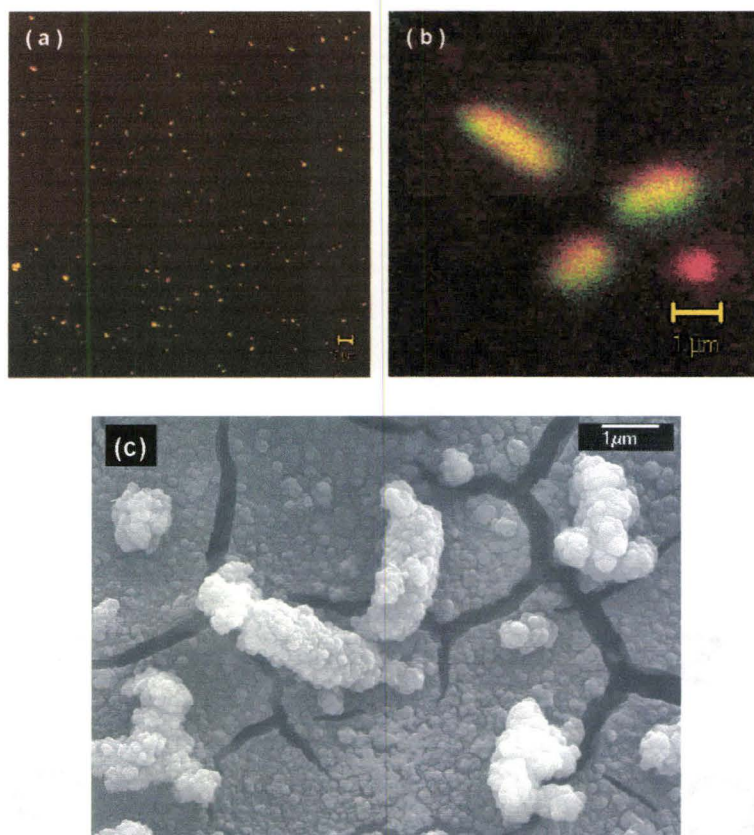
Figure 4-5 (a-b) The confocal microscope images of the mixture of GFP *E. coli* and EA

TiO$_2$ (fluorescent labeled with atto-610) and (c) a SEM image of the same mixture
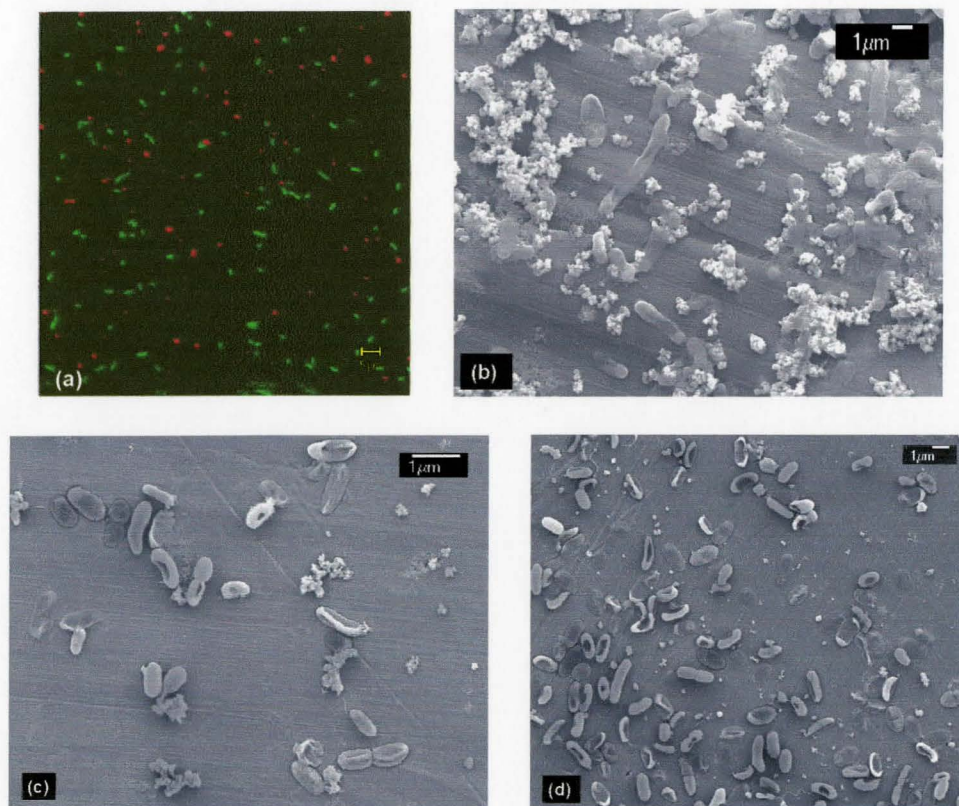
Figure 4-6 (a) A confocal microscope image of the control-2: the mixture of GFP *E. coli* and streptavidin-coated TiO$_2$ (fluorescent labeled with atto-610); (b) a SEM image of the control-1 or control-2. the mixture of GFP *E. coli* and control TiO$_2$, (c) a SEM image of the control-3 the mixture of *P putida* and EA TiO$_2$; (d) a SEM image of the control-4 or control-5 the mixture of *P putida* and control TiO$_2$
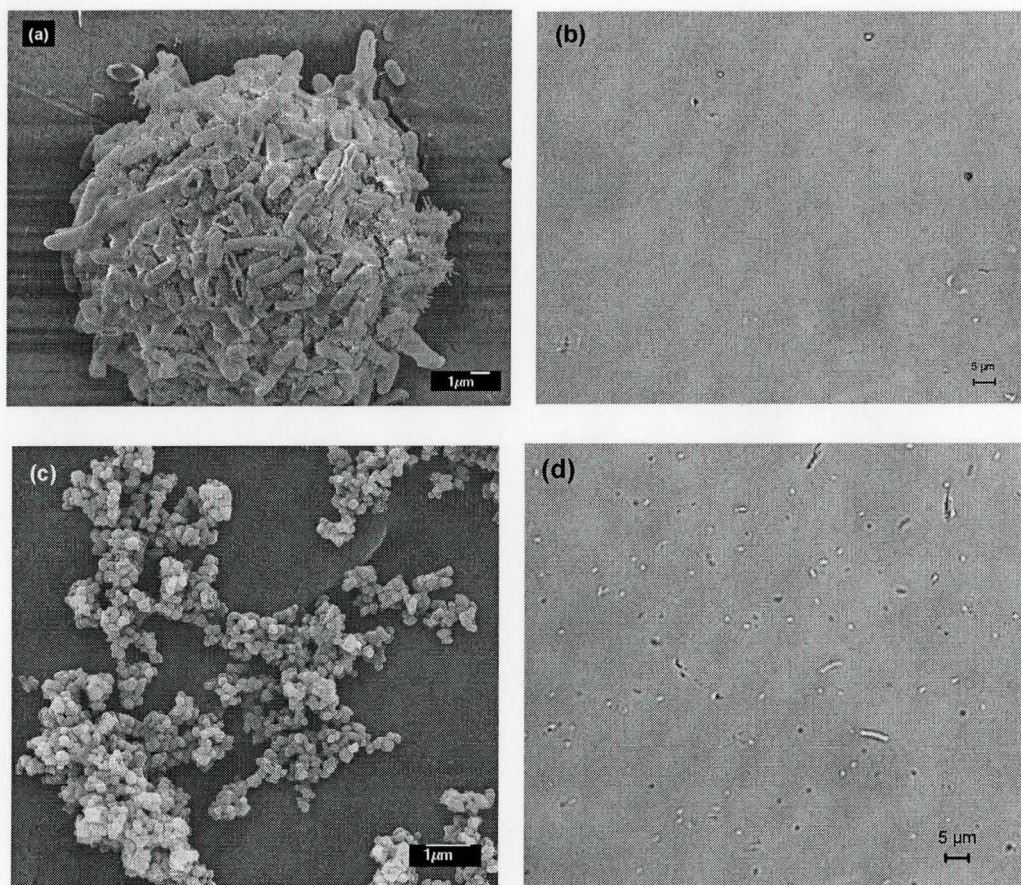
Figure 4-7 EA TiO$_2$ particles were mixed with *E. coli* bacterial at the ratio in excess of ~200 by shaking in dark for 1h and then the mixture was maintained quiescent for 2h to allow completely precipitation, after that, (a) the sediment was observed by SEM, and (b) the supernatant liquid was observed by optical microscopy;   Control TiO$_2$ particles (untreated or streptavidin-coated) were mixed with *E. coli* bacterial under the same experimental conditions. (c) the sediment was observed by SEM, and (d) the supernatant liquid was observed by optical microscopy;
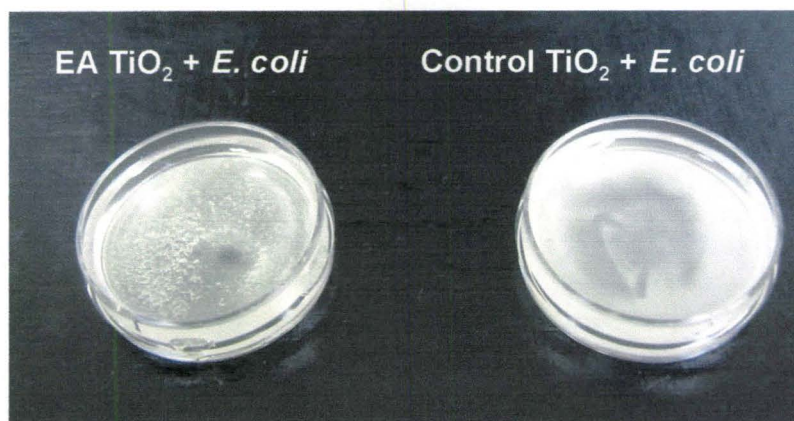
Figure 4-8 The mixture of EA TiO$_2$ and *E. coli* and the mixture of control TiO$_2$ (untreated TiO$_2$ or streptavidin-coated TiO$_2$) and *E. coli* were both mixed for 1 h and then maintained quiescent for 2 h in dark

(a)
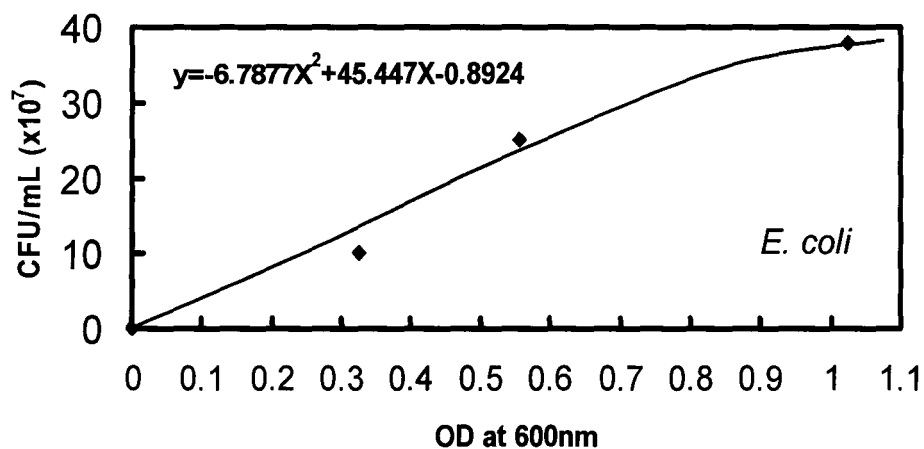
(b)
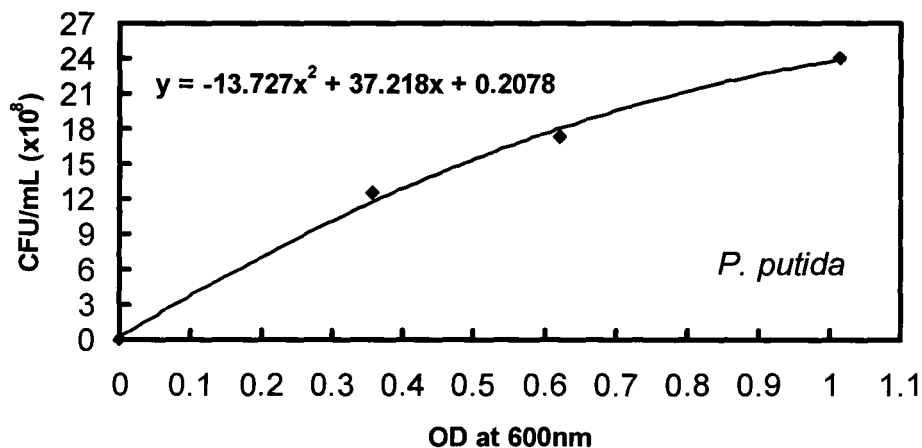
Figure 4-9   The calibration curves showing the relationship between the concentrations of bacteria in PBS buffer and the corresponding optical density values are obtained by measuring the absorbance of solution at 600nm wavelength. (a) for *E. coli* bacteria ; (b) for *P. putida* bacteria
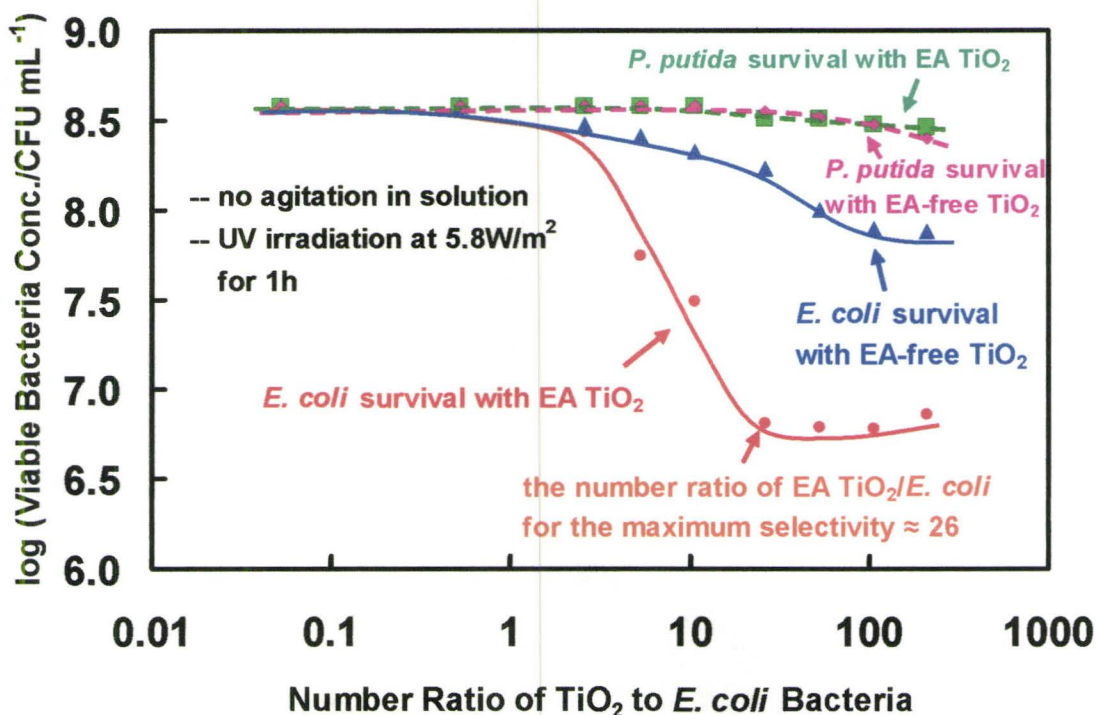
Figure 4-10 Bacterial survival (log (viable bacteria concentration/CFU mL^{-1})) changing with different number ratio of TiO$_2$ particles to *E. coli* cells, after 1h of 365nm irradiation at an intensity of 5.8 W/m^2 without agitation of solution; the red line representing *E. coli* survival with EA TiO$_2$; the blue line representing *E. coli* survival with streptavidin-coated TiO$_2$; the green dashed line representing *P. putida* survival with EA TiO$_2$; and the pink dashed line representing *P. putida* survival with streptavidin-coated TiO$_2$. The bacterial survival is represented by cell density (colony forming units per milliliter).
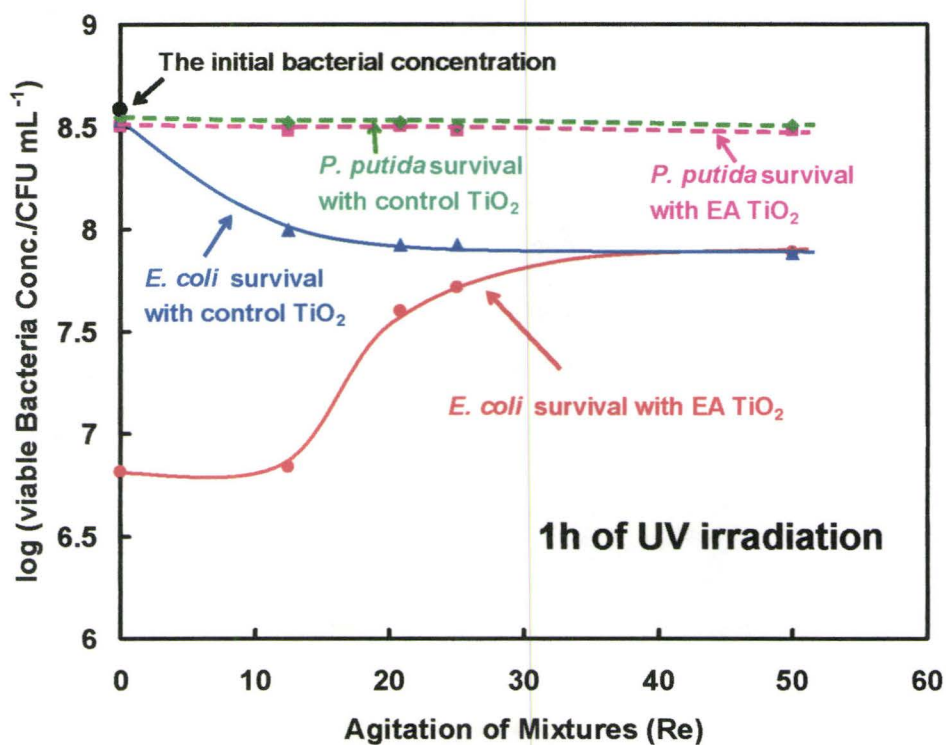
Figure 4-11   The change of log (viable bacteria concentration/CFU mL^{-1}) with EA TiO$_2$ and with the control TiO$_2$ against different Reynolds numbers of the agitated mixtures. The red line represents the case of killing *E. coli* with EA TiO$_2$; the blue line represents the case of killing *E. coli* with control TiO$_2$ (streptavidin-coated TiO$_2$); the pink line represents the case of killing *P. putida* with EA TiO$_2$; the green line represents the case of killing *P. putida* with control TiO$_2$ (streptavidin-coated TiO$_2$), and the black dot line represents the original concentration of bacteria. Data are obtained with the number ratio of particles to *E. coli* bacteria at 26 and 1h of 365nm irradiation at an intensity of 5.8 W/m^2.

	The original concentration of bacterial (CFU/mL)		Bacterial survival (CFU/mL) in the dark without agitation for 1h		Bacterial survival (CFU/mL) in the dark without agitation for 2h	
	E. coli	*P. putida*	*E. coli*	*P. putida*	*E. coli*	*P. putida*
Control 1(*E. coli* + *P. putida*)	3.8×10^8	3.8×10^8	3.7×10^8	3.8×10^8	3.7×10^8	3.8×10^8
Control 2 (untreated TiO_2+ *E. coli* + *P. putida*)	3.8×10^8	3.8×10^8	3.8×10^8	3.8×10^8	3.7×10^8	3.9×10^8
Control 3 (Streptavidin-coated TiO_2+ *E. coli* + *P. putida*)	3.8×10^8	3.8×10^8	4.1×10^8	4.0×10^8	3.8×10^8	3.8×10^8
EA TiO_2+ *E. coli* + *P. putida*	3.8×10^8	3.8×10^8	4.0×10^8	3.9×10^8	3.8×10^8	3.9×10^8

Table 4-4   Bacterial survival (CFU/mL) in the absence of TiO_2 and in the presence of different TiO_2 in the dark without agitation of solution for 0, 1 and 2 hours
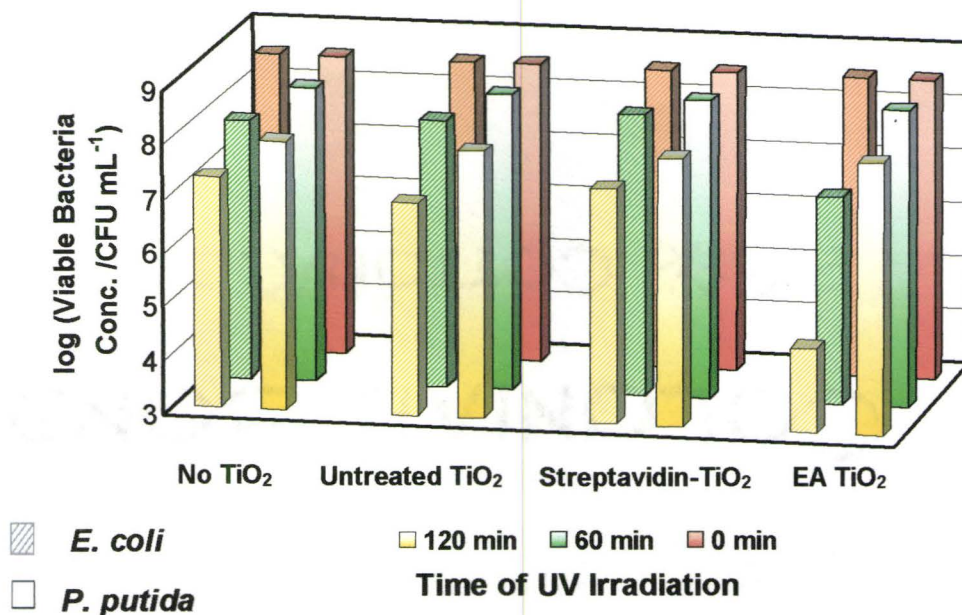
Figure 4-12 The change of log (viable bacteria concentration/CFU mL^{-1}) against different time of exposure to 365nm UV irradiation at an intensity of 5.8 W/m^2 in the absence of TiO$_2$ (the columns labeled by "no TiO$_2$"), or in the presence of untreated TiO$_2$ (the columns labeled by "untreated TiO$_2$"); or in the presence of streptavidin-coated TiO$_2$ (the columns labeled by "streptavidin-TiO$_2$"); or in the presence of EA TiO$_2$ (the columns labeled by "EA TiO$_2$"). Data are obtained with the number ratio of TiO$_2$ particles to *E. coli* bacteria at ~26 and without agitation of solution.

4.6   References

1. Matsunaga, T.; Tomoda, R.; Nakajima, T.; Wake, H., Photoelectrochemical sterilization of microbial cells by semiconductor powders. *FEMS Microbiology Letters* **1985,** 29, (1-2), 211-14.

2. Hashimoto, K.; Irie, H.; Fujishima, A., TiO$_2$ photocatalysis: A historical overview and future prospects. *Japanese Journal of Applied Physics, Part 1: Regular Papers, Brief Communications & Review Papers* **2005,** 44, (12), 8269-8285.

3. Hoffmann, M. R.; Martin, S. T.; Choi, W.; Bahnemann, D. W., Environmental Applications of Semiconductor Photocatalysis. *Chemical Reviews (Washington, D. C.)* **1995,** 95, (1), 69-96.

4. Fujishima, A.; Honda, K., Electrochemical photolysis of water at a semiconductor electrode. *Nature (London, United Kingdom)* **1972,** 238, (5358), 37-8.

5. Maness, P.-C.; Smolinski, S.; Blake, D. M.; Huang, Z.; Wolfrum, E. J.; Jacoby, W. A., Bactericidal activity of photocatalytic TiO2 reaction: toward an understanding of its killing mechanism. *Applied and Environmental Microbiology* **1999,** 65, (9), 4094-4098.

6. Hirakawa, K.; Mori, M.; Yoshida, M.; Oikawa, S.; Kawanishi, S., Photo-irradiated titanium dioxide catalyzes site specific DNA damage via generation of hydrogen peroxide. *Free Radical Research* **2004,** 38, (5), 439-447.

7. Hidaka, H.; Horikoshi, S.; Serpone, N.; Knowland, J., In vitro photochemical damage to DNA, RNA and their bases by an inorganic sunscreen agent on exposure to UVA and UVB radiation. *Journal of Photochemistry and Photobiology, A: Chemistry* **1997,** 111, (1-3), 205-214.

8. Linsebigler, A. L.; Lu, G.; Yates, J. T., Jr., Photocatalysis on TiO2 Surfaces: Principles, Mechanisms, and Selected Results. *Chemical Reviews (Washington, D. C.)* **1995,** 95, (3), 735-58.

9. Kawahara, K.; Ohko, Y.; Tatsuma, T.; Fujishima, A., Surface diffusion behavior of photogenerated active species or holes on TiO2 photocatalysts. *Physical Chemistry Chemical Physics* **2003,** 5, (21), 4764-4766.

10. Tatsuma, T.; Tachibana, S.-i.; Fujishima, A., Remote Oxidation of Organic Compounds by UV-Irradiated TiO2 via the Gas Phase. *Journal of Physical Chemistry B* **2001,** 105, (29), 6987-6992.

11. Kikuchi, Y.; Sunada, K.; Iyoda, T.; Hashimoto, K.; Fujishima, A., Photocatalytic bactericidal effect of TiO2 thin films: dynamic view of the active oxygen species

responsible for the effect. *Journal of Photochemistry and Photobiology, A: Chemistry* **1997**, 106, (1-3), 51-56.

12. Blake, D. M.; Maness, P.-C.; Huang, Z.; Wolfrum, E. J.; Huang, J.; Jacoby, W. A., Application of the photocatalytic chemistry of titanium dioxide to disinfection and the killing of cancer cells. *Separation and Purification Methods* **1999**, 28, (1), 1-50.

13. Marques, S.; Ramos, J. L., Transcriptional control of the Pseudomonas putida TOL plasmid catabolic pathways. *Molecular Microbiology* **1993**, 9, (5), 923-9.

14. Ward, P. G.; Goff, M.; Donner, M.; Kaminsky, W.; O'Connor, K. E., A Two Step Chemo-biotechnological Conversion of Polystyrene to a Biodegradable Thermoplastic. *Environmental Science & Technology* **2006**, 40, (7), 2433-2437.

15. Cazorla, F. M.; Duckett, S. B.; Bergstroem, E. T.; Noreen, S.; Odijk, R.; Lugtenberg, B. J. J.; Thomas-Oates, J. E.; Bloemberg, G. V., Biocontrol of avocado dematophora root rot by antagonistic Pseudomonas fluorescens PCL1606 correlates with the production of 2-hexyl 5-propyl resorcinol. *Molecular Plant-Microbe Interactions* **2006**, 19, (4), 418-428.

16. Zhao, X.; Hilliard, L. R.; Mechery, S. J.; Wang, Y.; Bagwe, R. P.; Jin, S.; Tan, W., A rapid bioassay for single bacterial cell quantitation using bioconjugated nanoparticles. *Proceedings of the National Academy of Sciences of the United States of America* **2004**, 101, (42), 15027-15032.

17. Gerard, E.; Guyot, F.; Philippot, P.; Lopez-Garcia, P., Fluorescence in situ hybridization coupled to ultra small immunogold detection to identify prokaryotic cells using transmission and scanning electron microscopy. *Journal of Microbiological Methods* **2005**, 63, (1), 20-28.

18. Huang, S.-H., Gold nanoparticle-based immunochromatographic test for identification of Staphylococcus aureus from clinical specimens. *Clinica Chimica Acta* **2006**, 373, (1-2), 139-143.

19. Naja, G.; Bouvrette, P.; Hrapovic, S.; Luong, J. H. T., Raman-based detection of bacteria using silver nanoparticles conjugated with antibodies. *Analyst (Cambridge, United Kingdom)* **2007**, 132, (7), 679-686.

20. Fu, Z.; Rogelj, S.; Kieft, T. L., Rapid detection of Escherichia coli O157:H7 by immunomagnetic separation and real-time PCR. *International Journal of Food Microbiology* **2005**, 99, (1), 47-57.

21. Kaittanis, C.; Naser, S. A.; Perez, J. M., One-Step, Nanoparticle-Mediated Bacterial Detection with Magnetic Relaxation. *Nano Letters* **2007**, 7, (2), 380-383.

22. Gao, P.; Xu, G.; Shi, X.; Yuan, K.; Tian, J., Rapid detection of Staphylococcus aureus by a combination of monoclonal antibody-coated latex and capillary electrophoresis. *Electrophoresis* **2006,** 27, (9), 1784-1789.

23. Xu, J.; Zhao, Y.-M.; Chen, C.-M.; Sun, Y.; Liu, G.-Y.; Yan, M.-M.; Jiang, Z.-Y., Oriented photo-killing tumor using antibody-nano-TiO2 conjugates and electroporation methods. *Huaxue Xuebao* **2006,** 64, (22), 2294-2300.

24. Bhaduri, A.; Das, K. P., Proteins at solid/water interface - a review. *Journal of Dispersion Science and Technology* **1999,** 20, (4), 1097-1123.

25. Talbot, J.; Tarjus, G.; Van Tassel, P. R.; Viot, P., From car parking to protein adsorption: an overview of sequential adsorption processes. *Colloids and Surfaces, A: Physicochemical and Engineering Aspects* **2000,** 165, (1-3), 287-324.

26. Green, N. M., Avidin. *Advances in Protein Chemistry* **1975,** 29, 85-133.

27. Chaiet, L.; Wolf, F. J., The Properties of Streptavidin, a Biotin-Binding Protein Produced by Streptomycetes. *Archives of biochemistry and biophysics* **1964,** 106, 1-5.

28. Savage, M. D.; Mattson, G.; Desai, S.; Nielander, G. W.; Morgensen, S.; Conklin, E. J., *avidin-biotin chemistry: a hanhbook.* Pierce Chemical Co.: Rockford, 1992.

29. Ye, L.; Pelton, R.; Brook, M. A., Biotinylation of TiO2 Nanoparticles and Their Conjugation with Streptavidin. *Langmuir* **2007,** 23, (10), 5630-5637.

30. http://solutions.3m.com/wps/portal/3M/en_US/Microbiology/FoodSafety/product-applications/indicator-organism-testing/?PC_7_RJH9U5230O0G602RVAFDHB3043_nid=C0WJ62882Vbe29BDXSBJ7Fgl, In.

31. Kitagawa, M.; Ara, T.; Arifuzzaman, M.; Ioka-Nakamichi, T.; Inamoto, E.; Toyonaga, H.; Mori, H., Complete set of ORF clones of Escherichia coli ASKA library (a complete set of E. coli K-12 ORF archive): unique resources for biological research. *DNA Research* **2005,** 12, (5), 291-299.

32. Wold, A., Photocatalytic properties of titanium dioxide (TiO2). *Chemistry of Materials* **1993,** 5, (3), 280-3.

33. Benabbou, A. K.; Derriche, Z.; Felix, C.; Lejeune, P.; Guillard, C., Photocatalytic inactivation of Escherichia coli. Effect of concentration of TiO2 and microorganism, nature and intensity of UV irradiation. *Applied Catalysis, B: Environmental* **2007,** 76, (3-4), 257-263.

34. Gumy, D.; Morais, C.; Bowen, P.; Pulgarin, C.; Giraldo, S.; Hajdu, R.; Kiwi, J., Catalytic activity of commercial of TiO_2 powders for the abatement of the bacteria (E.

coli) under solar simulated light: Influence of the isoelectric point. *Applied Catalysis, B: Environmental* **2006**, 63, (1-2), 76-84.

35. Cohen-Yaniv, V.; Narkis, N.; Armon, R., Photocatalytic inactivation of Flavobacterium and E. coli in water by a continuous stirred tank reactor (CSTR) fed with suspended/immobilised TiO2 medium. *Water Science and Technology* **2008**, 58, (1), 247-252.

36. Maccabe, W. J.; Smith, J. C.; Harriott, P., *Unit Operations of Chemical Engineering. 4th Ed.* 1985; p 960 pp.

37. Huang, S.-C.; Swerdlow, H.; Caldwell, K. D., Binding of biotinylated DNA to streptavidin-coated polystyrene latex. *Analytical Biochemistry* **1994**, 222, (2), 441-9.

38. Hendrickson, W. A.; Paehler, A.; Smith, J. L.; Satow, Y.; Merritt, E. A.; Phizackerley, R. P., Crystal structure of core streptavidin determined from multiwavelength anomalous diffraction of synchrotron radiation. *Proceedings of the National academy of Sciences of the United States of America* **1989**, 86, (7), 2190-4.

39. Weber, P. C.; Cox, M. J.; Salemme, F. R.; Ohlendorf, D. H., Crystallographic data for Streptomyces avidinii streptavidin. *Journal of Biological Chemistry* **1987**, 262, (26), 12728-9.

40. Furlong, D. N.; Parfitt, G. D., Electrokinetics of titanium dioxide. *Journal of Colloid and Interface Science* **1978**, 65, (3), 548-54.

41. Snoswell, D. R. E.; Duan, J.; Fornasiero, D.; Ralston, J., Colloid stability of synthetic titania and the influence of surface roughness. *Journal of Colloid and Interface Science* **2005**, 286, (2), 526-535.

42. Ye, L.; Miao, C.; Brook, M. A.; Pelton, R., Photoflocculation of TiO2 Microgel Mixed Suspensions. *Langmuir* **2008**, 24, (17), 9341-9343.

43. Dickson, J. S.; Koohmaraie, M., Cell surface charge characteristics and their relationship to bacterial attachment to meat surfaces. *Applied and environmental microbiology* **1989**, 55, (4), 832-6.

44. Rincon, A.-G.; Pulgarin, C., Effect of pH, inorganic ions, organic matter and H2O2 on E. coli K12 photocatalytic inactivation by TiO2. Implications in solar water disinfection. *Applied Catalysis, B: Environmental* **2004**, 51, (4), 283-302.

4.7 Appendix

Equation 1

$$D_{SA} = \frac{\left(\sum_{i=1}^{n} \frac{A_i \times V}{\varepsilon}\right) \times N_A}{M_{SA} \times m_{Ti} \times SSA_{B-Ti} \times 10^{18}}$$

D_{SA}: the density of streptavidin conjugated on TiO_2 surfaces ($/nm^2$)

ε: the extinction coefficient of streptavidin used in these experiments (ε_{282nm} = 3.4 L/g)

A_i: the absorbance value of the supernatant liquid at 282nm after each centrifugation during the washing process

V: the volume of the buffer solution used in each washing (V = 3 mL = 3×10^{-3} L)

N_A: Avogadro's constant (N_A = 6.02×10^{23} /mole)

M_{SA}: the molecular weight of streptavidin (M_{SA} = 60 KDa)

m_{Ti}: mass of TiO_2 used in the experiments (m_{Ti} =1.2mg=1.2×10^{-3} g)

SSA_{B-Ti}: the specific surface area of the biotinylated TiO_2 particles used in the experiments (SSA_{B-Ti} = 14.4 m^2 g^{-1}, measured by N_2 absorption)

Equation 2

$$D_{anti} = \frac{m_{anti} \times N_A}{M_{anti} \times m_{Ti} \times SSA \times 10^{18}}$$

D_{anti}: the density of biotinylated *E. coli* antibody on EA TiO_2 surfaces ($/nm^2$)

m_{anti}: mass of biotinylated *E. coli* antibody required for the conjugation with streptavidin-coated TiO_2 surfaces (m_{anti}=60 µg=60×10^{-6} g)

N_A: Avogadro's constant (N_A = 6.02×10^{23} /mole)

M_{anti}: the molecular weight of antibody (M_{anti} ≈ 150 KDa, data from Abcam company)

m_{Ti}: mass of streptavidin-coated TiO_2 used for the preparation (m_{Ti} = 1.2 mg= 1.2×10^{-3} g)

SSA_{EA-f}: the specific surface area of the streptavidin-coated TiO_2 particles used in the experiments (SSA_{EA-f}=13.5 m^2 g^{-1}, measured by N_2 absorption)

Equation 3 [36]

$$R_e = \frac{n \times D_a^2 \times \rho}{\eta}$$

Re: the modified Reynolds number

n: rotational speed (in our experiments, the agitation speeds are 30rpm, 50rpm, 60rpm, and 120rpm, which corresponding to 0.5/s, 0.83/s, 1/s, and 2/s)

D_a: the diameter of the impeller (5×10^{-3} m)

ρ: the density of the fluid (assuming the density of the bacterial mixtures is same as that of water, 1×10^3 kg/m^3)

η: the viscosity of the fluid (assuming the density of the bacterial mixtures is same as that of water, 1×10^{-3} kg/ms)
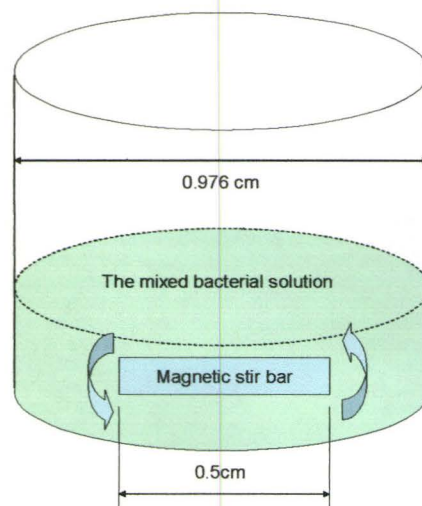
Figure 4A1 Photodisinfection experiments illustration

Chapter 5   Immobilization of TiO$_2$ nanoparticles onto cellulose fibers through bioconjugation[*]

5.1   Introduction

TiO$_2$ is an effective catalyst for the photoactivated oxidation of organic molecules. Such materials are used in applications ranging from water disinfection to environmental remediation of airborne organics. The immobilization of photoactive TiO$_2$ nanoparticles onto cellulose fibers can be used to prepare self-cleaning paper,[1-3] which may have a variety of potential applications such as food packaging. Currently, the methods for immobilizing TiO$_2$ nanoparticles onto fibers involve the use of additives such as cationic polymers, which can bind negatively charged particles and fibers together.[2,4-6] However,

---

[*] This work has led to one published paper in Journal of Materials Chemistry 2009, 19, XX. This paper, Immobilization of TiO$_2$ nanoparticles onto paper modification through bioconjugation, was authored by Lu Ye, Carlos Filipe, Mojgan Kavoosi, Charles Haynes, Robert Pelton, and Michael Brook. In this publication, *E. coli* containing the gene for the expression of CBM2a-strep tag II and the related techniques was provided by Mojgan Kavoosi, Charles Haynes. The research related to bacteria treatment and protein purification were guided by Carlos Filipe. These contributions make them co-authors, however, I did all the research described in that paper.

these additives can also induce significant aggregation of fines, fillers and fibers, resulting in deterioration of the quality of the paper.[7] More importantly, the aggregation dramatically decreases the specific surface area of the TiO_2 nanoparticles, resulting in a large number of photoinactive nanoparticles inside the aggregates, thereby significantly decreasing the efficiency of photocatalysis.

There is a need, therefore, to more effectively immobilize TiO_2 nanoparticles onto fibers. In principle, one feasible method to accomplish this is to adjust the pH of the solution to give the TiO_2 nanoparticle surfaces a positive charge, so that the positively charged nanoparticles can adhere to the negatively charged paper fibers.[3] A problem with this method, however, is that such adhesion depends strongly on the pH range of the environment. As the pH changes, the adhesion can be weakened significantly. Thus, more effective, alternative methods are required.

Carbohydrate-binding modules (CBMs), fourteen families of which are also known as cellulose binding domains (CBDs),[8] have a high affinity to cellulose ($K_a = 10^6$ M^{-1}).[9, 10] Fusion technology used to recombine CBMs with other biomolecules, such as streptavidin,[11] *Strep*-tag,[12] histidine tag,[9] Pro-A,[13, 14] and antibodies.[15, 16] These complexes offer the possibility of targeted immobilization of biomolecules of interest or other interesting moieties including quantum dots (QDs)[12] and polystyrene latices[16] onto a cellulose matrix for fiber modification,[17, 18] protein purification,[19, 20] diagnostics,[21, 22] or bacterial adhesion.[23, 24]

Biotin, vitamin H, involved in many important biochemical processes in the human organism, exists in every living cell.[25] Streptavidin, produced by *Streptomyces avidinii*,

binds exceptionally tightly to biotin ($K_a = 10^{15}$ M^{-1}).[26, 27] The biotin-streptavidin

interaction is widely used in bioprocessing, because one streptavidin molecule can bind

up to four biotin molecules. The broad usage of this linkage in biochemistry results from

the fact that most biomolecules can be biotinylated under mild conditions.[28] *Strep*-tag II,

a streptavidin ligand with a selected eight amino acids (WSHPQFEK), has been

developed on the basis of the high affinity between streptavidin and biotin.[29] The

interaction between *Strep*-tag II and streptavidin ($K_a = 10^4$ M^{-1})[30, 31] has been widely used

for the conjugation of the *Strep*-tag II fusion protein to streptavidin, particularly for the

one-step purification of the corresponding *Strep*-tag II-proteins through a streptavidin-

filled column.[32] TiO$_2$ nanoparticles can be covalently biotinylated by a chemical method,

which offers the possibility to attach biotinylated particles to streptavidin.[33]

Recently, much interest has developed in the preparation and application of TiO$_2$-

biomolecule hybrids because of the potential utility of combining their photocatalytic and

biological properties.[34, 35] A literature search shows that these hybrids have previously

been prepared by physisorption.[36, 37] In these UV-activated, TiO$_2$-biomolecule systems,

often rapid inactivation of these adsorbed biomolecules was found to occur because of the

free radicals generated on the UV-irradiated TiO$_2$ surfaces.[38, 39] It is therefore of interest

to establish if alternate methods can be found that will allow TiO$_2$ particles to be utilized

for their photoactive properties without concerns about degradation of the local

environment – cellulose fibers – on which the particles are supported.

In this research, we have developed a bioconjugation method for immobilizing TiO$_2$

nanoparticles onto cellulose fibers for the first time using multi-linker bioconjugation:

CBM2a-*Strep*-tag II – streptavidin – biotinylated TiO_2 nanoparticles. Such a system provides for explicit bioconjugation of the particles onto cellulose fibers and permits an analysis of the photoactivity of tethered TiO_2 particles for external oxidation as compared to oxidation of the tether and the local environment. The photocatalytic functionality of TiO_2-containing paper produced by this method is demonstrated by an assay involving decolorization of anionic reactive black 5 dye (RB5), and the resistance to oxidative degradation of the linker was roughly estimated.

5.2   Experimental Section

5.2.1.   Chemicals

Whatman qualitative filter paper (No.1) was purchased from Aldrich and used as received. The basis weight of the Whatman No.1 is 87 g m^{-2}, as provided by the Whatman Company. The specific surface area (SSA) of the paper was tested on a Quantachrome Nova 2200 by nitrogen adsorption and a Poremaster GT 60 by mercury intrusion porosimetry to be 6.154 m² g^{-1} and 16.106 m² g^{-1}, respectively. Streptavidin from *Streptomyces avidinii* was purchased from Fluka and used as received. Reactive Black 5 dye (RB5) was purchased from Sigma-Aldrich Canada and used as received. AEROXIDE® TiO_2 P 25 was donated by Degussa Corporation (Parsippany, NJ, USA). Biotinylated TiO_2 nanoparticles were prepared (Scheme 5-1) as described previously in Ye et al.[33] A glycerol stock solution of BL21 (DE3) *E. coli* cells containing the histidine-

CBM2a-*Strep*-tag II construct was provided by the Charles A. Haynes lab of the

University of British Columbia. The amino-acid sequence of the histidine-CBM2a-*Strep*-

tag II construct is shown in Figure 5-1. The CBM2a-*Strep*-tag II construct was cloned

into the NcoI/HindIII sites of the pET22 vector (Novagen). This vector has the pelB

signal sequence for expression into the periplasm, the ampicillin resistant gene and the T7

promoter. Hence, cells containing this vector are ampicillin resistant, and protein

expression is induced with isopropyl β-D-1-thiogalactopyranoside (IPTG). The antibiotic

ampicillin was purchased from Fluka and prepared at a concentration of 100mg/mL in

MilliQ grade water. The ampicillin solution was filtered through a 0.2μm filter disc to

remove bacteria and dust before use. IPTG (Fermentas, Burlington, ON, Canada) was

used to induce expression of histidine-CBM2a-*Strep*-tag II fusion protein in *E. coli*.

Luria-Bertani (LB) was used as the medium for *E. coli* culture, containing per liter:

tryptone (10g, EMD, Gibbstown, NJ), yeast extract (5g, EMD), and NaCl (10g, Aldrich).

Phosphate buffered saline (PBS) buffer (137 mM NaCl, 2.7 mM KCl, 4.2 mM Na_2HPO_4,

1.4 mM KH_2PO_4, pH 7.4) was prepared and autoclaved before use. Tris-

(hydroxymethyl)aminomethane-HCl buffer (20mM Tris-(hydroxymethyl) aminomethane,

50mM NaCl, pH 7.4) was prepared and autoclaved before use. MilliQ grade water was

used for preparing all aqueous solutions.

5.2.2. The expression and purification of histidine-CBM2a-*Strep*-tag II [40, 41]

E. coli stains BL21 (DE3), containing CBM2a-*Strep*-tag II construct, was cultivated in

500mL LB media supplemented with 0.1% ampicillin solution (100mg/ml). Shaker

flasks were inoculated from a single colony and cultured at 37 °C with a shaking rate of 180 rpm until the OD_{600} reached 0.6-1.0. IPTG was then added, to give a final concentration of 0.1mM, to induce expression of the histidine-CBM2a-*Strep*-tag II protein. The cells were then cultured for 14 h at 30 °C.

The cells were harvested by centrifugation at the rate of 10000 G for 15 min at 4 °C. The supernatant liquid was discarded and 10 mL Tris-HCl buffer was added to the centrifuge tube to suspend the cell pellets. The tube was then inserted in the ice-water sink to maintain low temperature when the cell pellets were disrupted by ultrasonication (4 times × 5 minutes, 25W energy output) using an ultrasonic cell disrupter (Vir Sonic 100, VirTis, USA). Then the cell debris was removed by centrifugation at 12000 G for 15 min at 4 °C. The resulting supernatant liquid was applied to a 5mL HisTrap FF column (GE Healthcare) according to the manufacturer's instructions. Finally, the protein purity was analyzed by SDS-page and stored in a -20 °C freezer before use.

5.2.3. Preparation of aminosilanized TiO₂ and biotinylated TiO₂ nanoparticles (Scheme 5-1)

Aminosilanized and biotinylated TiO₂ nanoparticles were prepared according to the method described in Ye et al.:[33] untreated TiO₂ (0.03g, 0.376mmol) was reacted with 3-aminopropyltriethoxysilane (0.15mL, 0.635mmol) in anhydrous DMSO (100mL) at 85 °C, stirring for 4 h under dry N₂. The solid particles were deposited by centrifugation and then washed with anhydrous DMSO (3×180mL) to remove the excess APTS. After washing, the particles were dispersed in anhydrous DMSO (100mL) again and cured in a

nitrogen stream at 120 °C for 2h. After curing, the preparation of aminosilanized TiO_2 was complete. Biotinylated TiO_2 particles were prepared by the reaction of aminosilanized TiO_2 (0.015g, 0.188mmol) with N-hydroxysuccinimidobiotin (0.1g, 0.29mmol) in anhydrous DMSO (50mL) at room temperature for 3h. Finally, the solid particles were washed with anhydrous DMSO (3×180mL), followed by MilliQ grade water (3×180mL), and then dried in vacuo at 65 °C to remove the residual solvents.

5.2.4. Immobilization of TiO_2 onto paper

The immobilization of AEROXIDE[®] TiO_2 P 25 nanoparticles onto paper was achieved by a bioconjugation method in three steps: (1) the adsorption of CBM2a-Strep-tag II protein to paper through the specific absorption of CBM2a to cellulose;[9, 10] (2) the binding of streptavidin to CBM2a-Strep-tag II protein by the bioconjugation of streptavidin with Strep-tag II;[30, 31] (3) the attachment of biotinylated P25 TiO_2 nanoparticles to streptavidin through the biotin-streptavidin interaction [33] (Figure 5-2).

After purification, the fusion protein of CBM2a-Strep-tag II was diluted with Tris-HCl buffer to obtain an appropriate concentration of about $3.96×10^{-5}$ mol/L (A_{280}=1.3126, ε=33125) for application to the paper. A 2 cm × 6 cm strip of Whatman No.1 filter paper was submerged in 3 mL of the CBM2a-Strep-tag II protein solution with the above-mentioned concentration in a Petri dish (100 × 20mm, BD Optilux™, BD Falcon™). The Petri dish was then shaken at a speed of 40rpm on a shaking bed (Barnstead/ Lab-Line USA Model No. 4633) at room temperature for 3 h for reaction (it was found that longer reaction times did not lead to more adsorption). After that, the paper was moved to

another Petri dish containing 15mL MilliQ grade water, and washed in a shaker at a speed of 80rpm for 15 min. The absorbance of the supernatant liquid of the CBM2a-*Strep*-tag II protein solution was tested at 280nm. The washing process was repeated and after each washing the absorbance value of the supernatant liquid of the solutions was tested at 280nm until the absorbance value was less than 0.0005, indicating that the unbound protein had all been washed off from the paper. The amount of adsorbed CBM2a-*Strep*-tag II protein onto the paper could be calculated using Equation 1.

Streptavidin solution at a concentration of 1.65×10^{-5} mol/L (A_{282}=0.9395, ε=57000) was prepared by dissolving the lyophilized streptavidin in Tris-HCl buffer. The paper, treated with CBM2a-*Strep*-tag II protein, was then treated and washed by the same procedures as used in attaching CBM2a-*Strep*-tag II protein. The amount of adsorbed streptavidin on the paper could be similarly calculated (Equation 1).

A biotinylated TiO_2 nanoparticle suspension, at a concentration of 0.4g/L, was prepared by dispersing nanoparticles in Tris-HCl buffer using ultrasonication (BRANSON 8510) for 10 min. Then the paper, treated with CBM2a-*Strep*-tag II and streptavidin, was submerged in 5mL of this biotinylated TiO_2 suspension for 20 s and immediately moved into 5mL of Tris-HCl buffer. The paper was then washed with the same procedure as described above. Finally, the paper was rinsed with 2L Tris-HCl buffer to remove the unbound particles.

The control-1, control-2 and control-3 experiments were preformed in the same way, except that specific materials were either omitted or replaced (see Table 5-1).

5.2.5.   Photodegradation of RB5 by TiO₂-containing paper

A Black-Ray® XX-15BLB UV Bench Lamp (365 nm) was used as the light source for photodegradation in the RB5 assay. The intensity of UV irradiation was measured by a Traceable® Ultra Violet Light Meter (VWR). An incident intensity of 23 W/m^2 to the TiO₂-containing paper in RB5 solution was established by adjusting the position of the light source. An RB5 solution with a concentration of 23ppm was prepared by dissolving the dye in MilliQ grade water. A strip of TiO₂-containing paper, prepared using the above-mentioned method, with a size of 1 × 2cm, and a magnetic stirring bar (7.9mm × 1.5mm) were placed in a quartz cuvette containing 1.7 mL of the RB5 solution. The cuvette was sealed and then irradiated with the UV lamp (365nm, 23W/m^2) for at least 12 h, while the solution was slowly agitated by the magnetic stirring bar with a speed of ~5 rpm. The absorbance of the supernatant solution at 597nm was measured every 2 h. The control experiment was performed using the control paper instead of TiO₂-containing paper. After 12 h of UV irradiation, the paper was characterized with scanning electron microscopy (SEM) and the solution was observed using both transmission electron microscopy (TEM) and optical microscopy.

5.2.6.   Measurements

1. Sodium dodecyl sulfate polyacrylamide gel electrophoresis (SDS-PAGE) analysis was performed on 17.5% polyacrylamide gels under denaturing conditions. Gels were stained with Coomassie brilliant blue R-250. A 10-kDa protein ladder (Fermentas) was used as a molecular mass marker.

2. The electrophoretic mobility of biotinylated P 25 TiO$_2$ was measured on the ZetaPlus zeta potential analyzer (Brookhaven Instruments Corp.) operating in phase analysis light scattering mode. Measurements were performed in Tris-buffer (20mM Tris-base, 50mM NaCl, pH 7.4). The mean and standard deviation (see below) were calculated from 10 runs (15 cycles per run).

3. UV-vis absorbances of samples were measured on a UV-vis spectrophotometer (Beckman Coulter DU800 Spectrophotometer, software version 2.0). For CBM2a-strep tag ($\varepsilon=33125$), the absorbance of the protein solution at 280nm was tested to quantify the concentration. The concentration of streptavidin was quantified at 282nm ($\varepsilon=57000$). A visible light source at 597nm was used for determining the concentration of RB5.

4. Scanning electron microscopy (SEM) observation and energy dispersive X-ray spectroscopy (EDS) analysis of the surfaces of the TiO$_2$-containing paper and the control papers were performed with a JEOL JSM-7000F scanning electron microscope and an EDS-INCA analyzer (Oxford), respectively. The papers were sputter-coated with platinum before testing.

5. The specific surface area (SSA) value of Whatman No.1 filter paper was tested by two methods: nitrogen adsorption performed on a Quantachrome Nova 2200 and

mercury intrusion porosimeter on a Poremaster GT 60 over a pressure range of 20-59352 psi and analyzed using the Washburn Equation.

6. Thermogravimetric analysis (TGA) of the TiO_2-containing paper and the control papers were performed with a Netzsch STA-409 DTA/TGA analyzer. The samples were heated in air at 10 °C/min from room temperature to over 800 °C.

7. Optical microscopy observation of the RB5 supernatant solution, after $UV-TiO_2$ irradiation for 12 h, was performed on a Zeiss EL-Einsatz microscope equipped with a QICAM QImaging camera.

8. Transmission electron microscopy (TEM) observation of the dried RB5 supernatant solution, after $UV-TiO_2$ irradiation for 12 h, was performed on a JEOL JEM-1200EX transmission electron microscope. The solution was dropped onto the copper grid to dry for observation.

5.3   Results

5.3.1.   Preparation of the Paper-CBD-Linker-TiO_2 Particles

Relatively large quantities of the cellulose binding domain (CBM) were required for studies on their use as biological adhesion promoters. Standard expression techniques

were utilized to prepare the material,[40, 41] and the SDS-PAGE test results showed, after isolation, that the fusion protein of CBM2a-*Strep*-tag II expressed in *E. coli* was effectively purified (Figure 5-3).

The CBD was used to link, through streptavidin, TiO_2 particles to paper. To do so, it was first necessary to surface modify the titania particles (P25) with amino groups, using aminopropyltriethoxysilane (APTS).[33] While aminosilane-modified particles are normally positively charged, in this aminosilanization, thermal curing was either omitted or carried out for very short time such that the organosilane coating incompletely capped the surface. As a consequence, the overall surface charge of the APTS modified TiO_2 nanoparticles in Tris-HCl buffer was negative. This reduces the likelihood of particle adsorption onto the negatively charged cellulose fibers. Subsequently, biotin was tethered to the particle surface using biotin-activated esters (Scheme 5-1). The electrophoretic mobilities of control materials showed that the entire series of particles was negatively charged in Tris-HCl buffer at pH 7.4: P25 TiO_2 -1.06±0.14 × 10^{-8}, APTS-modified P 25 TiO_2 -0.56±0.04) × 10^{-8} and biotinylated P 25 TiO_2 nanoparticles -0.71±0.04 × 10^{-8} m^2/Vs, respectively.

The biotinylated particles were exposed to streptavidin-CBM2a-*Strep*-tag II to give particles that were adhesive to cellulose. They were tethered to cellulose by three bioconjugation elements: biotin (on TiO_2 nanoparticles) / streptavidin, streptavidin / *Strep* tag II (on CBM2a) and CBM2a / cellulose (Figure 5-2). After the attachment experiments, it was found that many biotinylated P 25 TiO_2 nanoparticles were attached to the paper fibers and were distributed uniformly across fibers (Figure 5-4a and Figure 5-

5). By contrast, in the control experiments in which either there was no CBM2a-*Strep*-tag II protein present, or untreated or aminosilanized TiO_2 was used instead of biotinylated TiO_2 nanoparticles, it was found that very few particles were present on the fiber surfaces, apart from those occasionally trapped by holes (Figure 5-4 b-d). EDS tests were performed on the particle area and non-particle areas on the fiber surfaces.

Table 5-2 shows the EDS test results: where particles were located, the weight and atomic percentage of Ti were 10.46% and 3.33%, respectively; whereas no Ti could be detected in areas not bearing particles. These data indicate that the nanoparticles present on the fiber surfaces are TiO_2 based. The higher carbon concentration on the non-particle area (weight% 76.11, atomic% 85.61) than on the particle area (weight% 55.47, atomic% 70.5) is due to the higher percentage of cellulose on the test area. Platinum concentrations on the non-particle area (weight% 6.40, atomic% 0.44) and the particle area (weight% 6.59, atomic% 0.52) were similar, and are a consequence of Pt that was sputter-coated on the paper samples, which was required for the SEM assay. Sodium and chlorine concentrations on the non-particle and particle areas are similar and low, and result from the use of a buffer solution during the attachment experiments.

5.3.2. Binding the Particles to Paper

Biotinylated TiO_2 nanoparticles were bound to paper through multi-linker bioconjugation following the sequence: cellulose/CBM2a; *Strep* tag II on CBM2a/streptavidin; and, streptavidin/biotin on TiO_2 particles. The efficiency of binding TiO_2 to paper by this method can be evaluated by comparing the amounts of bound

proteins and particles obtained from the experiments with the theoretical values that would result from full attachment. Since CBM2a is the first protein loaded onto the paper, the amount of attached CBM2a plays a crucial role in determining the amount of the streptavidin molecules that can be subsequently attached. For the same reason, the density of TiO_2 nanoparticles on the paper depended on the coverage of the bound streptavidin.

In the experiments involving attachment of proteins (CBM2a and streptavidin) to paper, a strip of paper was submerged in the protein solution of known concentration. After shaking for a certain time, the paper was removed and then washed repeatedly with a known volume of water. In this method, proteins were initially adsorbed to paper by both chemisorption and physisorption. However, after subsequent washings, only chemisorbed proteins were retained on the paper. The amount of protein chemisorbed onto the paper could be calculated using Equation 1, after testing the UV absorbance (280nm for CBM2a-*Strep*-tag II, 282nm for streptavidin) of the resulting protein solutions. Further, by combining this with the SSA value and basis weight value of Whatman No.1 filter paper, the density of the adsorbed protein could be calculated using Equation 2. It was found that shaking the paper in the solution promotes the adsorption of protein. However, it was also found that shaking at high speed weakens the paper network. Our experimental results show that a shaking rate of about 30-50rpm is appropriate for maximum adsorption of proteins onto paper in a water medium, without degrading the properties of the paper support. It was found that protein chemisorption increased with the reaction time and eventually reached maximum values at about 2 hours: ~ 1.44 mg/m^2

(= 6.22 × 10^{-2}/nm^2) for the adsorption of CBM2a-*Strep*-tag to the paper; and ~ 1.92

mg/m^2 (= 1.93 × 10^{-2}/nm^2) for the further adsorption of streptavidin to *Strep*-tag II-

CBM2a-paper.

After attaching biotinylated P 25 TiO$_2$ nanoparticles to the streptavidin-*Strep*-tag II-

CBM2a-paper, the preparation of TiO$_2$-containing paper was complete. The amount of

TiO$_2$ on the paper was tested by TGA. Six replicate samples were tested, and on average

0.8wt% residual material was found after heating to 800 °C (Figure 5-6). The results for

the control papers showed the remaining material averaged only 0.12%. For Whatman

No.1 filter paper, the ash content is less than 0.06% (as provided by the Whatman

Company). The difference of the remaining material content after heating between the

control paper and the untreated paper indicates relatively low attachment of TiO$_2$ and the

presence of buffer salts on the control paper (Figure 5-4 b-d and Table 5-2).

Several attempts were made to understand in detail the surface density of TiO$_2$ and the

underlying bioconjugating elements, including TGA, nitrogen adsorption and mercury

porosimetry. Although the TGA results for the TiO$_2$-containing paper show that the TiO$_2$

is efficiently attached to paper by the bioconjugation method, it is impossible to get a

reliable datum of the attachment density based on the TGA results because the error of

TGA results is large and the accessibility to P25 TiO$_2$ nanoparticles of the cellulosic

surface is required for calculation. The latter number is unknown. BET data were

measured to obtain cellulosic surface area. The specific surface area (SSA) of cellulosic

fibers in the paper measured by nitrogen adsorption is 6.154 m^2 g^{-1}. However, these data

do not provide guidance on accessibility to larger particles, particularly to non-uniform

particles of varying roughness. Similarly, mercury porosimetry measurements on the

paper and TiO$_2$ tethered paper were undertaken. The SSA value of cellulosic fibers in the

paper measured by mercury porosimetry is 16.106 m^2 g^{-1}. However, these data similarly

do not discriminate between internal macropores accessible to mercury and macropores

that are truly accessible to the relatively large particles. Finally, the coverage and the

distribution density of TiO$_2$ on fibers were obtained by manually analyzing many SEM

images including Figure 5-4a to be ~24% and ~ 58 μm^{-2}, respectively.

5.3.3. Photocatalytic activity

The photocatalytic ability of the TiO$_2$-containing paper was demonstrated by

photodegradation of the dye RB5 (Figure 5-7 and Figure 5-8). One control experiment

was performed with the control paper (control-1, 2 and 3) and TiO$_2$-containing paper

without UV irradiation, showing that no photodegradation of RB5 dye observed after 24

hours. Another control experiment was performed with the control paper (control-3, no

biotin on the TiO$_2$ particles, Table 5-1), showing that only 10% dye decomposed after 12

hour UV irradiation. By contrast, an intensely colored aqueous solution of RB5 (23ppm,

A_{597}=0.5438) in the presence of 1cm × 2cm TiO$_2$-containing paper became completely

clear (A_{597}=0.0151) after irradiation for the same 12 hour period. After this time the

TiO$_2$-containing paper was observed by SEM and the supernatant solution was

characterized using optical microscopy and TEM. It was found that while many TiO$_2$

nanoparticles were still present on the fiber surfaces (Figure 5-11), many fibers and TiO$_2$

nanoparticles were also found in the solution (Figure 5-9 and Figure 5-10). These results

suggest that after 12 hours of UV irradiation, the fiber network and the bioconjugation were both partially destroyed due to photooxidation in the vicinity of the TiO_2 particle, resulting in the partial detachment of fibers and TiO_2 nanoparticles from the paper.

5.4   Discussion

TiO_2 is commonly used in paper chemistry to brighten the paper. Traditional methods for attaching inorganic particles to paper use additives such as cationic polymers. These additives produce aggregates of particles, which can be trapped by holes in the 3-dimensional network of the paper. The interaction between mineral/polymer and fiber is dominated by both physical and ionic interactions.[4, 6] Adhesion of the particles to the cellulose fiber is poor and TiO_2 aggregates perform relatively poorly as photocatalysts: much of the particle surface area is unavailable to UV irradiation.

In the present study, for the first time, unaggregated TiO_2 nanoparticles were attached to paper using bioconjugation, leading to the formation of photocatalytic paper. This conclusion is apparent from the physical characteristics of the product. Pulp fibers are negatively charged due to their intrinsic properties (the presence of some COOH groups).[42-44] The TiO_2 nanoparticles (untreated, aminosilanized and biotinylated) used in the experiments were also prepared with negatively charged surfaces, as confirmed by mobility test results at pH 7.4. Therefore, there will be no electrostatic attraction between fibers and TiO_2 nanoparticles. The observed adhesion is therefore due to bioconjugation.

The preparation process showed that complex molecular interactions of several different types were needed to effectively adhere TiO_2 nanoparticles to fibers with a uniform distribution (Figure 5-4a and Figure 5-5). The key interaction involved the specific adsorption of the cellulose binding domain (CBM2a), normally found in cellulase,[8] to cellulose. CBM2a-*Strep*-tag II was first loaded onto the paper to guarantee that the biological active site of CBM2a was occupied by the cellulose. The second and third bioaffinity events involved the binding of *Strep* tag II (on the CBM2a) and of biotin (on TiO_2 particles) to streptavidin. Thus, sufficient accessible biotin binding sites on the streptavidin is present to permit binding of the biotinylated TiO_2 nanoparticles,[33] linking them to the underlying paper.

Control experiments showed that particle/fiber adhesion depended on all these elements. Control paper prepared by the same procedure, but with the absence of the CBM2a-*Strep*-tag II protein, or the use of untreated/aminosilanized TiO_2 instead of biotinylated TiO_2 nanoparticles, led to paper that had very few attached particles (Figure 5-4 b-d). EDS results on both the particle area and the non-particle area confirmed that the adhering particles, observed with SEM, were TiO_2 based.

5.4.1. Factors affecting the attachment of TiO_2 particles to paper

The efficiency of photocatalysis of TiO_2 supported paper will depend on the number of particles that can be attached to the cellulose surface. Binding is affected by both the efficiency of biological conjugation (see next section), and by preparative methods. For example, mechanical energy during synthesis affects the efficiency of TiO_2 binding to

cellulose fibers. With appropriate agitation, TiO_2 particle adsorption was enhanced. This is probably because convection promoted the diffusion of biomolecules and particles to the fiber surfaces, as the attachment experiments were carried out in aqueous solutions. However, it was also found that excess agitation loosened the network structure of the paper, degrading its mechanical strength, which is unacceptable both for paper manufacturers and customers. It was determined that shaking at 30-50rpm was optimal for attachment of both biomolecules and TiO_2 nanoparticles to paper in the water medium, without degradation of the paper.

Tethering of TiO_2 particles depends on the efficiency of tethering of each of the elements – CBM2a-*Strep*-tag II to paper, streptavidin to *Strep* tag II on CBM2a, biotin on TiO_2 particles to streptavidin – to the paper surface. The affinity constants K_a of the three interactions are 10^6 M^{-1}, 10^4 M^{-1}, and 10^{15} M^{-1} for CBM2a-cellulose,[9, 10] *Strep*-tag II-streptavidin,[30, 31] and streptavidin-biotin,[26, 27] respectively. As factors such as temperature, pH and buffer properties affect the these interactions,[8-10, 28, 30, 31] Tris-HCl buffer (20mM Tris-(hydroxymethyl)aminomethane, 50mM NaCl, pH 7.4) at room temperature was chosen as a medium to maintain the biological functions of the biomolecules.

The theoretical values of full attachment of bio-molecules and nanoparticles on fiber surfaces can be simply calculated by the areas shadowed by the bound biomolecules or TiO_2 nanoparticles, assuming a monolayer surface coverage. According to this, the theoretical value for full attachment of CBM2a to the fiber surfaces is ~7.58×10^{-2} nm^{-2}, calculated by the maximum area (~13.2 nm^2) shadowed by a bound CBM2a molecule.[9] This theoretical value is similar to our experimental results for the adsorption of CBM2a-

Strep tag II to paper (6.22 × 10^{-2} nm^{-2}), indicating the coverage of CBM2a on the fiber surfaces under the reaction conditions discussed above was 82%.

The size of streptavidin is *ca.* 4.5×5.5 nm,[45, 46] suggesting the area shadowed by one streptavidin is ~ 25 nm^2 and the theoretical value for full attachment of streptavidin to the fiber surfaces is ~ 4×10^{-2} /nm^2. Our experimental results showed that the chemisorption of streptavidin to *Strep* tag II-CBM2a on paper was 1.93×10^{-2} nm^{-2}. Using these values, one can calculate that the efficiency of binding streptavidin onto CBM2a by this method was ~48 %.

The binding of TiO_2 nanoparticles to paper depended on the concentration of bound streptavidin on the fiber surface. The efficiency of binding of the former can be evaluated by analysis of SEM images manually (Figure 5-4a) and the results show the coverage and the distribution density of TiO_2 on fibers is ~24% and ~58 μm^{-2}, respectively. This coverage is surprisingly efficient given: (1) the size of streptavidin/biotin (5-6nm)[45] is small compared with the sizes of TiO_2 nanoparticles (P25 TiO_2 is comprised of 100 nm aggregates of ~30nm primary particles[47, 48]) and the fibers in the Whatman No. 1 filter paper used in the experiments; (2) the gravity of TiO_2 nanoparticles in an agitated aqueous solution leads to the detachment of the particles from the paper surface since the affinity between streptavidin and strep tag II is low 10^4 M^{-1};[30, 31] and (3) neither the surfaces of TiO_2 nanoparticles nor fibers are smooth, which reduces the efficiency of attachment.

5.4.2. Photoactivity

The attachment of P25 TiO_2 nanoparticles onto paper gives the paper photocatalytic capability.[1-3] Not surprisingly, the more non-aggregated TiO_2 nanoparticles on the paper, the higher is the photocatalytic capacity to decompose organic materials. This was demonstrated by photodegradation of the RB5 dye: RB5 was completely photodegraded after 12 hours of UV irradiation in the presence of TiO_2-containing paper (Figure 5-8). By contrast, in the control experiment in which either no UV irradiation was applied or paper containing very few TiO_2 particles was used, little color change of the RB5 solution was observed, implying very low efficiency of decomposition of RB5 (Figure 5-8): many more TiO_2 nanoparticles are attached to the TiO_2-containing paper than the control paper (Figure 5-4).

AEROXIDE® TiO_2 P 25 is a typical photocatalytic TiO_2, which is very capable of decomposing organic molecules under UV irradiation.[49] While the reactive oxygen species generated by UV-irradiated TiO_2 can photodecompose organic chemicals such as RB5, the complex biochemistry used to bioconjugate particles to paper should similarly be susceptible to UV-initiated damage. Our experimental results show that, after UV-TiO_2 irradiation for 12 hours in addition to complete decomposition of RB5, many TiO_2 nanoparticles had detached from the paper and entered the solution (Figure 5-9). In addition, the paper had undergone significant structural damage, as many fibrils appeared on the fibres and many fibers had detached from the paper (Figure 5-10). This result is in good agreement with Iguchi's reports,[2] which showed that the tensile strength of TiO_2-containing paper decreased by more than 30% after 240 hours of UV irradiation at an intensity of 20 W/m^2.

After 10 hours of UV irradiation, RB5 was completely degraded, while no damage to the photocatalytic paper could be determined. What is surprising, however, is that even after extensive irradiation/oxidation for 12 hours, many particles still remained bound to the paper (Figure 5-11). This demonstrates that the bioconjugation can partially resist damage due to free radicals produced from UV-irradiated TiO_2 nanoparticles.

The use of biological tethering strategies offers many benefits over traditional strategies of physical adsorption of minerals to surfaces. When TiO_2 particles are explicitly tethered to cellulose fibers using biomolecule linkages, higher densities of particles are found on the surface and, more importantly, the particles are found as individuals, rather than aggregated clumps. As a consequence, photooxidative efficiency per particle (and, parenthetically, brightening) is significantly enhanced over the aggregate structures. Perhaps most surprising is the resilience of the biological linker. While both cellulose fiber and linker undergo photooxidation after extended periods of UV irradiation, prior to that liquid borne materials are efficiently photooxidized without concomitant observable degradation to the biological linker.

5.5   Conclusions

1. Photocatalytic TiO_2 nanoparticles were uniformly immobilized onto paper surface at a coverage of ~24% and a density of ~58 /μm^2 by the bioconjugation of cellulose - CBM2a-*Strep*-tag II- streptavidin - biotinylated P 25 TiO_2 nanoparticles.

2. In the immobilization of TiO_2 nanoparticles onto paper, it was found that about 82% of the fibers in the Whatman No.1 filter paper are accessible for binding with CBM2a-*Strep*-tag II; CBM2a molecules on the fiber surfaces were further conjugated with streptavidin at a density of $1.93 \times 10^{-2}/nm^2$.

3. The photocatalytic capability of the TiO_2-containing paper was demonstrated by photodegradation of RB5: a strip of TiO_2-containing paper, with a size of 1cm × 2cm, was able to completely photodegrade 1.7mL of RB5 aqueous solution with a concentration of 23ppm, by 365nm irradiation at intensity of $23 W/m^2$ for 12 hours.

4. The bioconjugated fiber-CBM2a-*Strep*-tag II-streptavidin-biotinylated TiO_2 was more resistant to damage due to UV-irradiation than the dye RB5. However, degradation did occur; after extensive irradiation, the network of fibers is weakened.

5. The bioconjugating linkages are surprisingly stable to photooxidation when compared or other water borne organic species.

(a)
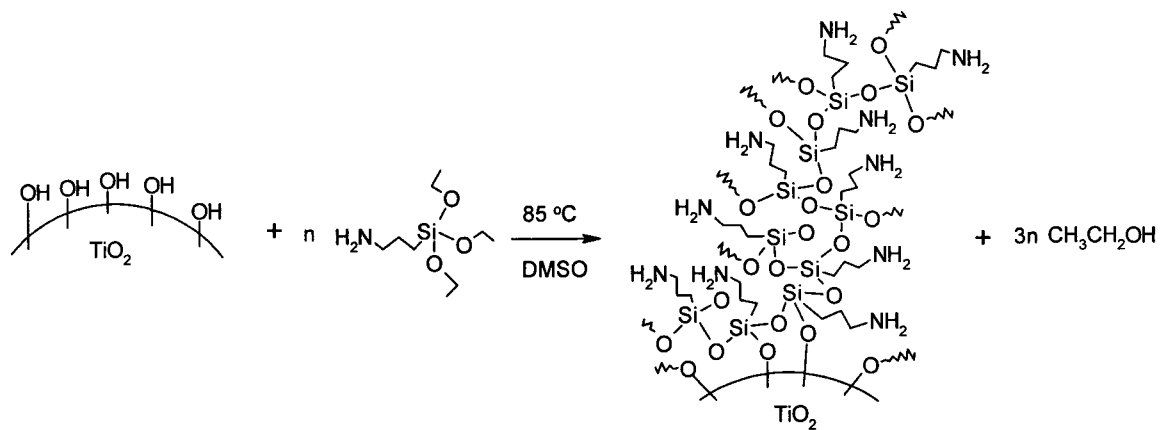
(b)
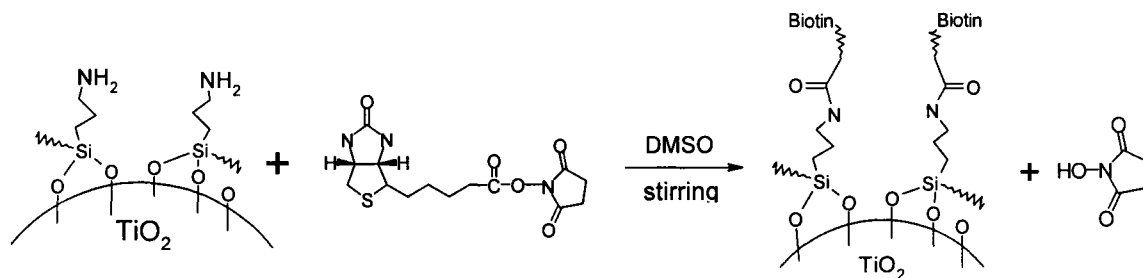
Scheme 5-1   (a) Silanization reaction of TiO$_2$ with APTS; (b) Biotinylation reaction of

Amino-TiO$_2$ with Biotin-NHS

MG

HHHHHHSSGPAGCQVLWGVNQWNTGFTANVTVKNTSSAPVDGWTLTFSFP

SGQQVTQAWSSTVTQSGSAVTVRNAPWNGSIPAGGTAQFGFNGSHTGTNAAPT

AFSLNGTPCTVG PTPTPT DDDDK ASWSHPQFEK

His 6 tag   CBM2a   (PT)₃ Linker   Entero-kinase cleavage site   *Strep*-tag II

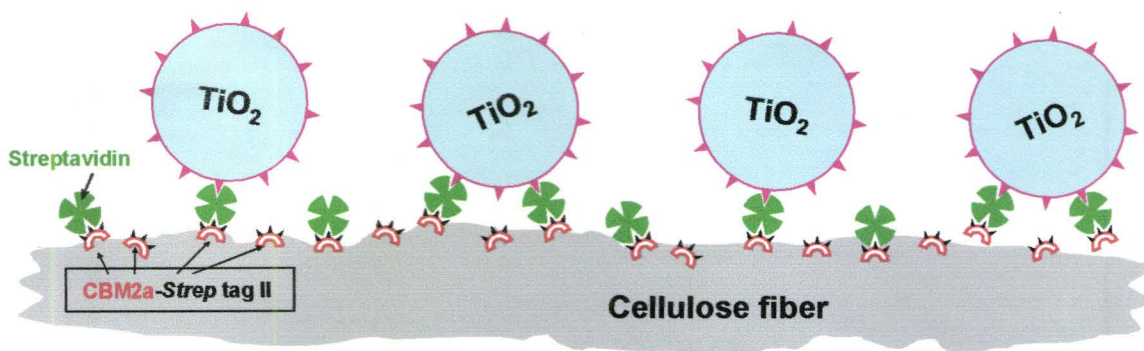**Figure 5-1**   the amino acid sequence of His-CBM2a-*Strep*-tag II fusion protein

Figure 5-2 Immobilization of P 25 TiO_2 nanoparticles onto paper by the bioconjugation

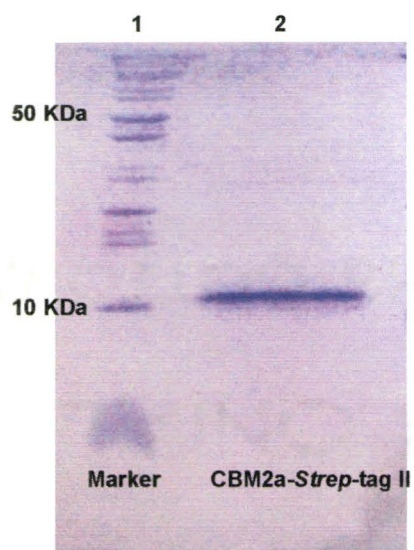of fiber- CBM2a-*Strep*-tag II - streptavidin - biotinylated TiO_2 nanoparticles

Figure 5-3 SDS-Page analysis; Lane 1: molecular weight markers; Lane 2: His-CBM2a-

Strep-tag II protein after the purification through the HisTrap FF column

experiment	paper	CBM2a-*Strep*-tag II	streptavidin	TiO$_2$
Immobilization experiment	Whatman No.1	Applied	Applied	Biotinylated TiO$_2$
Control-1	Whatman No.1	Not Applied	Applied	Biotinylated TiO$_2$
Control-2	Whatman No.1	Applied	Applied	Untreated TiO$_2$ (Aeroxide® P 25)
Control-3	Whatman No.1	Applied	Applied	APTS-modified TiO$_2$

Table 5-1 the materials applied in the immobilization of TiO$_2$ onto paper experiment and control-1, control-2 and control-3
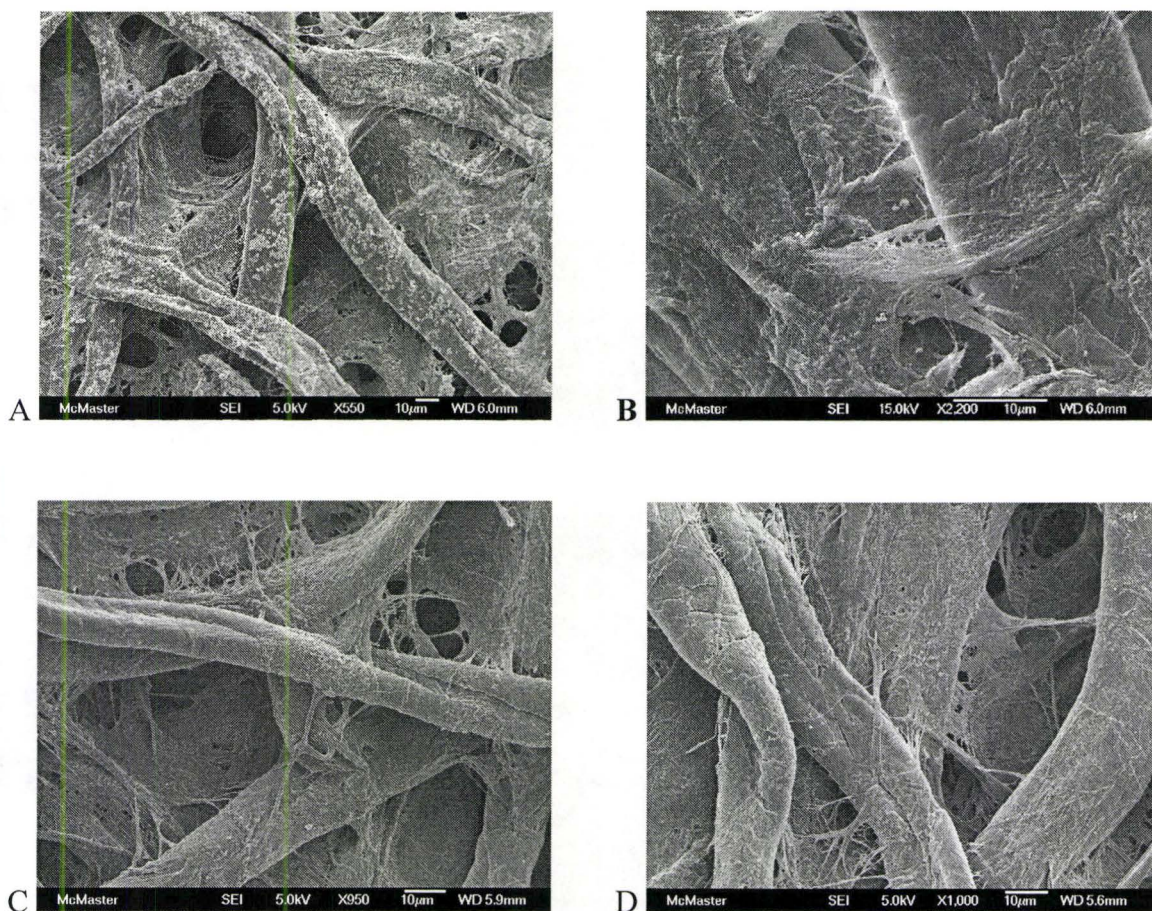
Figure 5-4   SEM images of (A) the paper treated with CBM2a-*Strep*-tag II, streptavidin and biotinylated TiO₂ nanoparticles; (B) the paper treated with streptavidin and biotinylated TiO₂ nanoparticles (the control-1 paper); (C) the paper treated with CBM2a-*Strep*-tag II, streptavidin and untreated TiO₂ nanoparticles (the control-2 paper); (D) the paper treated with CBM2a-*Strep*-tag II, streptavidin and aminosilanized TiO₂ nanoparticles (the control-3 paper);
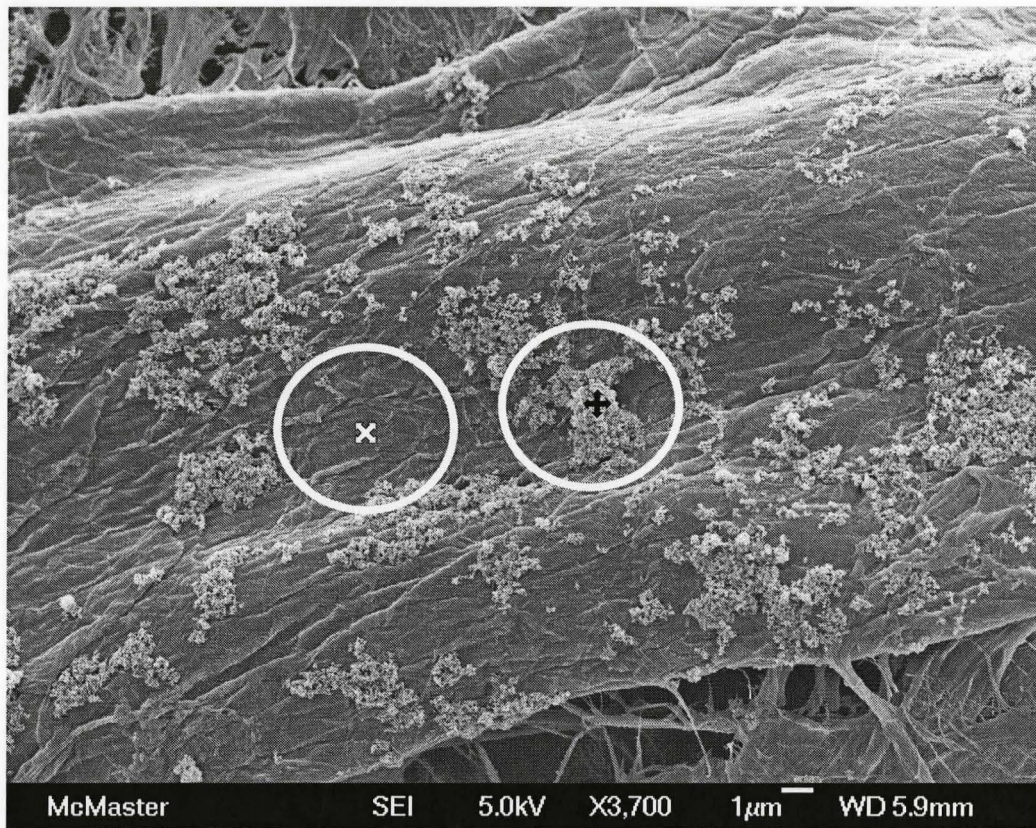
Figure 5-5 SEM image of paper treated with CBM2a-*Strep*-tag II, streptavidin and biotinylated TiO_2 nanoparticles; circled areas in which particles were found (✚) or absent (⊠) were demonstrated by EDS

Element	Particle area (✚)		Nonparticle area (⊠)	
	Weight %	Atomic %	Weight %	Atomic %
C	55.47	70.50	76.11	85.61
O	26.13	24.93	15.32	12.94
Ti	10.46	3.33	0	0
Pt	6.59	0.52	6.40	0.44
Na	0.59	0.39	0.90	0.53
Cl	0.75	0.32	1.26	0.48

Table 5-2 EDS test result of the particle area (✚) and nonparticle area (⊠) on the paper shown in Figure 5-5
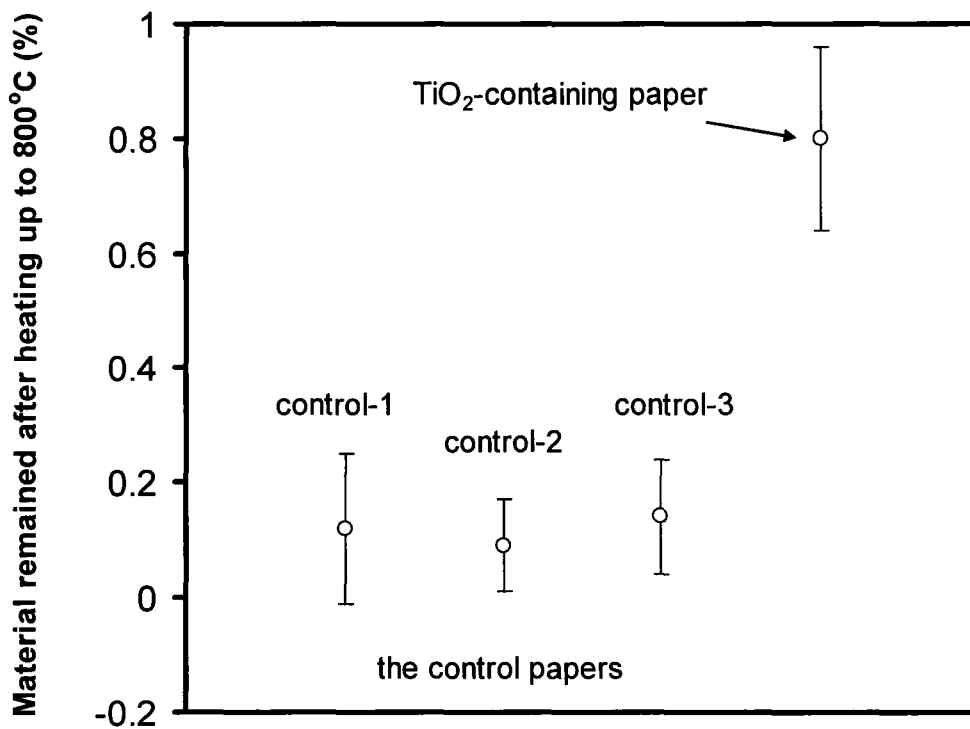
Figure 5-6 TGA results of TiO_2-containing paper prepared by the bioconjugation

method and the control papers (control-1, 2 and 3)
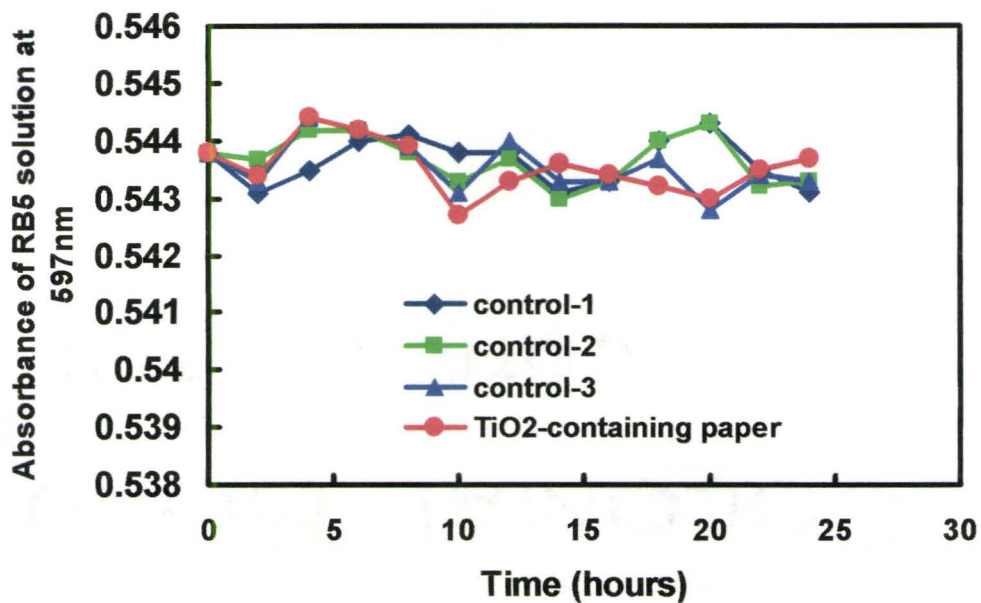
Figure 5-7 Absorbance of RB5 solutions containing control-1, 2, and 3 papers and the

TiO$_2$-containing paper without UV irradiation for 24 hours. The original concentration of

RB5 solution is 23ppm.
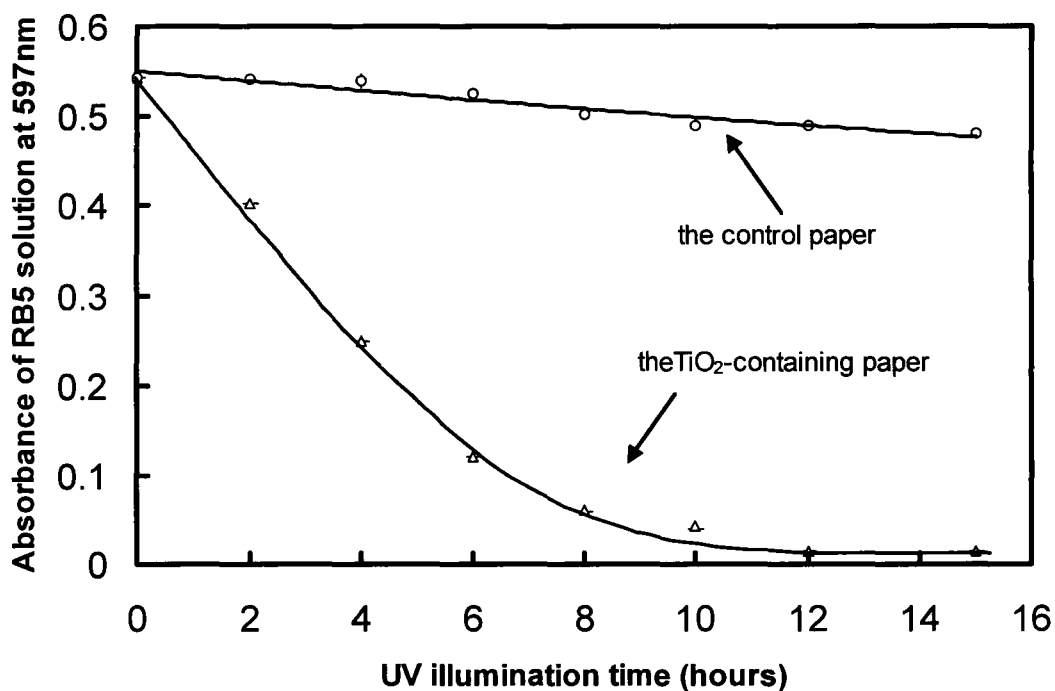
Figure 5-8 Photodegradation of RB5 with the TiO₂-containing paper and with the

control paper (control-3) in 1.7mL RB5 solution at a concentration of 23ppm, under

365nm UV irradiation with an intensity of 23W/m² for 12 hours
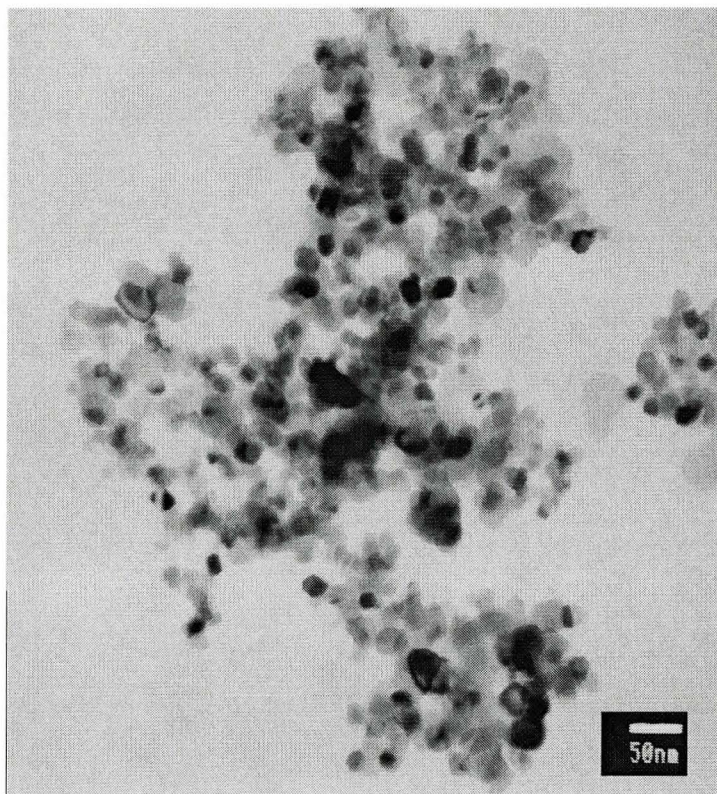
Figure 5-9   TEM image of RB5 supernatant solution, after 12 hours of UV-TiO$_2$-paper

irradiation (365nm, 23W/m^2).
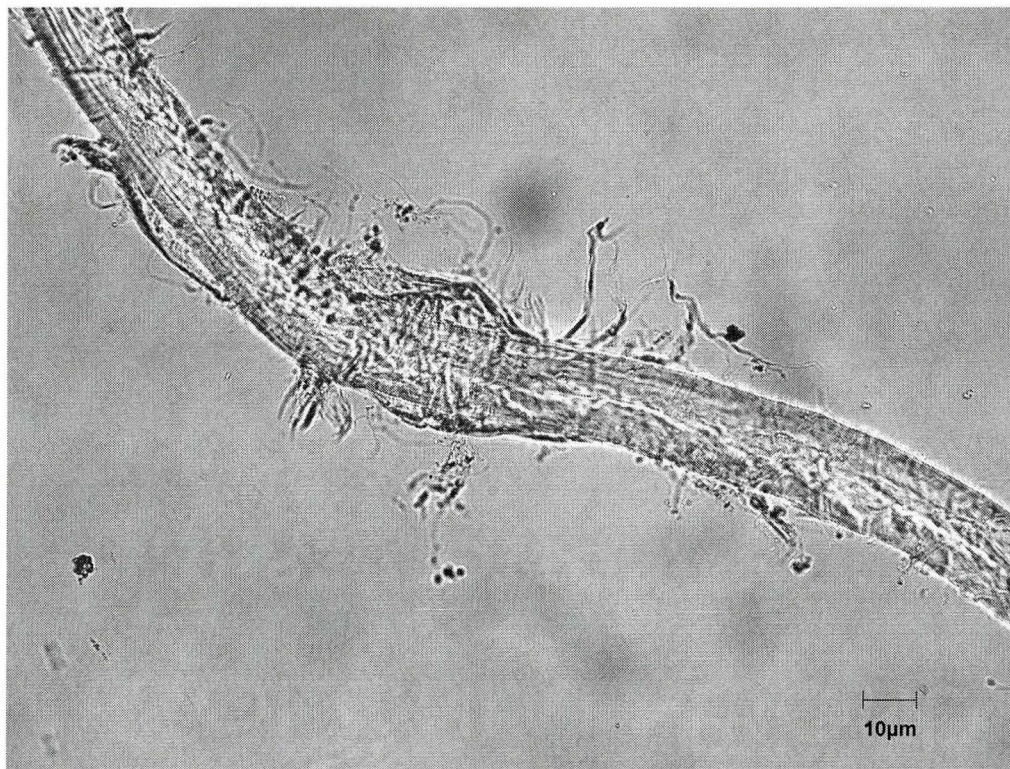
Figure 5-10   Optical microscope image of RB5 supernatant solution, after 12 hours of

UV-TiO$_2$-paper irradiation (365nm, 23W/m^2)
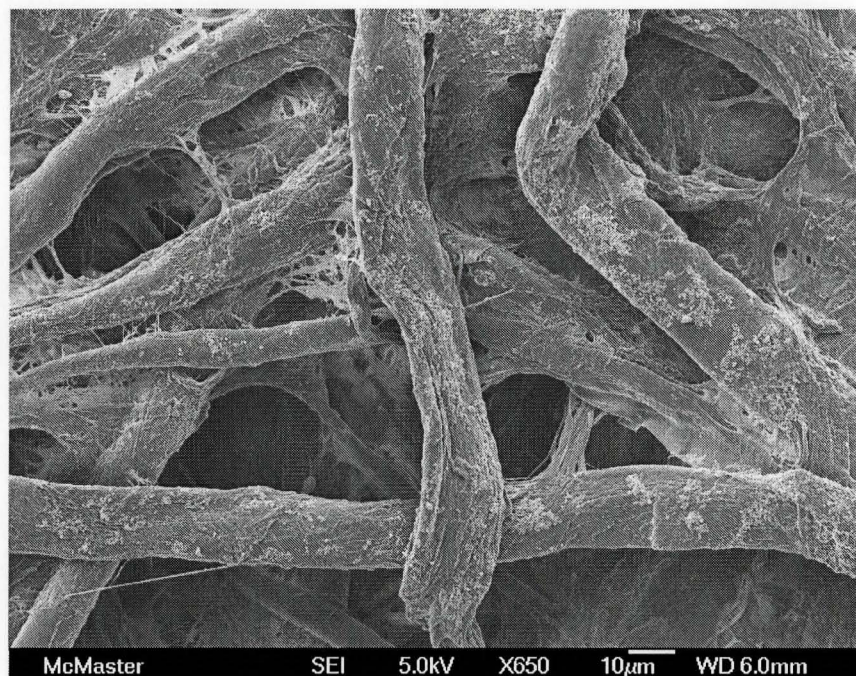
Figure 5-11   SEM image of the TiO$_2$-containing paper after irradiation for 12 hours

(365nm, 23W/m^2) in RB5 solution (1 7mL, 23ppm)

5.6   References

1. Matsubara, H.; Takada, M.; Koyama, S.; Hashimoto, K.; Fujishima, A., Photoactive TiO$_2$ containing paper: preparation and its photocatalytic activity under weak UV light illumination. *Chemistry Letters* **1995**, (9), 767-8.

2. Iguchi, Y.; Ichiura, H.; Kitaoka, T.; Tanaka, H., Preparation and characteristics of high performance paper containing titanium dioxide photocatalyst supported on inorganic fiber matrix. *Chemosphere* **2003**, 53, (10), 1193-1199.

3. Pelton, R.; Geng, X.; Brook, M., Photocatalytic paper from colloidal TiO$_2$ - fact or fantasy. *Advances in Colloid and Interface Science* **2006**, 127, (1), 43-53.

4. Moeller, H. W., Cationic starch as a wet-end strength additive. *Tappi Journal* **1966**, 49, (5), 211-14.

5. Alince, B., Cationic latex as a multifunctional papermaking wet-end additive. *Tappi Journal* **1999**, 82, (3), 175-187.

6. Gill, R. I. S.; Herrington, T. M., Floc size studies on kaolin suspensions flocculated with cationic polyacrylamides. *Colloids and Surfaces* **1988**, 32, (3-4), 331-44.

7. Gess, J. M.; Editor, *Retention of Fines and Fillers During Papermaking*. 1998; p 357pp.

8. Levy, I.; Shoseyov, O., Cellulose-binding domains. Biotechnological applications. *Biotechnology Advances* **2002**, 20, (3-4), 191-213.

9. McLean, B. W.; Bray, M. R.; Boraston, A. B.; Gilkes, N. R.; Haynes, C. A.; Kilburn, D. G., Analysis of binding of the family 2α carbohydrate-binding module from Cellulomonas fimi xylanase 10A to cellulose: specificity and identification of functionally important amino acid residues. *Protein Engineering* **2000**, 13, (11), 801-809.

10. Pinto, R.; Moreira, S.; Mota, M.; Gama, M., Studies on the Cellulose-Binding Domains Adsorption to Cellulose. *Langmuir* **2004**, 20, (4), 1409-1413.

11. Le, K. D.; Gilkes, N. R.; Kilburn, D. G.; Miller, R. C., Jr.; Saddler, J. N.; Warren, R. A. J., A streptavidin-cellulose-binding domain fusion protein that binds biotinylated proteins to cellulose. *Enzyme and Microbial Technology* **1994**, 16, (6), 496-500.

12. Ding, S.-Y.; Smith, S.; Xu, Q.; Sugiyama, J.; Jones, M.; Rumbles, G.; Bayer, E. A.; Himmel, M. E., Ordered arrays of quantum dots using cellulosomal proteins. *Industrial Biotechnology* **2005,** 1, (3), 198-206.

13. Shpigel, E.; Goldlust, A.; Eshel, A.; Ber, I. K.; Efroni, G.; Singer, Y.; Levy, I.; Dekel, M.; Shoseyov, O., Expression, purification, and applications of staphylococcal protein A fused to cellulose-binding domain. *Biotechnology and Applied Biochemistry* **2000,** 31, (3), 197-203.

14. Cao, Y.; Zhang, Q.; Wang, C.; Zhu, Y.; Bai, G., Preparation of novel immunomagnetic cellulose microspheres via cellulose binding domain-protein A linkage and its use for the isolation of interferon α-2b. *Journal of Chromatography, A* **2007,** 1149, (2), 228-235.

15. Craig, S. J.; Shu, A.; Xu, Y.; Foong, F. C.; Nordon, R., Chimeric protein for selective cell attachment onto cellulosic substrates. *Protein Engineering, Design & Selection* **2007,** 20, (5), 235-241.

16. Pangu, G.; Johnston, E.; Petkov, J.; Parry, N.; Leach, M.; Hammer, D. A., Targeted Particulate Adhesion to Cellulose Surfaces Mediated by Bifunctional Fusion Proteins. *Langmuir* **2007,** 23, (21), 10682-10693.

17. Lee, I.; Evans, B. R.; Woodward, J., The mechanism of cellulase action on cotton fibers: evidence from atomic force microscopy. *Ultramicroscopy* **2000,** 82, (1-4), 213-221.

18. Levy, I.; Nussinovitch, A.; Shpigel, E.; Shoseyov, O., Recombinant cellulose crosslinking protein: a novel paper-modification biomaterial. *Cellulose (Dordrecht, Netherlands)* **2002,** 9, (1), 91-98.

19. Ong, E.; Greenwood, J. M.; Gilkes, N. R.; Kilburn, D. G.; Miller, R. C., Jr.; Warren, R. A. J., The cellulose-binding domains of cellulases: tools for biotechnology. *Trends in Biotechnology* **1989,** 7, (9), 239-43.

20. Terpe, K., Overview of tag protein fusions: from molecular and biochemical fundamentals to commercial systems. *Applied Microbiology and Biotechnology* **2003,** 60, (5), 523-533.

21. Shoseyov, O.; Shpiegl, I.; Goldstein, M. A.; Doi, R. H. A novel cellulose binding domain with high affinity for cellulose and chitin and its applications. WO 9424158, 1994.

22. Bayer, E. A.; Morag, E.; Wilchek, M.; Lamed, R.; Shoham, Y. Modified cellulose-binding domain (CBD) proteins and their uses in affinity chromatography, immunoassays, enzyme reactors, and drug delivery. WO9613524, 1996.

23. Francisco, J. A.; Stathopoulos, C.; Warren, R. A. J.; Kilburn, D. G.; Georgiou, G., Specific adhesion and hydrolysis of cellulose by intact Escherichia coli expressing surface anchored cellulase or cellulose binding domains. *Bio/Technology* **1993,** 11, (4), 491-5.

24. Wang, A. A.; Mulchandani, A.; Chen, W., Whole-cell immobilization using cell surface-exposed cellulose-binding domain. *Biotechnology Progress* **2001,** 17, (3), 407-411.

25. Livaniou, E.; Costopoulou, D.; Vassiliadou, I.; Leondiadis, L.; Nyalala, J. O.; Ithakissios, D. S.; Evangelatos, G. P., Analytical techniques for determining biotin. *Journal of Chromatography, A* **2000,** 881, (1+2), 331-343.

26. Chaier, L.; Wolf, F. J., The properties of streptavidin, a biotin-binding protein produced by streptomycetes. *Archives of Biochemistry and Biophysics* **1964,** 106, (1), 1-5.

27. Green, N. M., Avidin. *Advances in protein chemistry* **1975,** 29, 85-133.

28. Savage, M. D.; Mattson, G.; Desai, S.; Nielander, G. W.; Morgensen, S.; Conklin, E. J., *avidin-biotin chemistry: a hanhbook.* Pierce Chemical Co.: Rockford, 1992.

29. Schmidt, T. G. M.; Skerra, A., The random peptide library-assisted engineering of a C-terminal affinity peptide, useful for the detection and purification of a functional Ig Fv fragment. *Protein Engineering* **1993,** 6, (1), 109-22.

30. Schmidt, T. G. M.; Koepke, J.; Frank, R.; Skerra, A., Molecular interaction between the Strep-tag affinity peptide and its cognate target, streptavidin. *Journal of Molecular Biology* **1996,** 255, (5), 753-66.

31. Skerra, A.; Schmidt, T. G., Applications of a peptide ligand for streptavidin: the Strep-tag. *Biomolecular engineering* **1999,** 16, (1-4), 79-86.

32. Schmidt, T. G. M.; Skerra, A., One-step affinity purification of bacterially produced proteins by means of the "Strep tag" and immobilized recombinant core streptavidin. *Journal of Chromatography, A* **1994,** 676, (2), 337-45.

33. Ye, L.; Pelton, R.; Brook, M. A., Biotinylation of TiO_2 nanoparticles and their conjugation with streptavidin. *Langmuir* **2007,** 23, (10), 5630-5637.

34. Cuendet, P.; Graetzel, M.; Pelaprat, M. L., Viologen derivatization of titanium dioxide particles and light-induced hydrogen evolution by immobilized hydrogenase. *Journal of Electroanalytical Chemistry and Interfacial Electrochemistry* **1984,** 181, (1-2), 173-85.

35. Ganadu, M. L.; Andreotti, L.; Vitali, I.; Maldotti, A.; Molinari, A.; Mura, G. M., Glucose oxidase catalyses the reduction of O_2 to H_2O_2 in the presence of irradiated TiO_2 and isopropyl alcohol. *Photochemical & Photobiological Sciences* **2002,** 1, (12), 951-954.

36. Topoglidis, E.; Cass, A. E. G.; Gilardi, G.; Sadeghi, S.; Beaumont, N.; Durrant, J. R., Protein Adsorption on Nanocrystalline TiO_2 Films: An Immobilization Strategy for Bioanalytical Devices. *Analytical Chemistry* **1998,** 70, (23), 5111-5113.

37. Topoglidis, E.; Campbell, C. J.; Cass, A. E. G.; Durrant, J. R., Factors that affect protein adsorption on nanostructured titania films. A novel spectroelectrochemical application to sensing. *Langmuir* **2001,** 17, (25), 7899-7906.

38. Hancock-Chen, T.; Scaiano, J. C., Enzyme inactivation by TiO_2 photosensitization. *Journal of Photochemistry and Photobiology, B: Biology* **2000,** 57, (2-3), 193-196.

39. Warner, W. G.; Yin, J. J.; Wei, R. R., Oxidative damage to nucleic acids photosensitized by titanium dioxide. *Free radical biology & medicine* **1997,** 23, (6), 851-8.

40. Gaberc-Porekar, V.; Menart, V., Potential for using histidine tags in purification of proteins at large scale. *Chemical Engineering & Technology* **2005,** 28, (11), 1306-1314.

41. Schmitt, J.; Hess, H.; Stunnenberg, H. G., Affinity purification of histidine-tagged proteins. *Molecular Biology Reports* **1993,** 18, (3), 223-30.

42. Diniz, J. M. B. F., Distribution of charge in wood pulps. *Langmuir* **1995,** 11, (10), 3617-19.

43. Herrington, T. M.; Petzold, J. C., An investigation into the nature of charge on the surface of papermaking woodpulps. 1. Charge/pH isotherms. *Colloids Surf.* **1992**, 64, (2), 97-108.

44. Sjoestroem, E., The origin of charge on cellulosic fibers. *Nord. Pulp Pap. Res. J.* **1989**, 4, (2), 90-3.

45. Hendrickson, W. A.; Paehler, A.; Smith, J. L.; Satow, Y.; Merritt, E. A.; Phizackerley, R. P., Crystal structure of core streptavidin determined from multiwavelength anomalous diffraction of synchrotron radiation. *Proceedings of the National Academy of Sciences of the United States of America* **1989**, 86, (7), 2190-4.

46. Weber, P. C.; Cox, M. J.; Salemme, F. R.; Ohlendorf, D. H., Crystallographic data for Streptomyces avidinii streptavidin. *Journal of Biological Chemistry* **1987**, 262, (26), 12728-9.

47. Hoffmann, M. R.; Martin, S. T.; Choi, W.; Bahnemann, D. W., Environmental Applications of Semiconductor Photocatalysis. *Chemical Reviews (Washington, D. C.)* **1995**, 95, (1), 69-96.

48. Wold, A., Photocatalytic properties of titanium dioxide (TiO_2). *Chemistry of Materials* **1993**, 5, (3), 280-3.

49. Janus, M.; Morawski, A. W., New method of improving photocatalytic activity of commercial Degussa P25 for azo dyes decomposition. *Applied Catalysis, B: Environmental* **2007**, 75, (1-2), 118-123.

50. Hong, J.; Ye, X.; Zhang, Y. H. P., Quantitative Determination of Cellulose Accessibility to Cellulase Based on Adsorption of a Nonhydrolytic Fusion Protein Containing CBM and GFP with Its Applications. *Langmuir* **2007**, 23, (25), 12535-12540.

Appendix   Calculation of the Densities of CBM2a-*strep* tag II and Streptavidin on Cellulose Fibers

Equation 1

$$m = M - \frac{A_1 \times V_1}{\varepsilon} - \sum_{i=2}^{n} \frac{A_i \times V_i}{\varepsilon}$$

m: mole of the protein attached to the paper

M: mole of the protein in the original solution before the paper is submerged

A_1: the absorbance of the protein solution after the paper is removed

V_1: the volume of the original protein solution

A_i ($i \geq 2$): the absorbance of the solution after the ith wash

V_i ($i \geq 2$): the volume of the solution for washing the paper at the ith time (25mL)

ε: extinction coefficient of the protein

Equation 2

$$D = \frac{m}{S \times BW \times SSA}$$

D: density of the adsorbed protein onto the paper (mol μm^{-2})

m: mole of the adsorbed protein onto the paper (calculated from Equation 1)

S: the area of paper applied in the experiments (S =2cm×6cm =12×10^8 μm^2)

BW: the basis weight of Whatman No.1 filter paper (BW =87g m^{-2})

SSA: the specific surface area of Whatman No.1 filter paper that is accessible to CBM

(SSA =9.76 m^2 g^{-1})[50]

Chapter 6   Summary and Contributions

The main objectives of this thesis were to explore the strategy of preparation of bioactive TiO_2 colloidal particles, study the properties of these bioactive particles, and develop their applications. These objectives have been achieved by covalently attaching biotin molecules to TiO_2 particles and then coupling various biotinylated biomolecules to the biotinylated TiO_2. The applications developed with bioactive TiO_2 colloidal particles include selectively binding and killing bacteria and immobilization of TiO_2 on cellulose fibers through bioconjugation, which verify their combined biological and photoactive functions.

6.1   *Surface modification of TiO_2 with silane coupling agent and biotin derivative:*

The surfaces of TiO_2 colloidal particles were modified with a silane coupling agent (3-aminopropyltriethoxysilane) through a chemical route to attach amino groups covalently.

The surface properties of the modified TiO$_2$ particles can be controlled by simply tuning the silanization reaction time and the curing process. Biotinylated TiO$_2$ colloidal particles are obtained by the reaction of aminosilanized TiO$_2$ with a biotin derivative (*N*-hydroxysuccinimidobiotin). Streptavidin molecules do not induce obvious flocculation of these biotin-TiO$_2$ particles, but they do conjugate with them. This theoretically allows the coupling of any desired biomolecules to TiO$_2$ by the bioconjugation of biotinylated biomolecule-streptavidin-biotinylated TiO$_2$ (Chapter 4, and 5). Biotinyltriethoxysilane, for the first time, was synthesized, purified, and characterized.

This work led to one published paper and two U.S. patents application. One paper concerning this part of work has been published in Langmuir 2007, 23 (10), 5630-5637. Authors include Lu Ye, Robert Pelton and Michael Brook. A US Patent (B&P File No. 3244-166), Biomolecule compatible silica particles, authored by Michael Brook, John Brennan, Robert Pelton, Rebecca Voss, and Lu Ye, has been submitted and is under review. In this patent, the work related to the conjugating biotin to particles was derived from this work described in this thesis. Another US Patent (B&P File No. 3244-157), "Surface modified particles", authored by Michael Brook, Robert Pelton, and Lu Ye, that resulted from this work was filed. However, this patent has been abandoned.

6.2   *The impact of UV irradiation on aminosilanized TiO$_2$:*

The rapid reduction of charges on aminosilanized TiO$_2$ colloidal particles under UV irradiation gives insight into the photo-oxidation process on TiO$_2$ surfaces: the organosilane coating is removed, thereby the surface charge is converted from positive to

negative. Based on the charge conversion, a novel photo-flocculation system was developed for the first time. This work has led to one published paper in Langmuir 2008, 24, 9341-9343. This paper, Photoflocculation of TiO$_2$ Microgel Mixed Suspensions, was authored by Lu Ye, Chuanwei Miao, Michael Brook and Robert Pelton. In this publication, the polymeric microgel was prepared and provided by Chuanwei Miao, otherwise, all the research work was undertaken by me.

6.3   Selective binding and disinfection with using E. coli antibody conjugated TiO$_2$:

Biotinylated *E. coli* antibodies are coupled to biotinylated TiO$_2$ by using streptavidin to obtain *E. coli* antibody conjugated TiO$_2$ colloidal particles. Selective binding and flocculation of *E. coli* antibody conjugated TiO$_2$ to *E. coli* bacteria were achieved. Selective killing of *E. coli* by exerting UV irradiation on *E. coli* antibody conjugated TiO$_2$ particles was also achieved. The ratio of bacteria to catalyst and the agitation were found to have influences on the selectivity of photodisinfection. This work will result in one paper, entitled, Selective flocculation and killing of *Escherichia coli* with antibody coated TiO$_2$, authored by Lu Ye, Robert Pelton, Carlos Filipe, Hai Wang, Luba Brovko, and Michael Brook. The paper is currently being prepared, and will be published soon. In this paper, knowledge related to *Pseudomonas putida* was provided by Hai Wang and Luba Brovko. This contribution makes them co-authors. The treatment of bacteria was guided by Carlos Filipe, which makes him a coauthor. While the research benefitted from the information provided by these researchers, all the research was undertaken by me.

6.4   Immobilization of TiO₂ on cellulose fibers through bioconjugation:

For the first time, TiO$_2$ particles were immobilized on cellulose fibers with a uniform distribution through the bioconjugation of cellulose - CBM2a-strep tag II – streptavidin – biotinylated TiO$_2$. The bioconjugation is sensitive to UV irradiation. The photoactivity of the resulting TiO$_2$-containing paper was studied by the decolorization of a UV sensitive dye. This work has led to one published paper in Journal of Materials Chemistry 2009, 19, XX. This paper, Immobilization of TiO$_2$ nanoparticles onto paper modification through bioconjugation, was authored by Lu Ye, Carlos Filipe, Mojgan Kavoosi, Charles Haynes, Robert Pelton, and Michael Brook. In this publication, *E. coli* containing the gene for the expression of CBM2a-strep tag II and the related techniques was provided by Mojgan Kavoosi, Charles Haynes. The research related to bacteria treatment and protein purification were guided by Carlos Filipe. These contributions make them co-authors, however, I did all the research described in that paper.

6.5   Contributions to the literature

Ten years ago, when examining photooxidation by TiO$_2$, Daniel M. Blake wrote in his review, "It remains to be seen if the efficiency and selectivity required by potential applications can be achieved (Application of the photocatalytic chemistry of titanium dioxide to disinfection and the killing of cancer cells, published in Separation and Purification Methods, 1999, 28, 1, 1-50)." The work in this thesis makes contributions that make more likely the success of this technology.

In this thesis, selective photodisinfection in a complex bacteria environment was first attempted and some associated issues such as optimizing ratio of catalyst vs. cells and the impact of the damage of the bioconjugation linker on the selectivity were also studied. One can see from Chapter 4 that conjugating antibodies to TiO_2 surface is the key to binding and killing the specific bacteria. In this work, one of the biggest challenges was to conjugate the antibody molecules in a right way: keep the region for binding to the antigen active. Although physisorption of antibodies on TiO_2 surface seems an easy strategy, it inactivates some of these adsorbed antibodies due to the random orientation in physisorption process.[1] In this thesis, the antibodies were firstly tagged by biotin, which was further tethered to the streptavidin conjugated TiO_2 surface. This strategy allows the antibody remain active to bind to antigen. Thus, we have successfully addressed one of the problems that has plagued the development of this technology in the past.

Many researchers have demonstrated that organic materials are degraded by TiO_2 when photolyzed. It was widely assumed that tethering titania particles to any organic structure would be non-productive, as the tether would be oxidized. That is, the destruction of the bioconjugating linker between the photocatalytic TiO_2 and the target (including the bacteria or the cellulose fiber, in this thesis) due to the ROS produced in the photocatalytic process should make impossible the development of processes to selectively killing bacteria. The experimental data (Chapter 5) showed the bioconjugation linker can partially resist the damage caused by UV-irradiated TiO_2; only after extensive oxidation – after it had killed bacteria – was it weakened significantly.

Some attempts to improve the resistance of the bioconjugating linkers to the ROS from the UV-TiO₂ system, including using biotin-PEG-NHS ester instead of biotin-NHS ester and using lower UV irradiation intensity, were not completely successful in that ultimately the killing efficiency and selectivity decreased. The fragility of bio-linker to UV-TiO₂ photooxidation is probably part of its intrinsic property, because ROS are capable of oxidizing almost all organic materials, particularly those nearby. Thus, our research is starting to allow one to apply limits of bioselectivity and catalyst efficacy. Ultimately, this sensitivity to oxidation means that, once used for selective degradation, the TiO₂ catalyst should be recoverable from the complex chemical and biological environment.

Another big challenge in developing selective binding and photodisinfection experiments is the choice of an appropriate control microorganism. At first, yeast was used because the big difference in the appearance of *E. coli* and yeast – they are relatively easy to distinguish one from the another. The specific binding to *E. coli* by the EA TiO₂ was first achieved. However, when *E. coli* was mixed with yeast and then applied in the binding experiment, there was no particular specificity in binding between *E. coli* versus EA TiO₂ for unknown reasons. Therefore, yeast was given up and *Pseudomonas putida* was used as the new control bacteria. Establishing the origins of the lack of differences is a problem that remains.

There was a secondary issue that had to be overcome: when examining bacteria, how could we independently identify these two types of bacteria in a mixed bacterial environment. Green fluorescent protein-containing (GFP) *E. coli* is increasingly being

exploited due to its fluorescent property, which may show the difference from the control bacteria. However, the fluorescence emitted by GFP in lab is not bright enough for visual identification, so that this technique was not viable. Finally, a special culture medium, *E. coli/coliform* count plate (Chapter 4) was adopted to overcome this problem. On this plate, after culture, only those *E. coli* colonies grow with visible trapped bubbles, whereas *P. putida* do not. However, during the experiments, it was found that although there was no problem with showing reliable *E. coli* colonies, the numbers of colonies *P. putida* that appeared without bubbles varied in each plate. Later, it was found, even when only *P. putida* was cultured in the plates, the same initial number of bacteria did not lead to same number of colonies after subculture: some plates showed many colonies, some showed very few, and some showed no colonies at all. The number of *P. putida* colonies grown on the plates was not reliable due to unknown reasons. To overcome this issue, I only used this *E. coli/Coliform* count plate to count *E. coli* colonies, while in the experiment simultaneously, used the regular LB-agar plate to count the total colonies of both of the two types of bacteria. By this strategy, the reliable numbers of *E. coli* and *P. putida* colonies in the mixed culture medium were obtained. The comparisons and analyses were made based on that data. Establishing better links between specific chemistry, and observed biological outcomes, remains a challenge that should be addressed.

6.6   Reference:

1. Ahluwalia, A.; De Rossi, D.; Ristori, C.; Schirone, A.; Serra, G., A comparative study of protein immobilization techniques for optical immunosensors. *Biosensors & bioelectronics* **1992,** 7, (3), 207-14.